The behaviour of a moored oil tanker in the Port of Leixões, Portugal
-With use of numerical models-

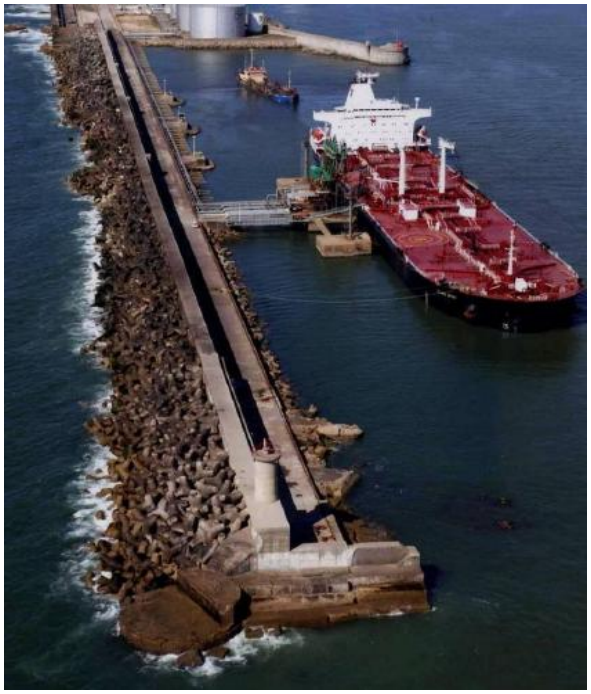

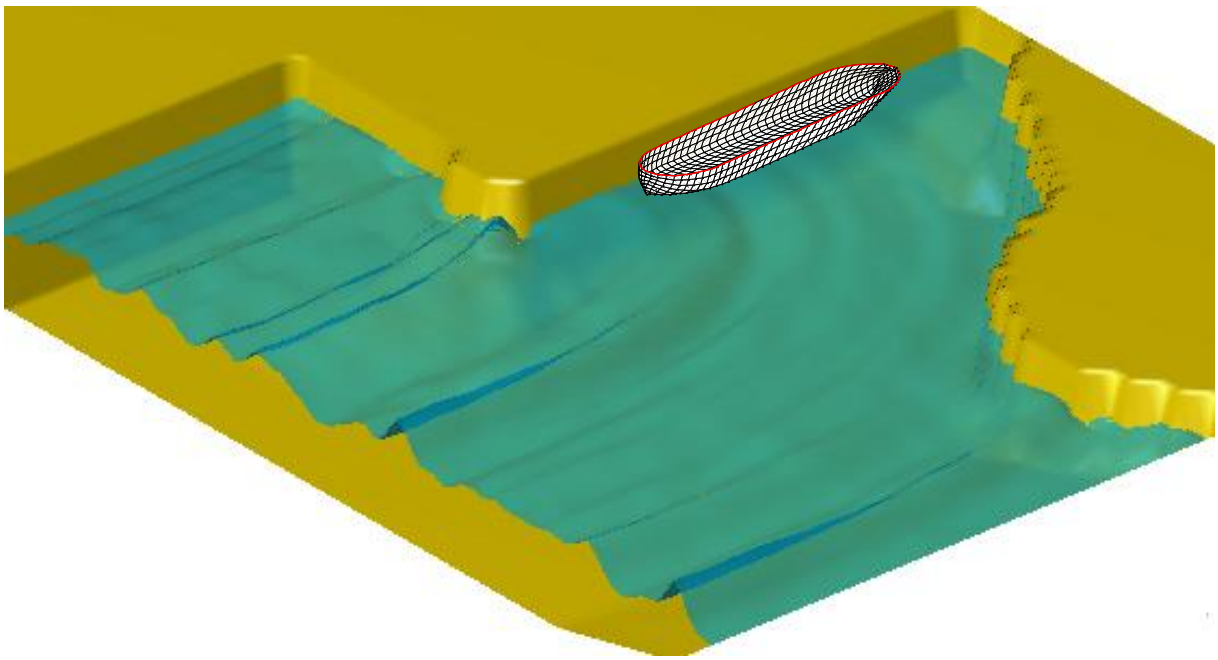

Martin van der Wel
Delft, The Netherlands
May 2011

The behaviour of a moored oil tanker in the Port of Leixões, Portugal
-With use of numerical models-

MSc. Thesis

Martin van der Wel

May 2011

Graduation committee:

Prof. Ir. H. Ligteringen	TU Delft	CiTG	Ports and Waterways
Prof. Dr. Ir. R.H.M. Huijsmans	TU Delft	3ME	Ship Hydromechanics
Dr. Ir. M. Zijlema	TU Delft	CiTG	Fluid mechanics
Ir. P. Quist	TU Delft	CiTG	Ports and Waterways
Dr. Eng. P. Rosa-Santos	FEUP		
Dr. Ir. W. van der Molen	CSIR		
Ir. A. van der Hout	Deltares		

In cooperation with:

Preface

This thesis presents a study about the numerical modelling of a moored oil tanker in the port of Leixões, Portugal. The research is carried out by a Hydraulic Engineering student from the Faculty of Civil Engineering and Geosciences of the Technical University of Delft, The Netherlands. The work has been carried out in cooperation with the Faculty of Engineering University Porto (FEUP), Portugal and the Council for Scientific and Industrial Research (CSIR), South-Africa and Deltares, The Netherlands.

Sometimes fellow students asked me why I would like to graduate in ports and waterways. To answer that question it may take some sentences, but the shortest possible answer is because of personal interest. A port cannot be designed without involvement of other specialism's. Subsequently a graduation student in the field of ports and waterways cannot graduate without having knowledge of other specialism's. Looking back, my graduation project was a journey along the beautiful places of Delft, Porto and Stellenbosch. But at the same time a journey along the fields of coastal engineering, port planning, ship hydromechanics, physical modelling and mainly numerical modelling.

During the journey many people contributed to the progress, while showing me the beautifulness of their specialism. All these contributions ensured small and sometimes large sidesteps on a path reaching the goals at the end of the journey. There are however some people whose contribution is indispensable and therefore I would like to show them my gratitude.
I would like to acknowledge Prof. Ir. H. Ligteringen for providing me this subject and the contacts I needed that came in at exactly the right times. The discussions and conversations through the progress definitely helped me reaching goals. From the Technical University of Delft I further would like to acknowledge Prof. Dr. Ir. R.H.M. Huijsmans, Dr. Ir. M. Zijlema and Ir. P. Quist for their guidance, suggestions and advises throughout the progress. From FEUP I would especially thank Dr. P. Rosa Santos who showed me the physical model, the prototype and the surroundings of Porto, meanwhile finishing his Phd. thesis. Special thanks to Dr. Ir. W. Van der Molen, without his work and knowledge I would not be able to translate the motions of waves into the motions of ships. Also his help during my weekends of stay in Stellenbosch are highly appreciated (having a flat tire after 30km was not bad for a weekend). I would like to thank the company of Deltares for offering me the opportunity to carry out additional simulations with their Boussinesq-type wave model. The knowledge of Ir. A.J. van der Hout was essential to discover the opportunities of the model and placing the results into a larger perspective. Looking from different perspectives to the same problem was necessary and the advises from Ir. B. van Vossen, Dr. Ir. M.P.C. De Jong and Ir. O. Weiler helped me by doing that. In general I would like to thank my family and friends for their endless support, either during graduation or otherwise.

Martin van der Wel

"Using a complex process based model, like Delft3D or Mike, cannot be used as an excuse for not understanding the main processes" D.J. Walstra, lecturer Coastal Dynamics II, TU Delft (2010)

"You are the intelligent part in the chain, the model is the calculator" D.J. Walstra again.

Summary

The Port of Leixões is located in the north of Portugal. The operational conditions at berth "A" are affected by several factors resulting in a down-time of the berth of about 20%. In order to describe the behaviour of the moored vessel physical model tests were performed at the Faculty of Engineering University of Porto within the research and development program DOLPHIN. Numerical simulations of wave propagation including non-linear wave interaction and the generation of both sub- and super-harmonics were not carried out in the DOLPHIN program.

Within this study a sequence of numerical models was applied to describe the moored ship motions and make a comparison with measurements from the physical model tests. An approach which combined a Boussinesq-type wave model with a panel model was selected as the appropriate approach for the present study. A Boussinesq-type wave model was selected, since diffraction around a breakwater, partial reflection from port structures and non-linear wave processes are important and relevant hydrodynamic processes to describe the wave field in the vicinity of the ship.

The output from the Boussinesq-type wave model describes the surface elevations as well as the velocity field of the waves in the vicinity of the ship. The successive panel model takes the presence of the ship within the incident wave field into account and calculates the wave forces on the ship. The calculated total wave forces are a summation of the Froude-Krylov, diffraction and second order wave forces. Time-series of wave forces serve as an input for a ship simulation model, which simulates the ship motions and the mooring forces, taking into account environmental forces and non-linear interactions with the mooring system.

The initial approach combined the Boussinesq-type wave model MIKE21 BW, with the panel model Harberth and the ship simulation model Quaysim. Due to numerical instabilities within MIKE21 BW an eddy with unreliable velocities was formed after longer period of simulation. This eddy was located in the vicinity of the ship. The subsequent computations with Harberth resulted in a continuous increase in second order wave forces on the ship. The first order wave forces on the ship did not increase continuously, but via an analysis it is shown that the calculated first order wave forces on the ship are not reliable. The finally simulated ship motions in Quaysim are not reliable as well. The unreliable wave forces on the ship as well as the unreliable subsquent simulated ship motions are a consequence of the pre-simulated instabilities within MIKE21 BW.

The cause of the numerical instabilities in MIKE21 BW could not be discovered during this study. Since longer period of simulations are required to obtain statistical reliable ship motions a switch was made to an alternative Boussinesq-type wave model called TRITON. Adaptations in the model set-up in TRITON ensured that numerical instabilities over longer periods of simulation in the simulated velocity field were avoided/minimized.

The emphasis in simulations with TRITON is on simulating and understanding the low frequency waves. The focus was on simulating the low frequency waves that caused significant moored ship responses within the physical model. The simulated waves in TRITON agree well with the measured waves in the physical model basin. It is shown that a standing wave is measured in the physical model basin, which caused measured surge responses of the ship. The obtained insight in the generation of these low frequency waves may be used when performing additional physical and/or numerical model tests.

It is recommended to simulate the total Port of Leixões with a Boussinesq-type wave model, taking into account all relevant hydrodynamic processes for moored vessel response. In that case a bound long wave should already be imposed in the incoming generated waves, since the generation of primary waves only may lead to an underestimation of the total content of low frequency waves.

The wave simulations, as performed with TRITON, are expected to be sufficiently accurate to serve as an input for vessel response computations. The recommended additional wave simulations and vessel response computations are expected to provide additional insight in the causes of excessive ship motions. New insight in the behaviour of waves as well as vessel response may lead to improvements of the operational conditions at berth "A" in the Port of Leixões.

Samenvatting

De haven van Leixões is gelegen in het noorden van Portugal. Door diverse factoren is afmeerplek "A" gedurende 20% van de tijd niet operationeel. Om het gedrag van de afgemeerde olie tanker te onderzoeken zijn fysieke model testen uitgevoerd aan de Universiteit van Porto in het kader van een onderzoeks- en ontwikkelingsprogramma genaamd DOLPHIN. Numerieke golfvoortplanting simulaties, inclusief niet-lineaire interacties tussen golven en het opwekken van zowel som- als verschilfrequente golven, ontbraken binnen het kader van het DOLPHIN programma.

Gedurende deze studie zijn diverse aaneengesloten numerieke modellen toegepast om het gedrag van de afgemeerde olie tanker te beschrijven. De resultaten van de numerieke simulaties worden geverifieerd met metingen verricht tijdens proeven met het schaalmodel. Voor deze studie is een combinatie van een Boussinesq-type golf model met een panelenmodel als meest geschikte aanpak gekozen. Een Boussinesq-type golf model was geselecteerd, omdat diffractie van golven om een golfbreker, partiële reflectie van golven door aanwezige havenconstructies en niet-lineaire interacties tussen golven beoordeeld waren als belangrijke en relevante golf processen om de scheepbewegingen door golfexcitatie accuraat te kunnen beschrijven.

De uitkomsten van het Boussinesq-type golfmodel bestaat uit oppervlakte-uitwijkingen en een beschrijving van het snelheidsveld door golven om het schip. Het panelenmodel simuleert de aanwezigheid van het schip binnen dit inkomende golfveld. De berekende totale golfkrachten op het schip bestaan uit een sommatie van de Froude-Krylov kracht, diffractiekracht en tweede-orde golfkrachten. De verkregen tijdseries van golfkrachten op het schip worden vervolgens gebruikt in een schip simulatiemodel. Het schip simulatiemodel simuleert de scheepsbewegingen en afmeerkrachten, hierbij rekening houdend met externe excitatiekrachten en niet-lineaire interacties met het afmeersysteem.

De initiële aanpak combineerde het Boussinesq-type golf model MIKE21 BW, met het panelenmodel Harberth en het schip simulatie model Quaysim. Gedurende lange perioden van simulatie raakte MIKE21 BW numeriek instabiel. Ten gevolge van het numeriek instabiel geraken werd er een neer gevormd in de buurt van het schip met onbetrouwbare snelheden. In de opvolgende berekeningen met het panelenmodel Harberth is er een continue oplopen van tweede orde krachten op het schip geconstateerd. De eerste-orde golfkrachten op het schip liepen niet op, maar uit een analyse is gebleken dat deze eerste-orde golfkrachten niet betrouwbaar zijn. De uiteindelijk gesimuleerde scheepsbewegingen met Quaysim zijn dientengevolge ook niet betrouwbaar. Ten gevolge van het numeriek instabiel raken van MIKE21 BW zijn zowel de berekende golfkrachten op het schip als de gesimuleerde scheepsbewegingen en afmeerkrachten onbetrouwbaar.

Waardoor MIKE21 BW numeriek instabiel is geraakt kon tijdens deze studie niet worden achterhaald. Omdat simulaties over langere periode benodigd zijn om scheepsbewegingen statisch betrouwbaar te kunnen beschrijven is een alternatief Boussinesq-type golfmodel genaamd TRITON toegepast. Veranderingen in de opzet van het model binnen TRITON hebben er toe geleid dat het numeriek instabiel raken van het model (zelfs na langere periode van simulatie) voorkomen/geminimaliseerd kon worden.

De nadruk van de simulaties uitgevoerd met TRITON lag op het simuleren en begrijpen van laag-frequente golven die excitatie van het afgemeerde schip in het fysieke schaalmodel hebben veroorzaakt. Het gesimuleerde golfveld in TRITON komt overeen met het gemeten golfveld in het fysieke schaal model. Het is aangetoond dat er een staande golf is gemeten tijdens proeven met het schaalmodel. De gemeten schrikbewegingen van het schip worden veroorzaakt door deze staande golf. Het inzicht verkregen met de uitgevoerde numerieke simulaties kan worden gebruikt in additionele proeven met het fysieke schaalmodel.

Het is aanbevolen om het golfveld binnen de gehele haven van Leixões te beschrijven met een Boussinesq-type golf model. Hierbij dienen alle relevante golfprocessen om het gedrag van de afgemeerde olie tanker te kunnen beschrijven meegnomen te worden. In dat geval dient een gebonden lange golf al opgelegd te worden in de gegenereerde inkomende golven, omdat het alleen opwekken van primaire golven kan leiden tot een onderschatting van de totale hoeveelheid laagfrequente golfenergie.

De verwachting is dat het golfveld binnen TRITON voldoende nauwkeurig is beschreven om als invoer te dienen voor het panelenmodel. Verwacht wordt dat de aanbevolen additionele golfsimulaties alsmede schipsimulaties vernieuwd inzicht zal geven in de oorzaken van de excessieve scheepsbewegingen. Het vernieuwde inzicht in het gedrag van golven en de daarmee gepaard gaande scheepsbewegingen kan leiden tot verbeteringen in de operationele condities ter plaatse van afmeerplek "A" in de haven van Leixões.

Contents

List of symbols

Roman symbols

Symbol	Unit	Designation
$\boldsymbol{A}$	$[kg]$	Added mass matrix
$\mathcal{B}$	$[-]$	Sea floor
$\boldsymbol{B}$	$[kg/s]$	Damping matrix
B_s	$[m]$	Breadth of ship
$\boldsymbol{C}$	$[kg/s^2]$	Hydrostatic restoring matrix
C_r	$[-]$	Reflection coefficient
c	$[m/s]$	Wave celerity
c_g	$[m/s]$	Group velocity
$\mathcal{D}$	$[-]$	Computational fluid domain
d	$[m]$	Still water depth
d_s	$[m]$	Draft of ship
$\mathcal{F}$	$[-]$	Free surface
$\vec{F}$	$[N]$	Force
$F_{x,y,z}$	$[N]$	Surge, sway and heave force
f	$[s^{-1}]$	Wave frequency
g	$[m/s^2]$	Gravitational acceleration
$\mathcal{H}$	$[m^2]$	Wetted surface of ship hull
h	$[m]$	Total water depth
$\boldsymbol{K}$	$[kg/s^2]$	Impulse response function matrix
L_{OA}	$[m]$	Length over all
L_{BP}	$[m]$	Length between perpendiculars
$\boldsymbol{M}$	$[kg]$	Mass matrix
$M_{x,y,z}$	$[Nm]$	Roll, pitch and yaw moment
n	$[-]$	Normal vector
p	$[N/m^2]$	Pressure
P	$[m^3/m/s]$	Depth integrated flux in x-direction
Q	$[m^3/m/s]$	Depth integrated flux in y-direction
S	$[m^2]$	Wetted surface of body
t	$[s]$	Time
$\vec{X}$	$[m]$	Body motion
u	$[m/s]$	Fluid velocity component in x-direction
v	$[m/s]$	Fluid velocity component in y-direction
W	$[m^2]$	Wetted surface of fixed structures
w	$[m/s]$	Fluid velocity component in z-direction
x	$[m]$	Longitudinal horizontal coordinate
y	$[m]$	Lateral horizontal coordinate
z	$[m]$	Vertical coordinate perpendicular to x-y plane

Greek symbols

Symbol	Unit	Designation
$\vec{\alpha}$	$[m]$	Total displacement
ζ	$[m]$	Wave surface elevation
Γ	$[-]$	Waterline of floating body
ρ	$[kg/m^3]$	Fluid density
Φ	$[m^2/s]$	Total potential
ϕ^I	$[m^2/s]$	Incident wave potential
ϕ^S	$[m^2/s]$	Scattered wave potential
ϕ^j	$[m^2/s]$	Radiation potential in mode j
χ	$[m^2/s]$	Time-varying part of radiation potential
ψ	$[m^2/s]$	Impulsive part of radiation potential
Ω	$[rad]$	Rotational displacement

Definitions

COG: Centre of gravity
COB: Centre of buoyancy
COF: Centre of floatation
DWT: Dead weight tonnage

Heave: Translation along z-axis
Surge: Translation along x-axis
Sway: Translation along y-axis
Yaw: Rotation around z-axis
Roll: Rotation around x-axis
Pitch: Rotation around y-axis

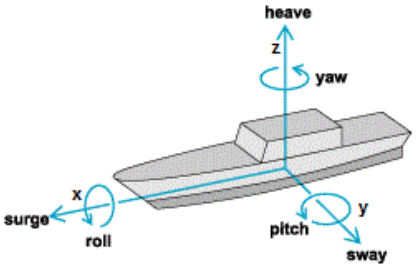

List of figures

List of tables

1 Introduction

The behaviour of moored ships in ports is a topic which is investigated for several decades. With increased computational efficiency and coupling of several numerical models it is nowadays possible to investigate moored ship behaviour in an alternative way than by performing physical model tests only. Results of both numerical and physical model simulations can be used to gain more insight in system behaviour and to give recommendations either about designing a port or improving a port.

1.1 Motive of study

Berth "A" in the Port of Leixões, see Figure 1-1, is affected by operational problems. As a consequence berth "A" is not in operation for 20% of the time. In order to improve the conditions at the berth, the behaviour of the moored oil tanker should be described. The Faculty of Engineering University of Porto (FEUP) was investigating the behaviour of the moored vessel by performing physical model tests. The behaviour of the moored vessel can be investigated by numerical model simulations. The results of both the numerical and physical models can be used to give recommendations how to improve the operational conditions at the berth.

1.2 Problem definition

The Port of Leixões is located in the north of Portugal. The port has an oil terminal, with three berths (respectively "A", "B" and "C"), see Figure 1-1. Berth "A" is located close to the harbour entrance and is protected by the Leixões North breakwater. Due to its location the berth is exposed to adverse maritime conditions. The operational conditions at berth "A" are affected by several factors resulting in a down-time of the berth of about 20%. The down-time of the berth leads to extra costs as well as security risks for the port authority (Veloso Gomes *et al.* 2005).
The 20% down-time of the berth does not only include the days that the berth cannot be used due to adverse maritime conditions, but also the days due to maintenance operations at the jetty or dredging works in the neighbourhood of the berth (Rosa-Santos *et al.* 2008).
Large motions of a moored oil tanker lead to a reduction of the (un)loading efficiency and in adverse conditions the vessel is not longer allowed to be kept at the berth safely. A research and development program (DOLPHIN) was initiated by FEUP and the Port of Leixões to study the behaviour of moored oil tankers and finally to improve the operational conditions at the berth. The berth "A" operational conditions are supposed to be influenced by (see Veloso-Gomes *et al.* 2005):

- Overtopping of the Leixões North breakwater.
- Wave diffraction around the head of the Leixões North breakwater.
- Possible resonance phenomena in the berth "A" area.
- Current transmission through the core of the breakwater.
- Characteristics of existing fenders and mooring system.

Figure 1-1: Overview of berths and location of the Port of Leixões.
Source: Rosa-Santos et al. (2010)

1.3 Objective of study

The objective of this study is to simulate the moored ship motions at berth "A" in the Port of Leixões by applying a sequence of numerical models. The calibrated and validated numerical models provide more insight into the behaviour of the moored tanker. Both physical and numerical model results may be used to improve the mooring conditions at berth "A" in the Port of Leixões.

During the study the original objective was adjusted. The focus of this thesis was shifted towards the understanding of the generated low frequency waves within the physical model. The emphasis is on simulating the low frequency waves that caused significant moored ship responses in the physical model. The shift was made since discrepancies in the numerical modelling were mainly concerned with the wave modelling.

1.4 Outline of the thesis

The thesis is divided in several chapters. In Chapter 1 a general introduction is made. Chapter 2 provides background information about the Port of Leixões, the DOLPHIN project, long waves, harbour oscillations and mooring of oil tankers in general. In Chapter 3 an analysis is made of the physical model and the relevant hydrodynamic processes. Chapter 4 contains the research methodology and gives a short description of the applied numerical models. During the study several numerical models are applied: MIKE21 BW in combination with Harberth and TRITON. In Chapter 5 the results after applying MIKE21 BW, Harberth and Quaysim will be discussed. Simulations carried out with TRITON will be explained in Chapter 6. In Chapter 0 the results from the physical model tests and the TRITON simulations will be compared. The model results obtained from both applied Boussinesq-type wave models will be discussed in Chapter 8. Final conclusions and recommendations will be given in Chapter 9.

2 Background information

2.1 Port of Leixões

The Port of Leixões is located in the North of Portugal, see Figure 1-1, and is one of the most important ports of the country. The port handles the major types of commodities within maritime transport. The port was established in 1890 when the first docks were completed. Port expansion took place in the 1930's and 1970's. Since the late 1990's Panamax container vessel can be handled in the port.

The Port of Leixões has an oil terminal which is under concession by Petrogal Petróleos de Portugal. The oil terminal is connected via a pipeline with the Petrogal refinery. The terminal is built nearby a breakwater, with a crest level at +15 m C.D. and has a total length of 700 m. Along the breakwater there are three berths, respectively berth "A", "B" and "C" , see Figure 2-1. Berth "A" is located behind a relatively new breakwater, while berth "B" and "C" are located behind a longer existing breakwater. The North breakwater protects berth "A" from direct wave action and is constructed over an old submerged breakwater. Permeability conditions of the breakwater are not known accurately. From observations it appeared that sediment is deposited near the inner breakwater toe, which was not noticed at the head of the breakwater. The depositing of sediments is supported by ship pilots which observed flows of sand coming from the breakwater at the stern of the ship, during adverse sea conditions (see Veloso-Gomes *et al.* 2005). The breakwater was damaged and repaired several times during the last decades. In order to protect the head of the breakwater a new submerged breakwater was installed in front of the older existing breakwater, see Figure 2-1.

Berth "A" can accommodate vessels up to 100,000 dwt carrying crude oil and other refined products. Berth "B" can accommodate vessels up to 27,000 dwt that carry crude oil, refined products, liquefied gasses and aromatic products. Berth "C" can accommodate vessels up to 5,000 dwt carrying liquefied petroleum gasses, refined products and aromatic products.

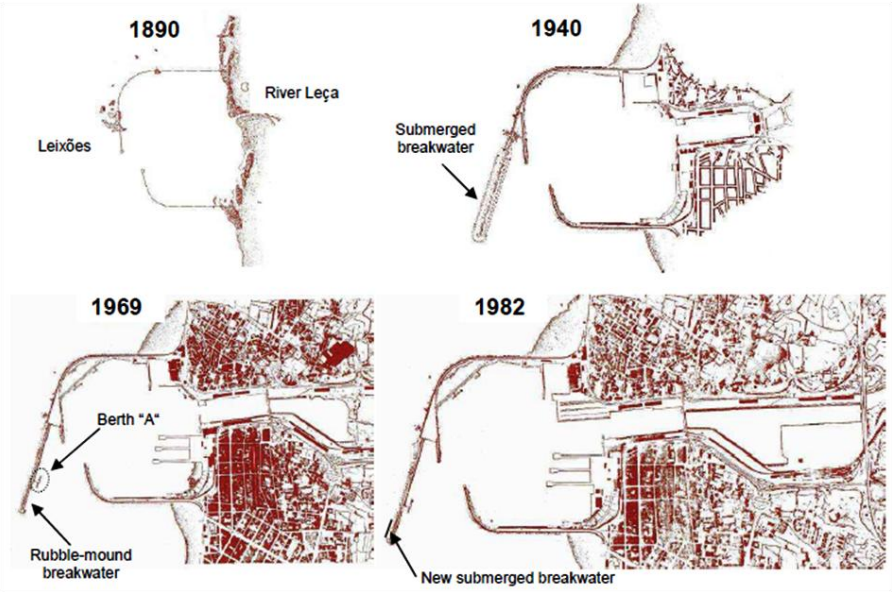

Figure 2-1: Evolution of the Port of Leixões. Source: Rosa-Santos et al. (2008).

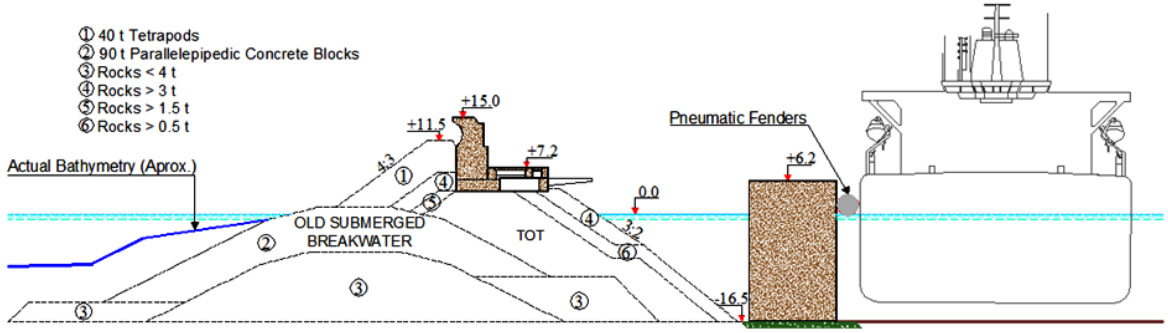

Figure 2-2: Cross section of breakwater at berth "A". Source: Rosa-Santos et al. (2008).

2.1.1 Berth "A"

The jetty structure of berth "A" consists of two breasting dolphins (equipped with a pneumatic fender and double mooring hooks) and a loading platform, see Figure 2-2 and Figure 2-3. In Figure 2-4 the most common mooring arrangement for the largest oil tankers that use the berth is given. In this arrangement eight mooring legs are used with double mooring lines. The largest oil tankers are usually moored with steel mooring lines with a synthetic mooring tail (usually nylon).
A detailed analysis of the wave records shows that, in general, berth "A" is operational when the deep water wave height is less than 2.5 meter and for wave periods between 7 and 15 seconds. The berth is predominantly inoperative for wave height higher than 2.5 meter and for wave periods between 8 and 20 seconds (Veloso-Gomes *et al.* 2005).
Previous studies have concluded that the downtime of berth "A" was mainly associated with waves coming from the West and North-West directions. Terminal operators and the ship pilots have stated that the most problematic sea states were the waves approaching from the West (almost perpendicular to the North breakwater), since those waves can diffract around the head of the breakwater more easily (Rosa-Santos *et al.* 2010). Waves from the South-West do not occur very often and their significant wave height is usually small compared with waves originating from other directions (Taveira Pinto *et al.* 2008).

Figure 2-3: Overview of berth "A".

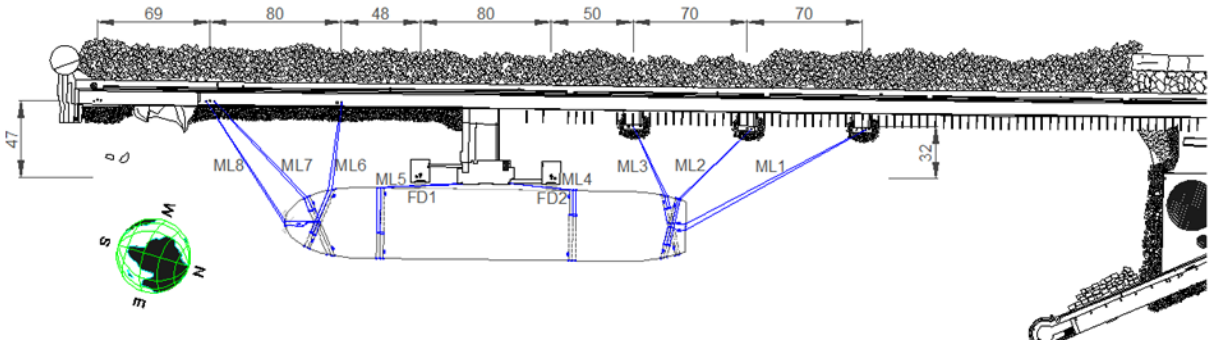

Figure 2-4: Asymmetrical mooring lay-out. Source: Rosa-Santos et al. (2008).

2.2 Physical model tests

2.2.1 DOLPHIN project

The investigation on improving berth "A" has been done within a Research and Development program called DOLPHIN. The main objective of the DOLPHIN project was to investigate the moored ship behaviour at berth "A". An adapted overview of the DOLPHIN program is given in Figure 2-5. Three different methods are applied to investigate the behaviour of the moored ship:

- Prototype measurements.
- Physical modelling.
- Numerical modelling.

Before the DOLPHIN project started the following studies were carried out:

- Analysis of inoperativeness records of berth "A".
- Physical model tests for the Leixões North breakwater.
- Numerical modelling of wave propagation.
- Analysis of the bathymetry evolution nearby berth "A" (alongside the North breakwater).

The analysis of down-time records and the numerical modelling of wave propagation provided wave conditions which are tested within the physical model. Results of numerical wave propagation simulations agreed with ship pilot reports and showed that during high tide, waves of 2.5 meter height may be expected in the surrounding area of berth "A" during certain (extreme) wave conditions.

In the region of Leixões harbour two ranges of long period waves can often occur: the first one with periods ranging from 2 to 5 minutes and the second with periods ranging from 15 to 20 minutes. Simulations with monochromatic long waves showed that the water mass in the neighbourhood of berth "A" can experience resonance for waves with periods close to both ranges and a standing long wave node in the region of berth "A" can occur for some of these wave periods (Veloso-Gomes *et al.* 2005 and Rosa-Santos *et al.* 2008). Numerical simulations of wave propagation including non-linear wave interaction and the generation of both sub- and super-harmonics have not been carried out.

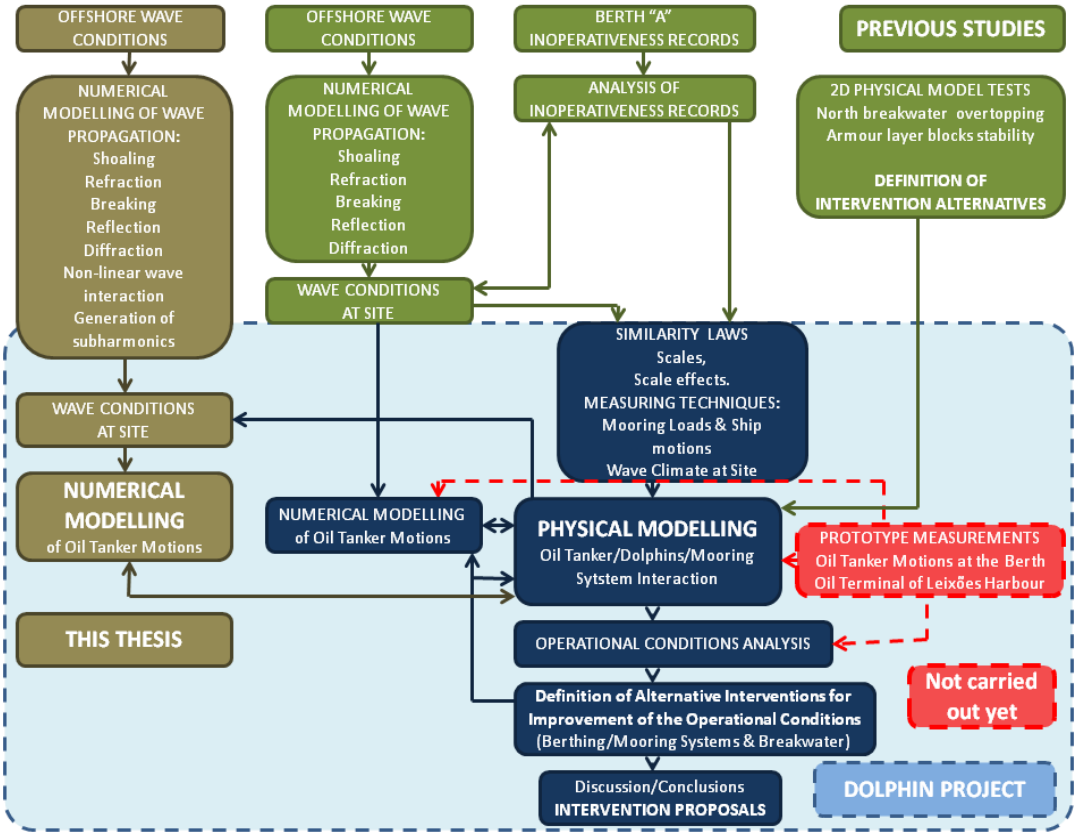

Figure 2-5: Overview of the DOLPHIN project. Source: Taveira-Pinto et al. (2008) (adapted).

2.2.2 Physical model

Physical model tests have been carried out at the Faculty of Engineering of University Porto within a test basin with outer dimensions of 28 by 12 meters. Before testing the ship was ballasted and calibrated and the mooring line and fender characteristics were reproduced. The physical model tests were carried out according to Froude criteria of similitude at a geometrical scale of 1:100. The wave maker consists of multi-elements and has a dynamic wave absorption system. During the first phase of physical model tests moored ship behaviour was investigated in case of head waves in a simplified reproduction of the berth arrangement, see Figure 2-6. During the first phase only the berthing structure was reproduced according to prototype characteristics, since ship behaviour was investigated in the case of head waves only. Those waves are expected to reach berth "A" after diffraction around the head of the breakwater. During the second phase a more detailed construction of the surrounding areas of berth "A" was represented, see Figure 2-7.

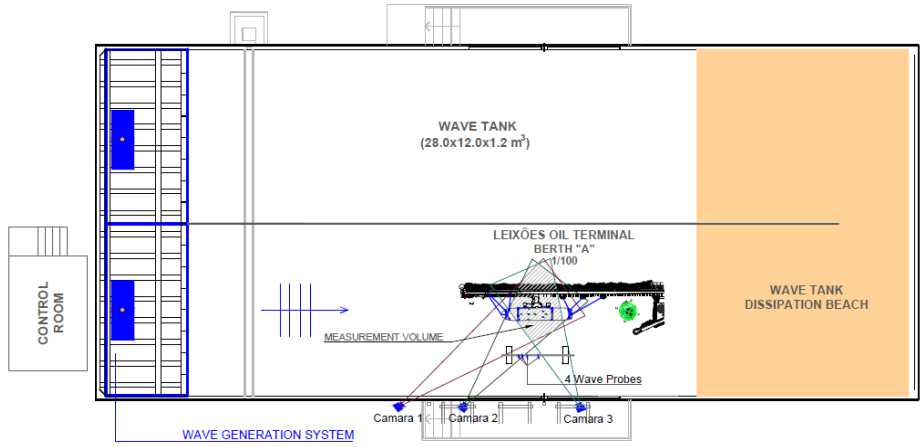

Figure 2-6: Physical model of the first phase. Source: Rosa-Santos et al. (2010)

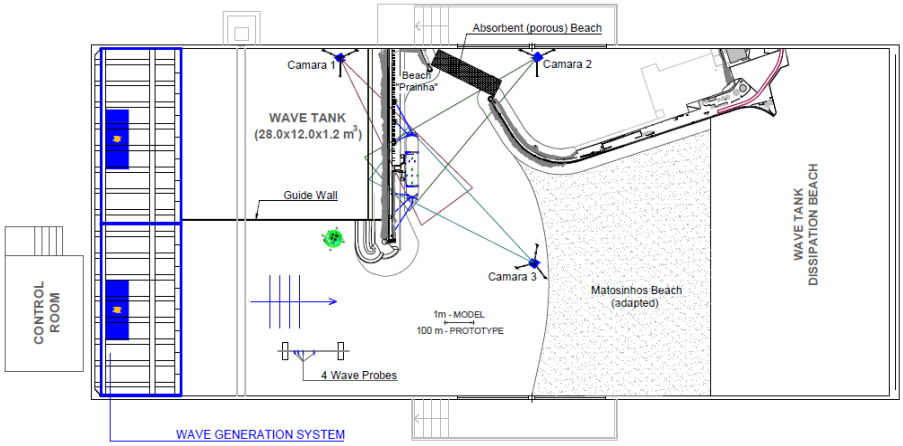

Figure 2-7: Physical model of the second phase. Source: Rosa-Santos et al. (2010)

An overview of the second phase of the physical model tests is given in Figure 2-7 and Figure 2-8. Numerical computations will be carried out for the second phase of the study and compared with physical model measurements. Some remarks should be made regarding the wave forcing by the wave maker and the set-up of the physical model with respect to the inclusion of beaches and breakwaters.

Beach and breakwaters

- The dissipation beach at the end of the physical model (see V in Figure 2-8) is adapted compared to the first phase of the study to avoid wave reflections from the side walls of the physical model.
- The beach (see V in Figure 2-8) is curved in long-shore direction, but has a uniform profile in cross-shore direction.
- Both the North and South breakwater structure are represented as accurate as possible.
- A wave guide wall is placed halfway in front of the wave maker (see III in Figure 2-8). The North breakwater (at VI in Figure 2-8) is made impermeable for the major tests. Wave penetration through the North breakwater can therefore be neglected.
- A porous (absorbing) beach (see VII and detail Figure 2-8) was designed and installed at the entrance to the inner harbour basin to reduce reflections. Reflection analysis of this porous beach was not made.

Wave maker

- During the physical model tests waves were generated according to a standard JONSWAP spectrum, combined with theoretical set-down compensation and dynamic wave absorption.
- The generated waves were long crested waves without directional spreading.
- The wave maker provides a set-down compensation, in real time, in the form of a second-order driven signal that is added to the primary waves to ensure that (unwanted) free long spurious incoming waves are minimized.
- Dynamic wave absorption is used to absorb reflected waves. The efficiency of the absorption is depending on the frequency, see Figure 2-9. Notice that the defined frequency axis in Figure 2-9 is on model scale. At a geometrical scale of 1:100 the frequency should be divided by 10 (according to Froude scaling) to obtain prototype values.
- The efficiency of the dynamic wave absorption for long waves with periods above 50 seconds is low. Long waves reflected from the beach (V in Figure 2-8) are not absorbed by the wave maker, but should instead be absorbed along other model boundaries.

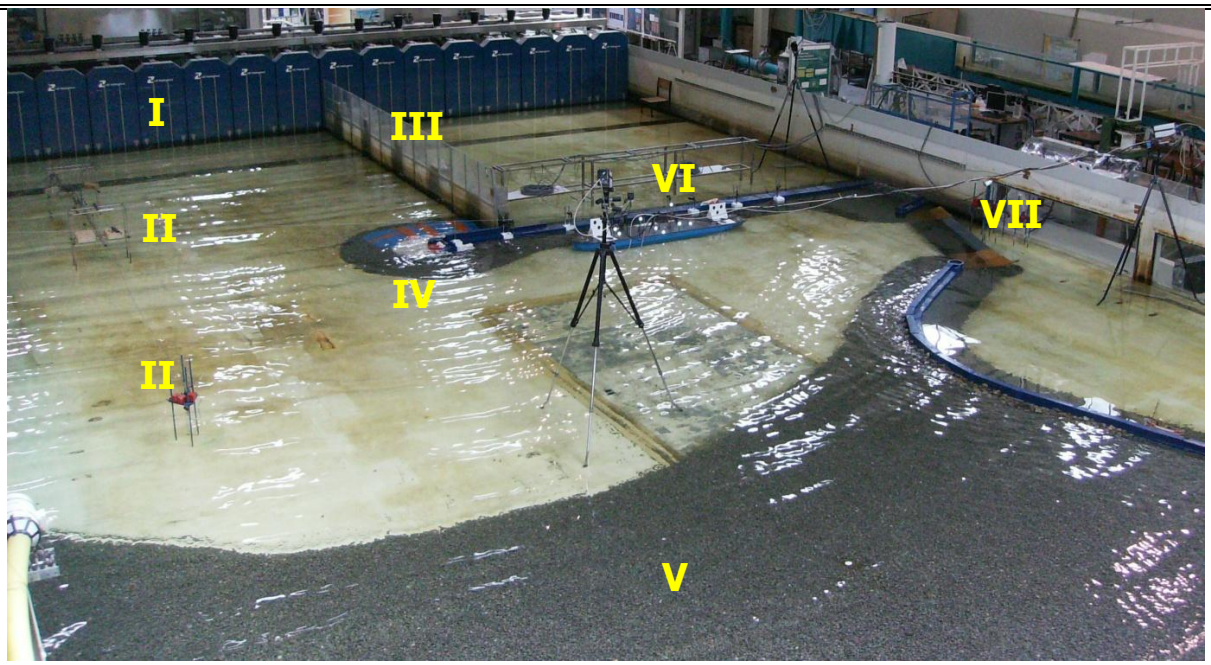

I	Wave maker
II	Wave gauges
III	Wave guide wall
IV	Breakwaterhead
V	Absorbing beach
VI	Ship
VII	Porous (absorbing) beach

Figure 2-8: Overview of physical model. Source: Rosa-Santos (2010).

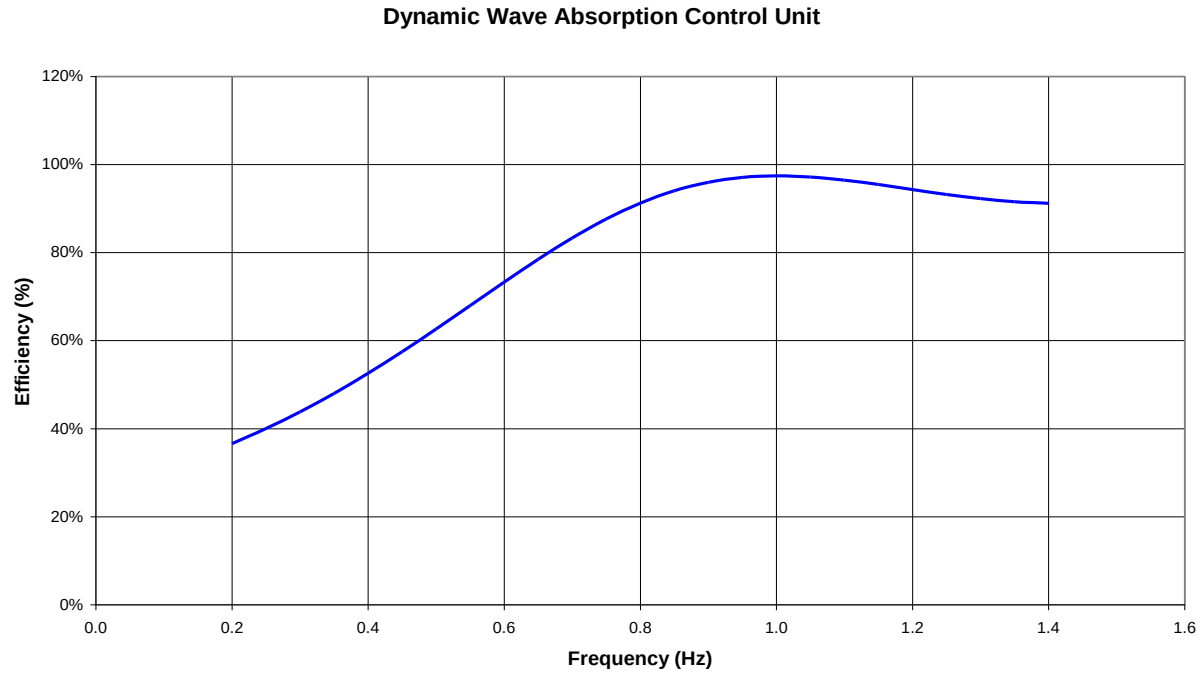

Figure 2-9: Efficiency of dynamic wave absorption control unit .

2.2.3 Tanker and mooring system characteristics

The ship that regularly moors at berth "A" is a 105,000 dwt oil tanker. The ship used during physical model tests was calibrated for maximal loaded conditions and has the dimensions according to Table 2-1, a visualization of the wetted ship hull (described by 676 panels) is given in Figure 2-10.

Designation	Symbol	Magnitude	Unit
Displacement volume	Δ	122714	[tons]
Length over all	L_{OA}	245.05	[m]
Length between perpendiculars	L_{BP}	236.00	[m]
Breadth	B	43.00	[m]
Draft	d	14.10	[m]
Depth	D	21.00	[m]
Transversal metacentric height	GM_T	5.83	[m]
Longitudinal metacentric height	GM_L	314.14	[m]
Vertical position COG above keel	KG	12.46	[m]
Longitudinal position COG in relation to the stern	$Z_{COG,L}$	128.36	[m]
Transversal position COG in relation to longitudinal central axis	$Z_{COG,T}$	0.00	[m]
Vertical position COB above keel	Z_{COB}	7.35	[m]
Longitudinal position COB in relation to the stern	$Z_{COB,L}$	128.41	[m]
Longitudinal position COF in relation to the stern	$Z_{COF,L}$	119.94	[m]
Waterplane area	A_W	9368.80	[m^2]
Transverse radius of gyration	k_{xx}	15.10	[m]
Longitudinal radius of gyration	k_{yy}	61.40	[m]

Table 2-1: Prototype ship dimensions.

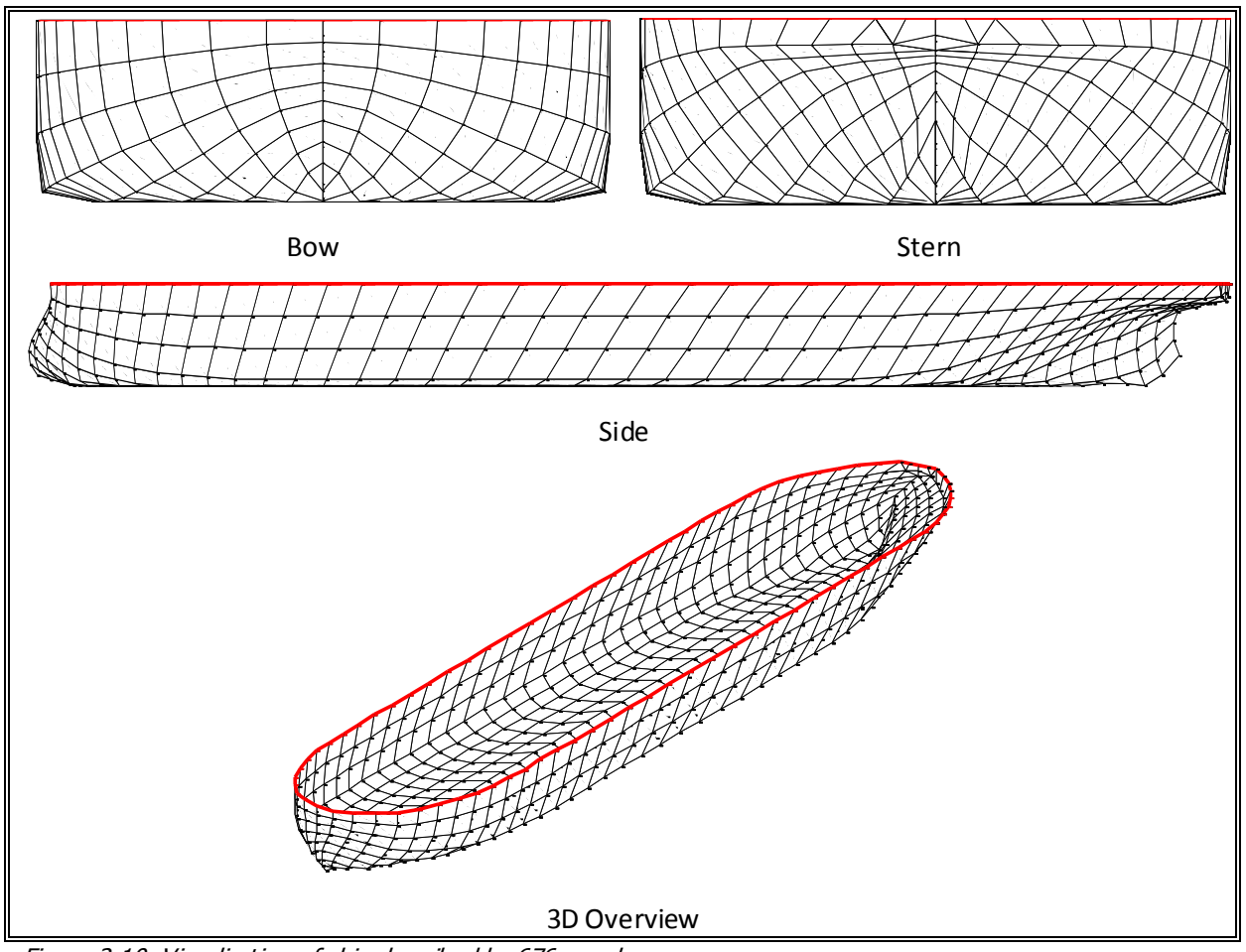

Figure 2-10: Visualisation of ship described by 676 panels.

During the calibration phase of the physical model tests the ship mooring lines as well as the fenders were simulated. The load elongation curves of the ship mooring lines were simulated using a combination of precision springs and taking into account the stiffness of the corresponding force transducer. The non-linear behaviour of the mooring lines (see Figure 2-11 left) as well as the fenders (see Figure 2-11 right) was linearized for the model ship. The non-linear mooring lines were linearized such that the energy absorption capacity of an equivalent linear mooring line was equal. An inelastic kevlar string and a combination of two precision springs were used to reproduce each one of the eight double mooring lines of the prototype. Precision coil springs were carefully selected to furnish the appropriate elasticity to each mooring element (Rosa-Santos *et al.* 2008 and 2010).

An example of the calibration and linearization of the mooring lines and fenders is included in Figure 2-11, whereas the equivalent constant stiffness coefficients of the mooring lines and fenders are included in Table 2-2.

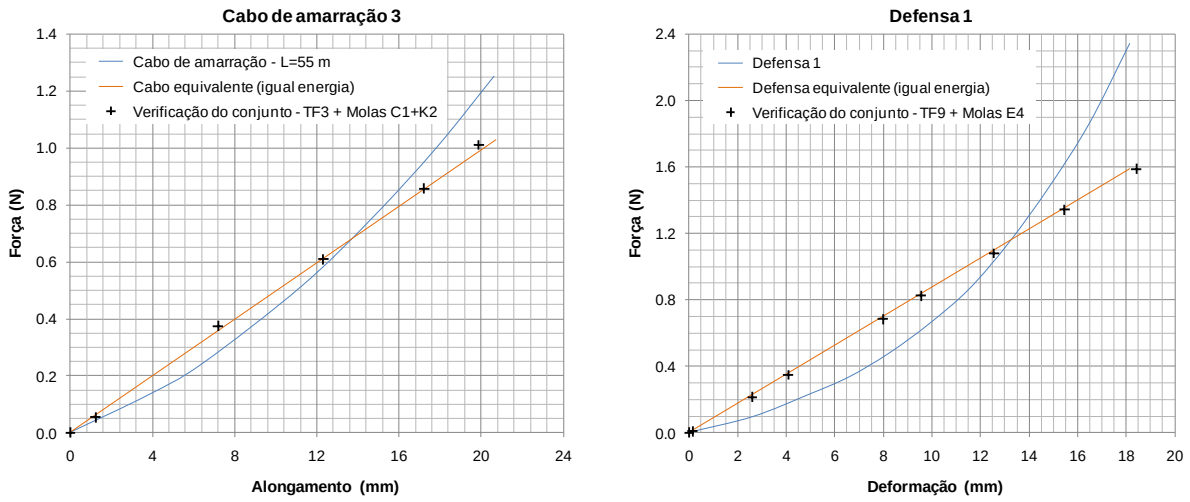

Load versus elongation mooring line 3. *Load versus elongation fender 1.*

Figure 2-11: Examples of load elongation curves.

Mooring line & Fender	Approximate length		Stiffness	
	Prototype [m]	Model [m]	Prototype [kN/m]	Model [N/mm]
ML 1 (ASY & SYM)	150	1,50	173,53	0,0169
ML 2 (ASY & SYM)	90	0,90	349,83	0,0341
ML 3 (ASY & SYM)	55	0,55	510,76	0,0498
ML 4 (ASY & SYM)	55	0,55	504,84	0,0493
ML 5 (ASY & SYM)	82	0,82	352,69	0,0344
ML 6 (ASY & SYM	82	0,82	351,99	0,0343
ML 7 (ASY & SYM)	90	0,90	349,42	0,0341
ML 8 (ASY)	120	1,20	317,49	0,0310
ML 8 (SYM)	167	1,67	168,61	0,0165
FD1 (ASY & SYM)	--	--	886,63	0,0865
FD2 (ASY & SYM)	--	--	877,40	0,0856

Table 2-2: Equivalent constant stiffness coefficients of the mooring lines and fenders.

2.2.4 Physical model results

Wave conditions

A total number of 15 wave conditions were tested in the physical model, see Table 2-3. Waves were generated perpendicular to the wave maker paddles without directional spreading using a standard JONSWAP spectrum with 2nd order wave steering (see also section 2.2.2).

T_p [sec]	d=16 [m]	d=18 [m]	d=20 [m]
10	√	√	√
12	√	√	√
14	√	√	√
16	√	√	√
18	√	√	√

Table 2-3: Tested wave conditions.

Measurements

During the 2nd phase of the physical model tests the following aspects were measured:

- Surface elevations of waves by 7 resistance wave gauges, without presence of the ship for a simulation duration of 2~3 hours (in prototype time).
- Ship motions, tracked by an infrared motion capture system (*Qualisys system*).
- Mooring lines and fender forces by a total of 8+2 force transducers, see Figure 2-12.

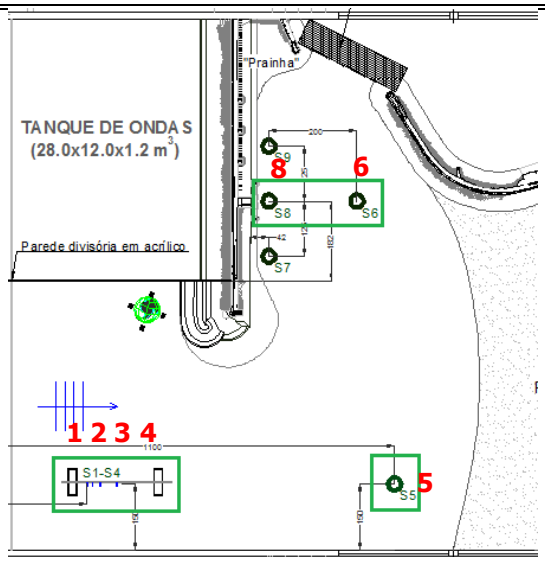

Locations of wave gauges.

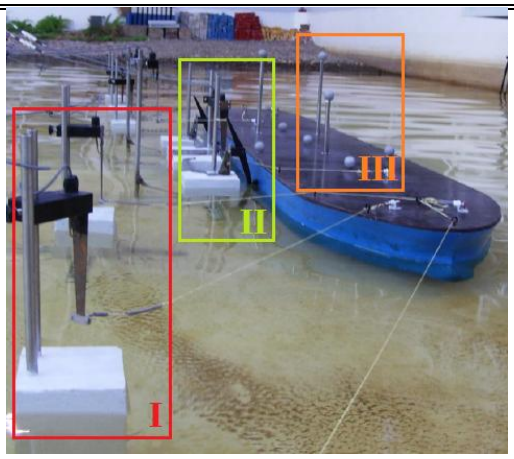

Moored ship measurements
I: Force transducer mooring lines.
II: Force transducer fenders.
III: Infrared ship motion capture system .

Figure 2-12: Measurements in physical model.

Conclusions

A brief overview of the conclusions from the physical model tests will be presented in this thesis, for more details one is further referred to Rosa-Santos *et al.* (2008A, 2008B, 2009 and 2010).
From the physical model tests it was concluded that:

- Modification of the berthing lay-out by relocating a headline had a negligible influence on the ship motions.
- Increasing the breast lines pretension effectively reduces the moored ship motions, especially in combination with high friction fenders.
- The tidal level is an important factor to control the behaviour of the moored ship. The ships added inertia as well as damping increases with decreasing water depth, but the increase of low frequency wave energy with decreasing water depth leads to a worsening of moored ship responses.

Relevant measurements from physical model tests can be found in Appendix B.

2.3 Relevant physics

2.3.1 Wave forcing

Waves can be classified into several groups. For a moored ship the most relevant waves are short waves (periods of 5~20 seconds) and infra-gravity waves (periods of 25~300 seconds), see section 2.3.3, section 2.3.4 and Figure 2-13. At the ocean free infra-gravity waves may be generated due to e.g. seismic activity and storm surges. These waves are for this study not relevant. Relevant is the forced bound long wave (also referred to as set-down wave) that propagates with the primary waves at the scale of wave groups, see Figure 2-14 and e.g. Longuet-Higgins and Stewart (1962).

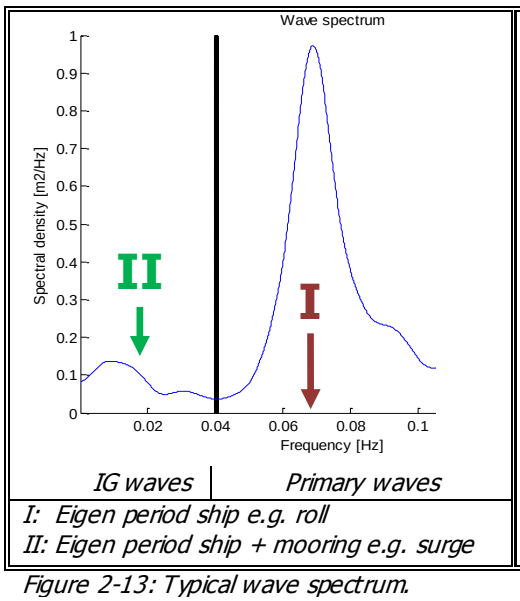

Figure 2-13: Typical wave spectrum.

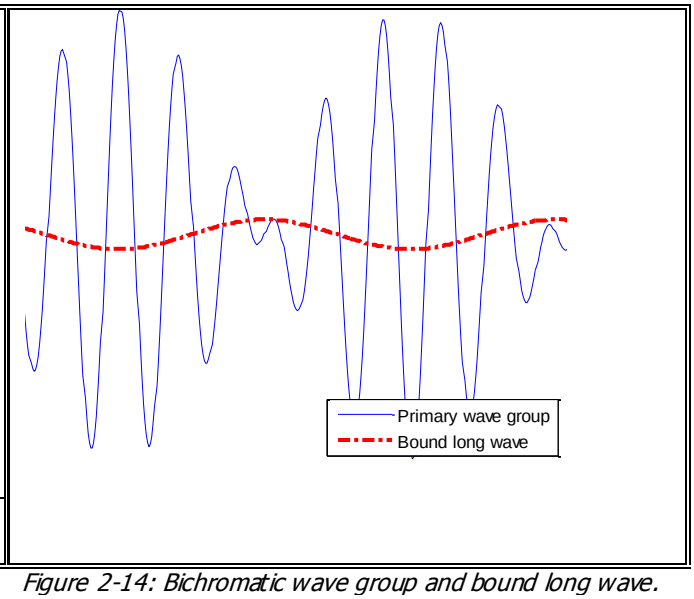

Figure 2-14: Bichromatic wave group and bound long wave.

Bound long waves release as free long waves after wave breaking of the primary waves. Wave breaking at a shoreline occurs in the surfzone, where the bound long wave reflects as a free wave from the shoreline. In case the angle of incidence and the shore normal is small, the reflected free wave may leak from the surfzone to deeper water (also referred to as leaky waves). In case the angle of incidence and the shore normal is large the reflected waves may be trapped in the surfzone due to depth refraction (also referred to as edge waves). The total motion due to incoming and outgoing long waves is also referred to as surfbeat, see Figure 2-15. Discontinuities in either bathymetry or geometry may release free long waves as well, see e.g. Bowers (1977). The amount of bound long wave energy depends on the local wave field and water depth, whereas the amount of free long wave energy depends on the surrounding shelf and nearby shores, see Herbers *et al.* (1994).

The main difference between a bound long wave and a free long wave is the propagation speed of the waves and the shoaling ratio. The wave celerity of both bound long wave and free long waves are given by Eq. 2-2 and Eq. 2-1 respectively. Bound long waves travel with the speed of wave groups, whereas free long waves travel with the speed of individual waves according to the linear dispersion relationship.

$$c_{free} = \frac{\omega}{k} = \sqrt{\frac{g}{k}\tanh(kd)} \qquad \text{Eq. 2-1}$$

$$c_{bound} = \frac{\Delta\omega}{\Delta k} = \frac{\partial\omega}{\partial k} = nc_{free} = \frac{1}{2}\left(1+\frac{2kd}{\sinh(2kd)}\right)\sqrt{\frac{g}{k}\tanh(kd)} \qquad \text{Eq. 2-2}$$

In which:

g	=	Gravitational acceleration	[ms^{-2}]
d	=	Water depth	[m]
k	=	Wave number	[m^{-1}]
ω	=	Wave frequency	[s^{-1}]
c	=	Wave celerity	[ms^{-1}]
n	=	Ratio between group celerity and higher phase celerity	[-]

Another important difference between bound long waves and free long waves is the shoaling ratio when long waves enter shallower areas.

Free long waves shoal according to Green's law: $\zeta \propto d^{-0.25}$.

Bound long waves shoal, depending on the slope, between $d^{-0.25} < \zeta < d^{-2.5}$.

In which:

ζ = Wave amplitude [m]

The existence of infra-gravity waves is supported by theories, field observations and experiments. For more detail one is referred to (amongst others): Baldock *et al.* (2000 and 2002), Battjes *et al.* (2004), Gallagher (1971), Herbers *et al.* (1994,1995A and 1995B), Huntley *et al.* (1981), Longuet-Higgins and Stewart (1962), Munk (1949), Sand (1982), Schäffer (1993), Symonds *et al.* (1982) and Tucker (1950).

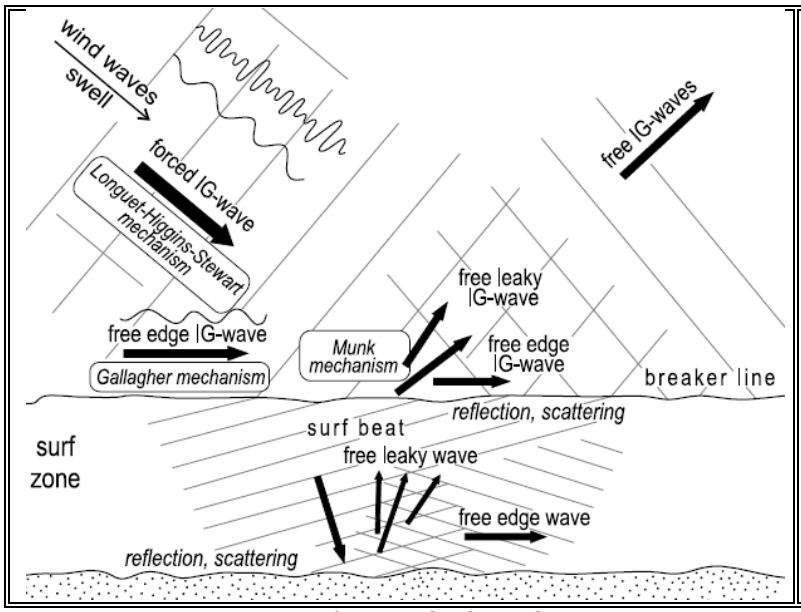

Figure 2-15: Generation mechanisms for free infra-gravity waves at the shoreline. Source: Rabinovich (2009).

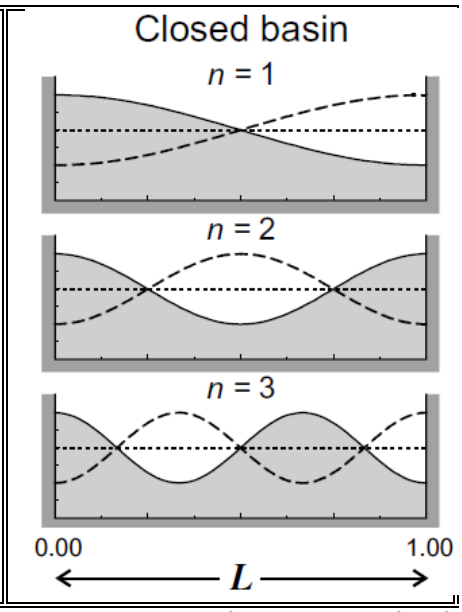

Figure 2-16: Standing waves in closed basins. Source: Rabinovich (2009).

2.3.2 Harbour oscillations

Although the amplitudes of long waves are of the order of centimetres they are important in harbours. The amplitude of the infragravity waves increases with decreasing water depth in harbours and may cause harbour oscillations. Because the frequency of infragravity waves is close to the eigen periods of ship and mooring system, large horizontal moored ship motion responses are expected. Bowers (1977), showed that differences in wave height in and outside a harbour entrance causes an imbalance in bound long waves. The imbalance in bound long waves causes the generation of free long waves. Bound long wave energy is thus partly released as free long waves, which may amplify in case of basin resonance. A visualisation of the generation of free long waves due to a discontinuity in the bathymetry is given in Figure 2-17.
Alternative analytical solutions of harbour resonance for simplified configurations are made by Mei and Agnon (1989) and Wu and Liu (1990). When harbour configurations become complex, distinct numerical or physical models may be used to investigate harbour resonance. Many numerical models are available to simulate harbour oscillations. Woo and Liu (2004) showed that Boussinesq-type wave models are able to describe the set-down beneath wave groups and can be used to investigate harbour resonance under influence of ocean waves.

When the length of the wave equals the basin length a standing wave may develop, see Figure 2-16. These standing waves can be recognized as local maxima in the infra-gravity wave spectrum at the eigen frequencies of the basin. This local maximum is more pronounced when measured in an anti-node of the standing wave. For rectangular basins with an uniform depth the eigen period of a closed basin can be approximated with the well known Merian's formula (Eq. 2-4), whereas Eq. 2-3 should be applied for open basins (in that case the 0-th mode is the well known Helmholtz mode). For approximations of eigen periods for other harbour configurations one is referred to Rabinovich (2009).

Open basins: $$T_n = \frac{4L}{(2n+1)\sqrt{gd}} \qquad n = 0,1,2,3... \qquad \textit{Eq. 2-3}$$

Closed basins: $$T_n = \frac{2L}{n\sqrt{gd}} \qquad n = 1,2,3... \qquad \textit{Eq. 2-4}$$

In which:

T_n	=	Eigen period of oscillation	[s]
L	=	Basin length	[m]
n	=	Mode number	[-]

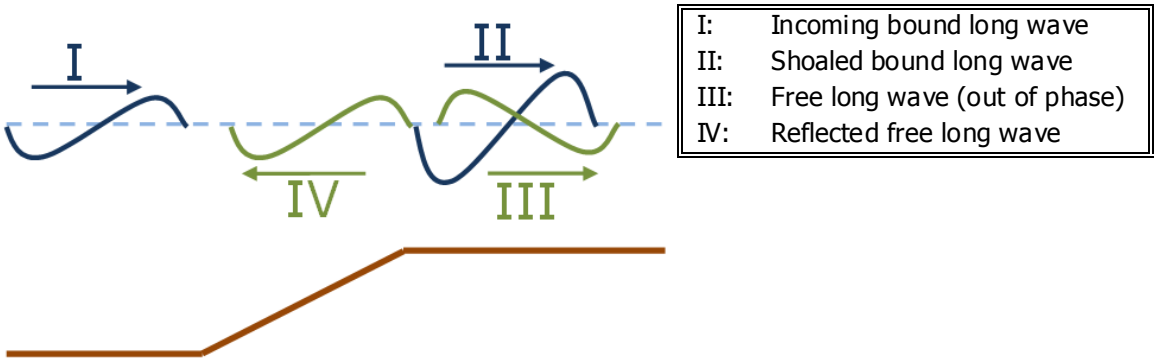

Figure 2-17: Generation mechanisms for free infra-gravity waves due to discontinuity in bathymetry

2.3.3 Ship motions in infragravity waves

Although the amplitude of long waves in harbours are of the order of centimeters they may cause large moored ship responses. Damping in the horizontal plane of a moored ship at the eigen frequency of both ship and mooring system is low. Infra-gravity waves have frequencies close to the eigen periods of ship and mooring system in the horizontal plane. These infra-gravity waves may cause harbour oscillations resulting in standing wave patterns. The resulting ship motions in the horizontal plane are mainly depending on whether the moored ship is placed in a node or an anti-node of the standing wave, see Figure 2-18.

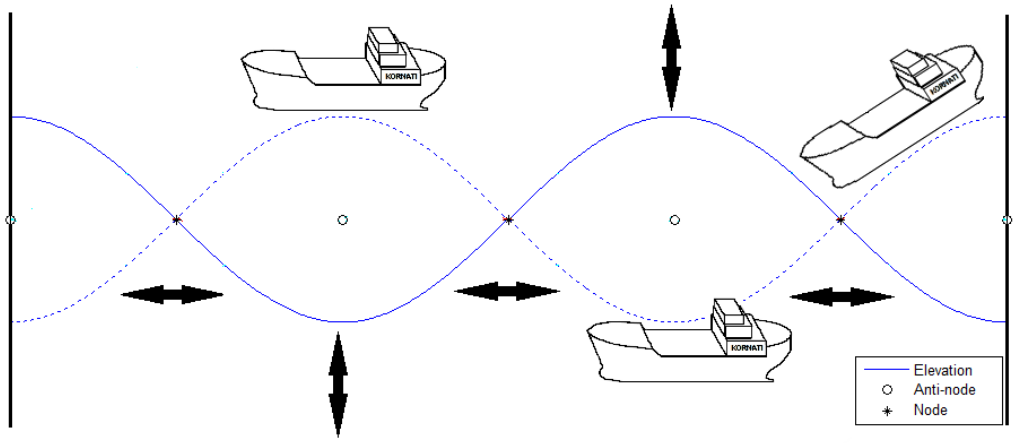

Figure 2-18: Ship motions in standing waves.

Ship placed in a node:

- The orbital velocity of the standing wave is horizontally directed, whereas the surface elevation of the standing wave is zero.
- As a result of the horizontal velocities drag forces are acting on the ship. The ship responds by a surge motion.
- Due to the gradient in the surface elevation the ship will make a pitch movement. The pitching motion may result in surge motions of the ship.

Ship is placed in an anti-node:

- The orbital velocity of the standing wave is vertically directed, whereas the surface elevation of the standing wave is maximal.
- The wave forces on the ship are vertically directed.
- The ship responds by a heave motion.

Many harbour configurations are more complex than the illustrated example in Figure 2-18. In order to describe moored ship behaviour in a harbour configuration it is important to take standing waves into account.

2.3.4 Mooring arrangement of an oil tanker

A moored oil tanker is subjected to several environmental forces like: wind, currents, tide, seiches, swell, waves, changes in draft or trim, surges from passing ships and ice. The motions of a moored oil tanker are characterized by low frequency (periods ~ 1 to 2 minutes) horizontal motions: surge, sway and yaw and high frequency (periods ~ 5 to 20 seconds) vertical motions: heave, roll and pitch. The efficiency and security during berth operations in case of a moored oil tanker are mainly depending on the ship motions in the horizontal plane (surge, sway and yaw). These motions can be effectively restrained by the mooring arrangement. Motions in the vertical plane of the oil tanker are less dependent on the mooring arrangement (in case of vertical motions the restoring forces are due to buoyancy). A typical mooring arrangement for oil tankers consists of mooring dolphins (for stern- and headlines) and breasting dolphins (for the breast and spring lines). A typical mooring arrangement is given in Figure 2-19 whereas the governing line names are given in Table 2-4.

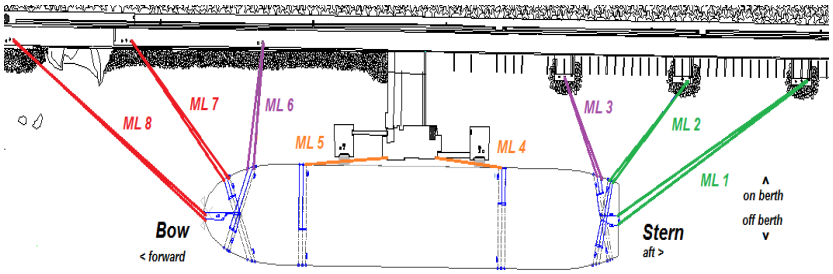

Figure 2-19: Typical mooring arrangement.

Line	*Colour*	*Name*
ML 1	Green	Stern
ML 2	Green	Stern
ML 3	Purple	Breast
ML 4	Orange	Spring
ML 5	Orange	Spring
ML 6	Purple	Breast
ML 7	Red	Head
ML 8	Red	Head

Table 2-4: Mooring lines.

General recommendations for effective mooring of oil tankers are given by OCIMF (2008). Based on the recommendations given by OCIMF an asymmetrical as well as a symmetrical mooring arrangement is investigated during physical model tests. The general recommendations for safe and efficient mooring of oil tankers will not be given in this thesis, one is referred to the given reference.

In order to guarantee safe working conditions when a ship is moored, criteria for the ship motions are set. These criteria are set to avoid or minimize accidents with line breaking. When the criteria are exceeded the cargo handling operations should be slowed down or stopped. In extreme conditions the ship should leave the berth. The most common applied criteria for oil tankers are given by PIANC (1995) and can be found in Table 2-5.

Degree of freedom:	Heave [m]	Surge [m]	Sway [m]	Roll [^{0}]	Yaw [^{0}]
	1.5	2.5	2	4	2

Table 2-5: Maximum allowable motions amplitudes for a moored oil tanker. Source: PIANC (1995)

3 Physical model analysis

3.1 Hydrodynamic processes

The main hydrodynamic processes which occur in the physical model are:

- Diffraction
- Refraction
- Shoaling
- Reflection
- Non-linear wave interaction

Diffraction of waves takes place at the Leixões North breakwater. Refraction causes waves to bend towards shallower depth contours (e.g. beaches and breakwaters). Shoaling of waves will mainly occur at the beach. Reflected waves are expected from the model boundaries e.g. breakwaters, beaches and side walls. For an explanation of theses basics wave processes one is referred to Bosboom and Stive (2010) and Holthuijsen (2007).
Non-linear wave interaction will occur in the entire model basin creating both sub- and super-harmonics. The generated bound long waves from the wave maker may release as free waves from beaches and breakwaters. Release of free waves may also be caused by discontinuties in the bathymetry, which is particulary relevant for waves that diffract around the head of the breakwater.

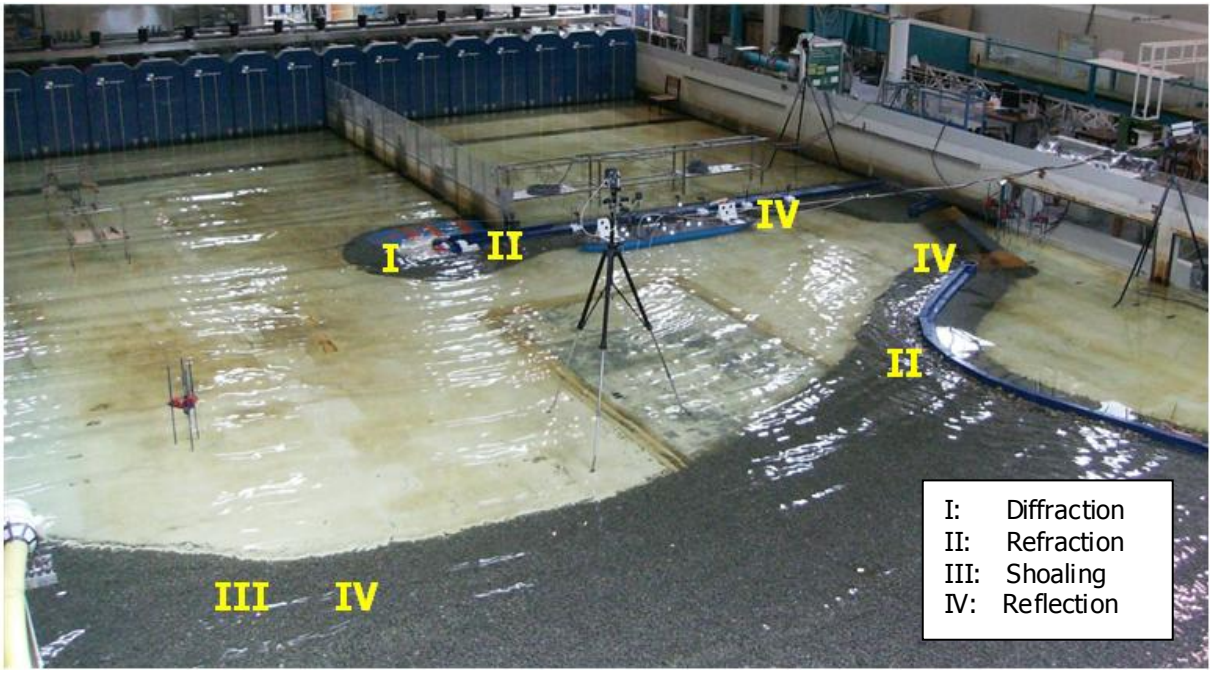

Figure 3-1: Hydrodynamic processes in physical model basin.

3.2 Analysis of measurements

After obtaining a time-serie of wave surface elevations a wave spectrum can be obtained by means of a Fast Fourier Transformation (FFT) analysis, see e.g. Holthuijsen (2007). The FFT is used to obtain the amplitude, phase and frequency of wave components in the timeserie. The spectral density per frequency obtained after FFT is divided over a number of frequency bins. Some smoothing to present the wave spectra is often used. As a result of smoothing some detail may be lost. In this thesis the presented wave spectra are based on a smoothing technique, for which the spectral shape and total wave height is retained, see Van der Molen (2010). By selecting a constant smoothing factor for all time-series the spectra can be compared directly, see Figure 3-2.

A high level of detail in the low frequency spectrum is useful to recognize possible standing waves and/or spurious basin resonance. These standing waves and/or basin resonance may affect the ship motions, see section 2.3. Analysis of the wave spectra for all wave conditions at wave probe 6 and 8 (vicinity of the ship), showed a local peak at a frequency of 0.006Hz, see Figure 3-3 and Figure 3-4.

In the case of small smoothing the spectrum looks "grassy" and the error (defined as the difference between the expected value and computed value) is relatively large. In order to obtain a more reliable wave spectrum the spectral resolution decreases. A compromise should be found between spectral resolution and acceptable reliability. One method to obtain a compromise between spectral resolution and acceptable reliability is quasi-ensemble averaging, see also Holthuijsen (2007). Quantifying the reliability of the wave spectra in terms of confidence intervals is not made during this study.

For illustration of the errors made in spectral density the following example may be used:
A wave record with a measured duration of 2.5hour has a frequency resolution of $\Delta f = 0.000111$Hz. Averaging the spectral density over larger frequency bins for example $\delta f = 0.00125$Hz gives an absolute error in spectral density of:

$$\frac{100\%}{\sqrt{0.00125/0.000111}} \approx 8.9\%$$

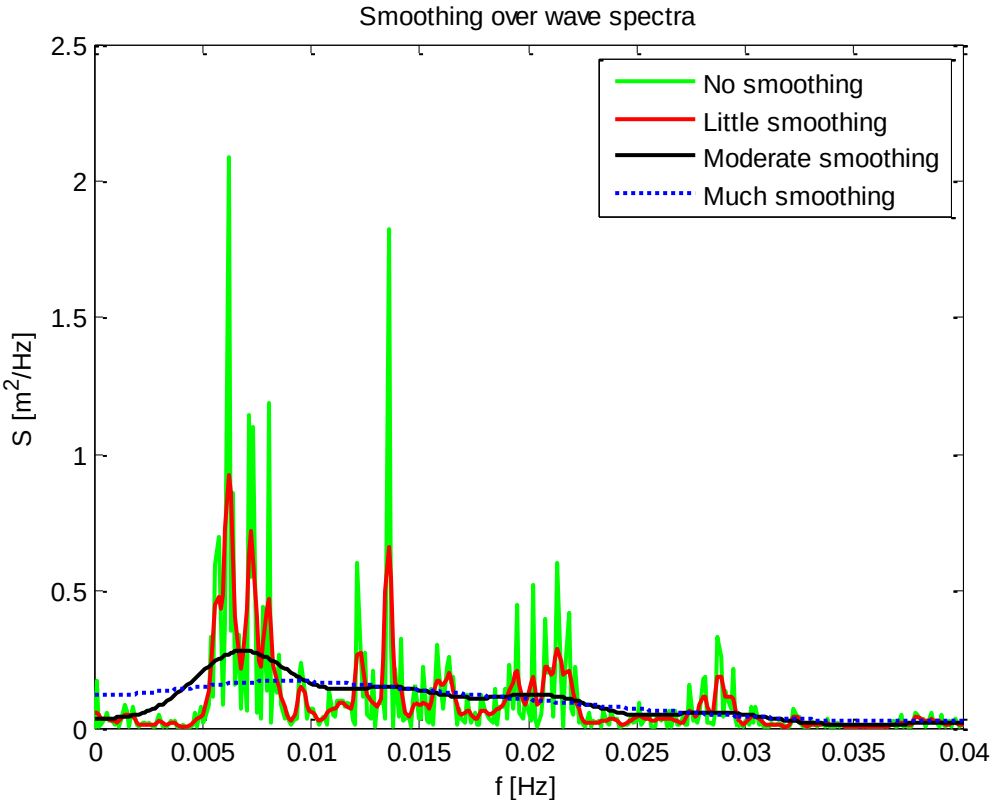

Figure 3-2: Smoothing over wave spectra

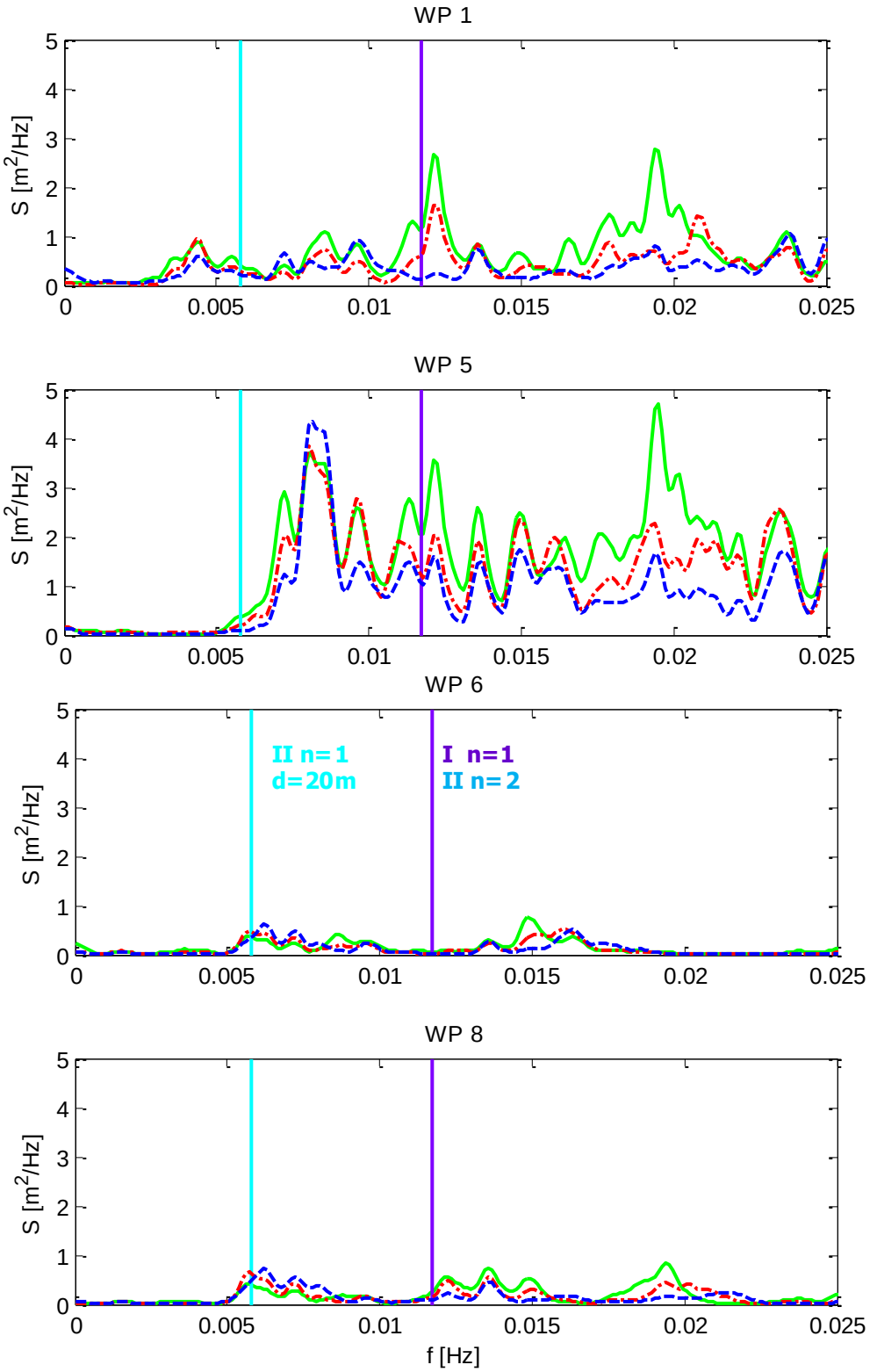

Figure 3-3: Measured wave spectra.
With constant smoothing.
Tidal level: d= 16, 18 and 20 [m].
Peak period: T_p=14 [sec].

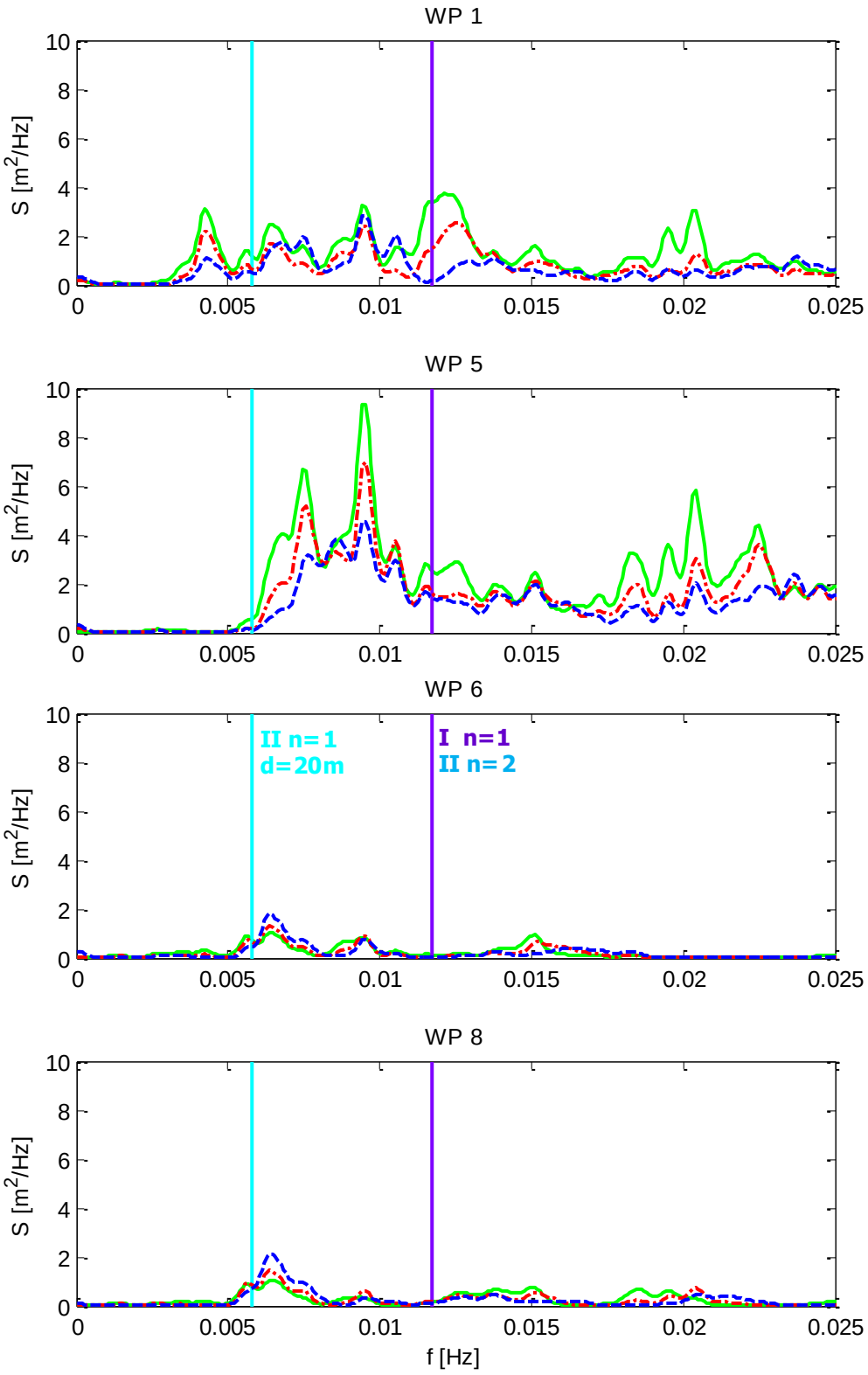

Figure 3-4: Measured wave spectra.
With constant smoothing.
Tidal level: d = 16, 18 and 20 [m].
Peak period: T_p=18 [sec].

Eigen periods

Within the physical model spurious standing waves can be generated. Basin resonance is expected when the basin length corresponds to a multiple of the wavelength, see Figure 2-16.
Three possible areas for standing waves are distinguished:

- Area I: Between wave guide wall and side wall = 600 meter.
- Area II: Between side wall and side wall = 1200 meter.
- Area III: From wave maker to absorbent beach ≈ 2000 meter.

The eigen periods for harbour oscillations can be approximated by applying Eq. 2-4 for the distinguished areas, see Figure 3-5. The eigen periods are presented in Table 3-1, whereas the corresponding eigen frequencies are presented in Table 3-2.

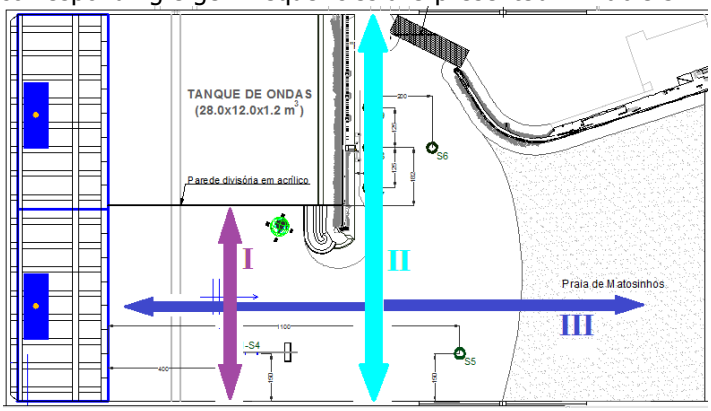

Figure 3-5: Distinguished areas for calculation eigen periods.

n	I (d=20m)	II (d=20m)	III (d=20m)
1	85.7 [sec]	171.3 [sec]	285.6 [sec]
2	42.8 [sec]	85.7 [sec]	142.8 [sec]
3	28.6 [sec]	57.1 [sec]	95.2 [sec]

Table 3-1: Calculated eigen periods

n	I (d=20m)	II (d=20m)	III (d=20m)
1	0.0117 [Hz]	0.0058 [Hz]	0.0035 [Hz]
2	0.0234 [Hz]	0.0117 [Hz]	0.0070 [Hz]
3	0.0350 [Hz]	0.0175 [Hz]	0.0105 [Hz]

Table 3-2: Calculated eigen frequencies

The peak at 0.006Hz is noticed at wave gauge 1 to 4, but not pronounced. Possibly a standing wave is formed between both side walls of the physical model, since the calculated eigen frequency is close to the frequency of the found peak (see, Figure 3-3 and Figure 3-4). This standing wave cannot exist at wave gauge 1 to 4, since the basin length at those gauges is different. At wave probe 1 a peak is noticed at a frequency of 0.0117Hz, which is possibly a standing wave between the wave guide wall and the side wall of the basin.
Assuming that a transverse standing wave is measured in the basin this may explain part of the enhancement of measured wave energy at wave probe 5. At wave probe 6 and 8 the measured low frequency energy is less compared to wave probe 5, this is probably because these probes are placed closed to a node. Wave gauge 5 is placed in an anti-node at which the amplitude of the standing wave and hence the spectral density is higher. This presumption is endorsed by the measured ship motions where both surge and pitch motions do show similar trends, see Figure 3-6. Local peaks at the same frequencies can be found in the spectra of heave, pitch, spring lines, stern lines and head lines, see Appendix B.
Other resonant mechanisms in the physical model may well exist. An alternative resonant mechanism with resemblance in prototype is given in Appendix E. From this study and/or report no conclusion can be withdrawn which resonant mechanism was dominant to find the corresponding measured surge responses of the ship.

3.3 Summary of physical model analysis

- From an analysis of the available measured data it is observed that there is an enhancement of low frequency energy in the vicinity of the ship at frequencies around 0.006Hz.
- This frequency is close to an eigen period of the physical model basin.
- Possibly a transverse standing wave is measured.
- The existence of a transverse standing wave may explain some resulting ship motions.

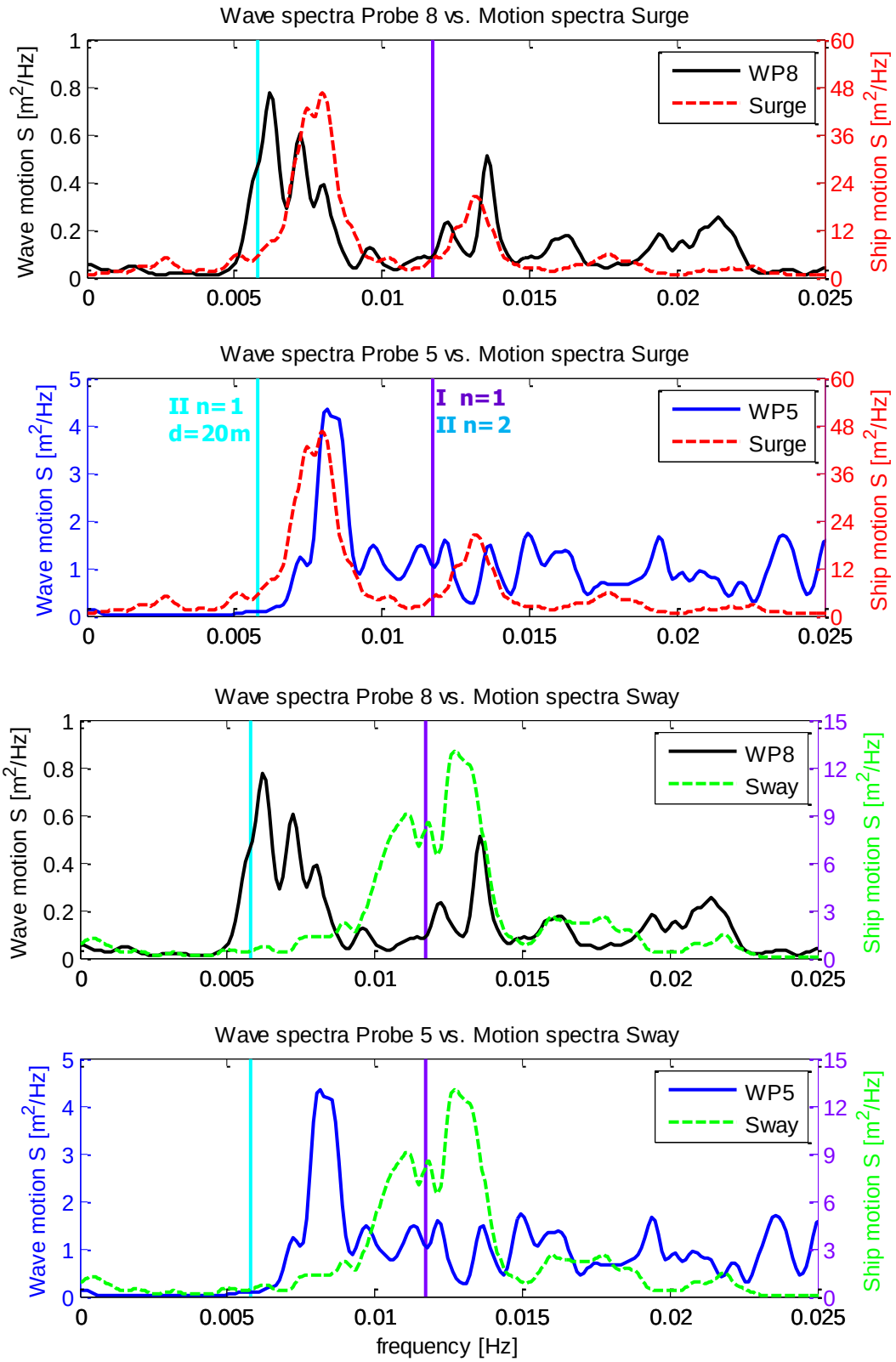

Figure 3-6: Measured wave and ship motion spectra.
With constant smoothing.
Tidal level: d = 20 [m].
Peak period: T_p=14 [sec].
Two different vertical axis.

4 Research methodology

4.1 Methodology

When a ship is moored at an open jetty in deep water at a non-sloping seabed it is possible to describe the motions and mooring forces with a ship simulation model and a deep water wave spectrum only. In case of complex harbour lay-outs with a shoreline close by, coastal processes and reflections from port structures need to be included. Based on the work of Van der Molen (2006B) two different numerical approaches can be used to describe moored ship behaviour within ports. The approach which combines a Boussinesq-type wave model with a panel model was selected as the appropriate approach for the present study, since:

- Diffraction of waves is important.
- Partial reflection of waves from beaches and especially port structures needs to be included.
- Non-linear wave processes need to be included.

By coupling a Boussinesq-type wave model, a panel model and a ship simulation model moored ship behaviour in a port can be simulated. The proposed flow diagram for moored ship behaviour in ports is given in Figure 4-1. Summarized, the three successive models are used to:

- The Boussinesq-type wave model takes into account the propagation of ocean waves into the harbour.
- The panel model takes into account the presence of the ship in the wave field at the berth and subsequently calculates the wave forces on the ship.
- The ship simulation model calculates ship motions and mooring forces, taking into account environmental forces and interactions with the mooring system.

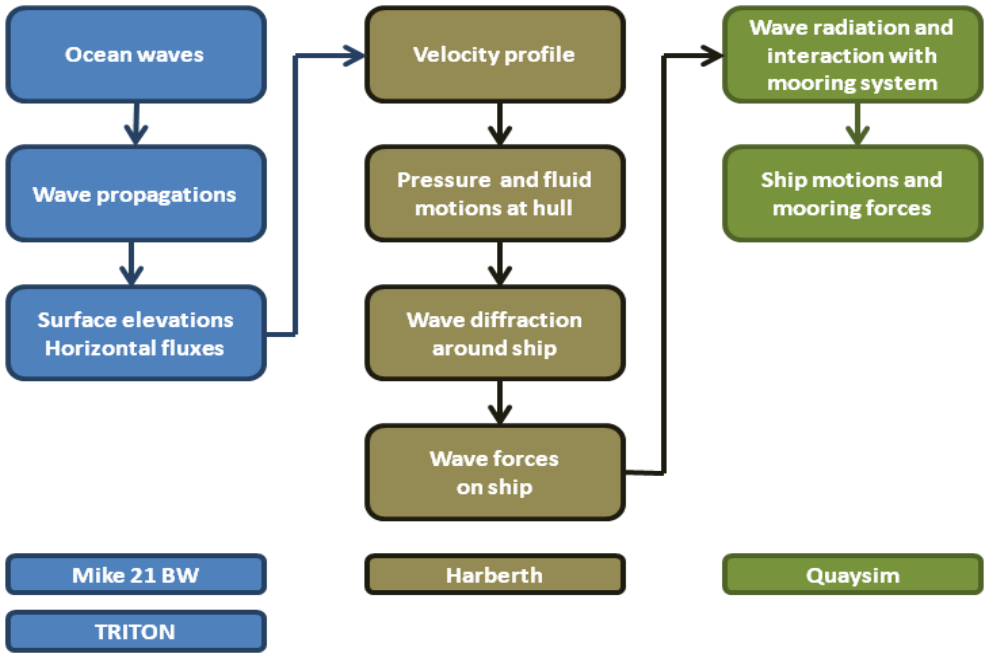

Figure 4-1: Proposed coupling of numerical models to described moored ship behaviour within ports. Source: Van der Molen 2006A (adapted).

4.2 Description of the Boussinesq-type wave models

The numerical models used to calculate the propagation of ocean waves into the harbour are the Boussinesq-type wave models MIKE21 BW and TRITON. In this section general information about the models is given, for more detail and formulations one is referred to DHI (2005, 2006A and 2006B) in case of MIKE21 BW and Borsboom *et al.* (2000) + Deltares (2008) for TRITON.
Making a detailed comparison between both Boussinesq wave models is not the purpose of this thesis and is therefore not done. A general comparison between both models is given in section 4.2.3.

General principles of the applied Boussinesq-type wave models

- Boussinesq-type wave models are phase resolving, they describe individual wave behaviour.
- Within the Boussinesq-type wave model the 3D flow is written in 2D equations.
- The Boussinesq-type wave models are capable of reproducing the most important wave phenomena like: shoaling, refraction, diffraction, wave breaking, bottom dissipation, moving shoreline (run-up and run-down), partial reflection, wave transmission, non-linear wave-wave interactions, frequency spreading and directional spreading.

4.2.1 MIKE21 BW

MIKE21 BW is part of the package MIKE21 from DHI and is successfully applied in several wave modelling propagation studies for coastal areas. MIKE21 BW solves the time-dependent vertically integrated Boussinsesq equations of mass and momentum. The Boussinesq-type equations are solved using a flux-formulation with improved frequency dispersion characteristics (see Madsen *et al.* 1991, 1992, 1997A and 1997B).

MIKE21 BW is restricted to the following conditions:

- In case of enhanced equations: linear frequency dispersion up to $\mu = k_p d < 3.1$.
- In case of classical Boussinesq equations: linear frequency dispersion up to $\mu = k_p d < 1.4$.

In which:

μ	=	measure of linear dispersion	[-]
k_p	=	wave number belonging to the peak wave period	[m^{-1}]

Program structure

For correct modelling of waves in MIKE21 BW at least the following need to be defined:

- Bathymetry: Up to a predefined minimum water depth.
- Sponge layers: For the absorption of short waves along model boundaries e.g. beaches. A wider sponge layer should be selected if longer waves should be absorbed as well.
- Porosity layers: these layers are applied at breakwaters and walls to model wave transmission and partial reflections. The porosity value is depending on the wave height and period, water depth in front of the structure and the reflection coefficient of the structure.
- Wave generation: Waves are generated at an internal wave generation line. The wave generation line serves as an internal source for the generation of waves. A sponge layer after the wave generation line is usually applied. This sponge layer absorbs the outgoing waves, as well as the radiated waves from the internal wave generation line.

4.2.2 TRITON

TRITON is a Boussinesq-type wave model from Deltares. TRITON is in development and for that reason not yet commercially available. Although in development, TRITON is able to model wave propagation up to the following restrictions:

- Linear frequency dispersion up to $\mu = k_p d < 4$.
- Non-linear effects up to $\varepsilon = ad^{-1} < 0.25$.
- Non-linear effects up to $\varepsilon\mu^2 < 0.25$.
- Wave shoaling up to $\mu\mu_s \approx 0.5$.

In which:

ε	=	Measure for the non-linearity of waves	[-]
a	=	Wave amplitude	[m]
μ_s	=	$\{k_p L_{bottom,p}\}^{-1}$	[-]
k_p	=	Representative wave number	[m^{-1}]
$L_{bottom,p}$	=	Typical horizontal length scale over which bottom changes take place	[m]

Program structure

TRITON uses three modules:

- TriGrid: computational grid and model boundaries.
- TriBath: create depth file such that each computational grid point has a certain depth.
- TriGui: defining the boundary conditions and output locations.

Within TRITON the following boundary conditions can be used:

- Closed: in case of closed boundaries or full reflecting walls.
- Partial: in case of partial reflecting walls.
- Outflow: in case of zero reflecting walls.
- Monochromatic: for the generation of monochromatic waves.
- Spectrum: for defining a wave spectrum from which a time-serie is made.
- Time-serie: for defining a time-serie.

4.2.3 Comparison MIKE21 BW and TRITON

Based on the model equations which are solved by the models MIKE21 BW and TRITON, it can be concluded that both models have the same order of accuracy and can therefore be applied for the same range of applications. The main difference between MIKE21BW and TRITON is the inclusion and treatment of the boundary conditions along the harbour structures and internal wave generation.

MIKE21 BW uses sponge and porosity layers to include physical processes as wave energy dissipation and partial reflection transmission, see Madsen (1983). Wave generation is done by an internal wave generation line, see Schäffer and Sørenson (2006). TRITON does not use sponge or porosity layers, nor a internal wave generation line backed up by a sponge layer. The model is equipped with a absorbing boundary procedure, which adapts based on the local wave field, see Borsboom *et al.* (2000 and 2001). Properties of waves, reflected off structures, are based on a typical celerity and direction of the outgoing wave. Within TRITON mass and momentum are strictly conserved. Although several model approximations are made, these physical properties are retained.

The main difference between MIKE21 BW and TRITON is in the applied numerical techniques to solve the boundary conditions, on which an illustration is given in Figure 4-2. Besides the differences in techniques used at the model boundaries, different numerical schemes are used to solve the equations. The (dis)advantages of these schemes for e.g. the robustness of the numerical models are not investigated.

It should be remarked that there is no standard option to include a theoretical bound long wave in the wave generation in MIKE21 BW. A theoretical bound long wave can however be imposed in the generated waves within TRITON.

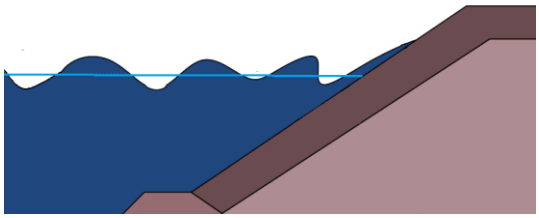

Physical model

Bathymetry and reflection are determined as accurate as possible by scaling. The reflection coefficient of the breakwater is determined based on physical model tests.

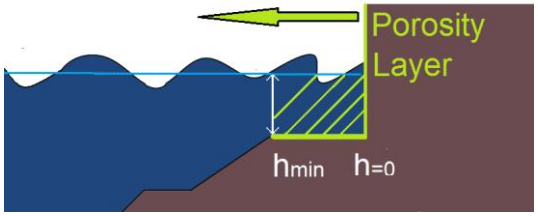

MIKE21 BW

Bathymetry defined to h_{min}. From h_{min} to the water line the water depth is kept constant at h_{min}.
A porosity layer is defined which is build out from the water line. The defined porosity value is depending on H, T and Cr. The width of the layer is determined based on the wave length.

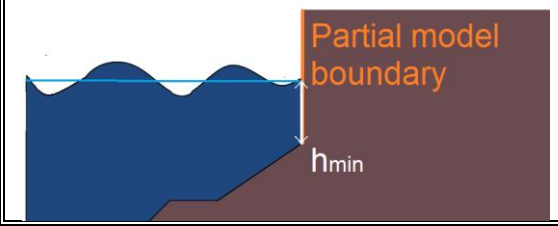

TRITON

Bathymetry is defined for the full domain, but the user may define a h_{min} and apply a partial model boundary condition. The partial boundary condition is selected on Cr only. The boundary condition procedure calculates the reflected wave.

Figure 4-2: Inclusion of partial boundary conditions.

Remarks

- In both Boussinesq-type wave models it is not possible to include partial reflection coefficients as a function of the wave frequency. Partial reflection should be modelled correctly for waves with a period corresponding to the peak period of the waves.
- Recent research by De Jong *et al.* (2009) showed that, in particular situations, bound long wave energy in TRITON is underestimated compared to theoretical values, see Figure 4-3. Recently improvements are made, see De Jong *et al.* (2011), but these were not included in these simulations yet. For long primary waves periods and relatively shallow water conditions, the bound long waves are however described with sufficient accuracy. The range for which the bound long waves are sufficiently well described was defined as $kd < 0.5-1.0$. The criterion to accurately describe the bound long waves is thus more strict than the criterion for the primary waves. For the tested wave conditions in the physical model the bound long waves are, according to this criterion, described with sufficient accuracy.
- Criteria for accurately describing bound long waves in MIKE21 BW are unknown. In Madsen and Sørenson (1993) a comparison between non-linear effects and theoretical values, according to Stokes theories are given, but only for super-harmonics. It is stated that the accuracy of modelling super-harmonics is not depending on selecting the enhanced equations (i.e. irrespective of the B value in case of the enhanced equations). In both Madsen and Sørenson (1993) and Sørenson *et al.* (2004) it is stated that the enhanced Boussinesq equations tend to underestimate energy transfer to super-harmonics, but statements about energy transfer to sub-harmonics are not given.

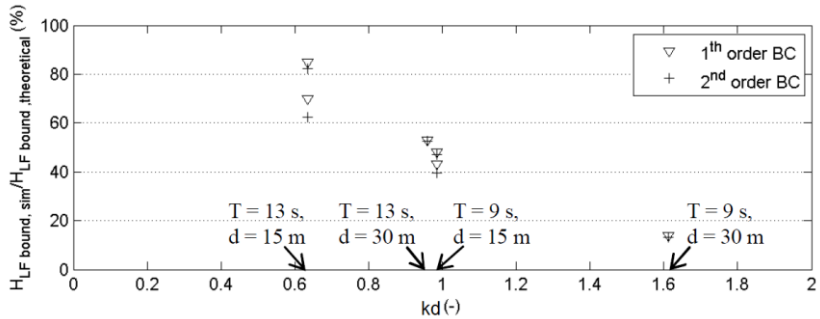

Figure 4-3:Bound long wave height in TRITON.
Comparison with theoretical values for different kd values. Source: De Jong et al. (2009)

4.3 Description of the 3D panel model

The numerical model used to compute the forces on the ship in the irregular and inhomogeneous wave field is the 3D time-domain panel model Harberth. In this section general information about the model is given, for more detail and formulations one is referred to Appendix A and Van der Molen (2006B, 2008 and 2009).

General principles 3D panel model Harberth

- The 3D panel model can be applied on arbitrarily shaped bodies, with a zero mean forward speed.
- The angles of rotation of the ship are assumed to be small (<0.1 radians), such that linearization and superposition of motions can be applied. Since the angles of rotation are small the moored ship can be defined as a linear mass-spring system.
- The resulting motion of the ship in waves may be seen as a superposition of the motion of the body in still water and the forces on the restrained body in waves, see Figure 4-4.
- The oscillation amplitudes of the fluid and the body should be small relative to the cross-sectional dimensions of the body.
- The fluid flow around the ship is assumed to be homogenous, incompressible and irrotational such that it can be described by a velocity potential, Φ . The gradient of the velocity potential is equal to the flow velocity ($u = \frac{\partial \Phi}{\partial x}$, $v = \frac{\partial \Phi}{\partial y}$ and $w = \frac{\partial \Phi}{\partial z}$).
- Due to the use of potential theory, effects of flow separation are neglected.
- The potential flow around the body can be calculated based on the principle of Green's second theorem. According to this theorem the pressures in the volume of water around the ship are transformed in the pressures on the surface of the ship hull. The applied boundary conditions on the computational domain, as well as interaction with port structures in the vicinity of the ship, are considered in the formulation of the Green functions, see Appendix A.
- Within Harberth waves are not considered as the sum of regular wave components, but as a summation of impulsive sources.
- The hydromechanical coefficients (added mass and damping) are calculated in the frequency domain to minimize numerical instabilities (contrary to Van der Molen (2009)).
- The first order free waves do fulfill the linear dispersion relationship in Harberth.

Program structure

Harberth considers the radiation problem (wave due to the moving body in initially still water) and calculates the wave forces due to the incident and scattered wave on the restrained body, see Figure 4-4. The solution of the radiation problem consists of generated waves due to a moving ship. The solution of the radiation problem provides the added mass and damping coefficients for each incident wave direction and wave frequency and is solved in the frequency domain. The matrices serve as an input in the dynamical simulation with Quaysim. The used retardation functions in Harberth were verified against measurements of Van Oortmerssen (1976) and the numerical frequency domain panel model DELFRAC (Pinkster (1995)), see Van der Molen (2006B).
The incident waves to calculate the wave forces on the restrained body are determined with the Boussinesq wave model. The Boussinesq wave model cannot take into account the presence of a ship in the incident wave field, therefore Harberth calculates the scattered and diffracted wave due to the presence of the ship. The output from the Boussinesq-type wave model (MIKE21 BW) consists of the two horizontal depth integrated fluxes (P and Q) and the water surface elevation ζ . Harberth transforms these data to velocities and pressures at the ship hull using an inverse transformation applied to the variables of the original Boussinesq-type wave model equations. The backward transformation of the depth-averaged velocity and pressure is required to obtain the distributions over the water depth. The hull is divided into a large number panels, such that the pressure and velocity at each panel is assumed to be constant. The transformation provides therefore mean values of pressures and velocities at each panel.

Integration of the pressures from the incident waves provides the so called Froude-Krylov force, which is the wave force due to the incident wave. The Froude-Krylov force includes the force due to nonlinearities in the incident wave field (also referred to as the second order force due to the second order potential).

Integration of the pressures from the scattered waves provide the diffraction force and the second order force. Other contributions to the second order force are products of first order quantities and are obtained based on the calculated incident, scattered and radiated waves and the ship motions. The total wave force is given by the summation of the Froude-Krylov, diffraction force and the second order force.

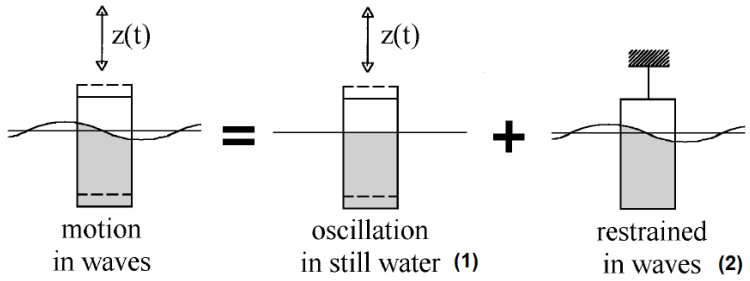

Figure 4-4: Visualization of ship motions in waves. Source: Journée and Massie (2001). Decomposition into the radiation problem (1) and wave exciting motions (2).

Input Harberth

The main input for the simulations in Harberth consists of the following components:

- Ship characteristics and description of the ship hull.
- Positioning of structure (quay wall or breakwater) relative to the ship-bound coordinate system.
- Transmission coefficient ε_t, to include friction and viscous effects between ship and structure, such that partial reflecting walls in the vicinity of the ship can be included. The transmission coefficient ε_t, can be approximated as $1-C_r$, in which C_r is the reflection coefficient as defined in the porosity layer in the MIKE21 BW computations.
- Incident wave file (obtained from Boussinesq-type wave model simulation).

Output Harberth

The main output files of Harberth consists of the following components:

- A hydrodynamic file containing the hydrodynamical coefficients.
- A wave force file containing time series of wave forces.

Remark

The program description for Harberth as given within this thesis is based on a coupling with the Boussinesq-type wave model MIKE21 BW. A coupling between TRITON and Harberth is available and works according to the same principles as described for the coupling MIKE21 BW and Harberth. Besides the coupling with Harberth, TRITON can also be coupled to DELMULTI, see Wenneker *et al.* (2006). DELMULTI calculates time-series of wave forces on a ship and works according to the same principles as Harberth. The diffraction forces in DELMULTI are determined by solving the diffraction problem for all frequencies separately, whereas the diffraction forces in Harberth are calculated using the Haskind relations, see Van der Molen (2008).

4.4 Description of the ship simulation model

The numerical model to compute the ship motions as well as the mooring line and fender forces due to external forces acting on the ship is the ship simulation model Quaysim. Quaysim is a time domain simulation program to analyze the dynamic behaviour of moored ships. In case of moored ship behaviour non-linear restoring forces and wave drift forces fluctuate with respect to time. Linear superposition cannot be applied in this analysis, contrary to frequency domain calculations, therefore a time domain simulation should be applied. Quaysim is based on similar formulations as the ship simulation models Shipmoorings, BAS and Termsim.

General principles ship simulation model Quaysim

- The angles of rotation of the ship are assumed to be small (<0.1 radians), such that linearization and superposition of motions can be applied. Since the angles of rotations are small the moored ship can be defined as a linear mass-spring system.
- The hydromechanical reaction forces and motions, due to time varying ship motions, can be described by using the formulations of Cummins (1962).
- The inertia matrix depends on the mass distribution of the ship. The matrices for added mass, linearized viscous damping, hydrostatic restoring and impulse response functions are determined by Harberth and serve as an input for Quaysim. These matrices are the linear contributions of the hydrodynamic forces due to the moving body.
- The external force may consist of several components, both linear and non-linear. The external force on the ship may be due to waves (including non-linear contributions), currents, wind and interactions with the mooring system. The external forcing due to waves acting on the ship are calculated by Harberth and serve as an input for Quaysim.
- Viscosity effects due to the ship motions are included in the simulations.

The Cummins equation to describe time-varying ship motions is given by:

$$\sum_{j=1}^{6}\{(\boldsymbol{M}_{kj}+\boldsymbol{A}_{kj})\ddot{\vec{X}}_j(t)+\boldsymbol{B}_{kj}\dot{\vec{X}}_j(t)+\boldsymbol{C}_{kj}\vec{X_j}(t)+\int_0^{\infty}\boldsymbol{K}(\tau)_{kj}\dot{\vec{X}}_j(t-\tau)d\tau\}=\vec{F}_k(t) \qquad \textit{Eq. 4-1}$$

In which:

$\boldsymbol{M}$	Inertia matrix
$\boldsymbol{A}$	Added mass matrix
$\boldsymbol{B}$	Linearized viscous damping matrix
$\boldsymbol{C}$	Hydrostatic restoring matrix
$\boldsymbol{K}$	Impulse response functions matrix
$\vec{X}(t)$	Body motion
$\vec{F}(t)$	External force
$j=1\sim 6$	Degree of freedom of the body
$k=1\sim 6$	Coupled degree of freedom of the body

Input Quaysim

- A hydrodynamic file containing the hydrodynamical coefficients.
- A wave force file containing time series of wave forces.
- Ship characteristics.
- Description of mooring system, including mooring line and fender characteristics.

Output Quaysim

- Statistics of ship motions.
- Statistics of mooring line, fender and environmental forces.
- Time series of ship motions.
- Time series of mooring line, fender and environmental forces.

5 Numerical simulations with MIKE21 BW, Harberth and Quaysim

5.1 Wave propagation simulations

5.1.1 Model set-up

General settings

The first step in MIKE21 BW is to decide whether or not the enhanced equations with improved linear frequency dispersion characteristics should be solved. The spatial grid size and time step are more strict when applying the enhanced equations compared to the classical equations and hence the computational time is much larger. According to the included MIKE21 BW model set-up planner a spatial cell grid size of $\Delta x=4$ meter is appropriate for the purposes of wave modelling for this study. The model set-up planner is based on selecting a minimum period for the waves, which should be modelled correctly to a certain defined minimal water depth. Using the linear dispersion relationship for the selected minimum wave period in the minimum water depth gives the shortest wavelength, which can be modelled correctly in MIKE21 BW. Based on a rule of thumb of 20 spatial cell grid points per wave length and applying the linear dispersion relationship a practically smaller spatial grid size would be found. Based on the following considerations a spatial cell grid spacing of $\Delta x=4$ meter was selected as appropriate, since:

- Only waves with a small wave length at the defined minimal water depth are not modelled accurately.
- The ship is located at a water depth which is much larger than the defined minimal water depth.
- Waves with a small wave length are not the cause of excessive ship motions.
- The most energetic short waves and long waves are modelled correctly.
- The numerical phase error for the shortest waves is expected to be small.

A time step of $\Delta t=0,1$ seconds was selected to ensure numerical stability based on the CFL condition. The selected time step is a conservative choice which resulted in a lower computational efficiency.

During all simulations both wave breaking and moving shoreline (run-up and run-down) were excluded. Wave breaking and moving shoreline will increase the computational time and are for the purposes of this study not important. Wave breaking at the beach was avoided due to an applied sponge layer build out from the minimal water depth. The moving shoreline technique, as proposed by Madsen *et al.* (1997B), may introduce some numerical instability problems due to the artificial slot-technique. By excluding the moving shoreline, numerical instability due to this technique is avoided and computational time decreased.

Boundary conditions

Three boundary conditions applied in MIKE21 BW are distinguished:

- Sponge layers.
- Porosity layers.
- Wave generation .

Both porosity and sponge layers are created by the applied MIKE21 tools. A large sponge layer was applied behind the internal wave generation line, which should absorb both the radiated short and long waves from the internal wave generation line. A shorter sponge layer was applied at the beaches, since these layers should only absorb the short waves and reflect the long waves. Porosity layers were designed based on expected wave heights, water depths in front of the structure and reflection coefficients as obtained from physical model tests. The width of the porosity layer (in terms of grid cells) is based on the wave length for the most energetic waves. Several porosity and sponge layers were designed to calibrate and validate the model results. Waves were generated at an internal wave generation line for which a time-serie was designed with the supplied MIKE21 tools. The applied boundary conditions are visualized in Figure 5-1.

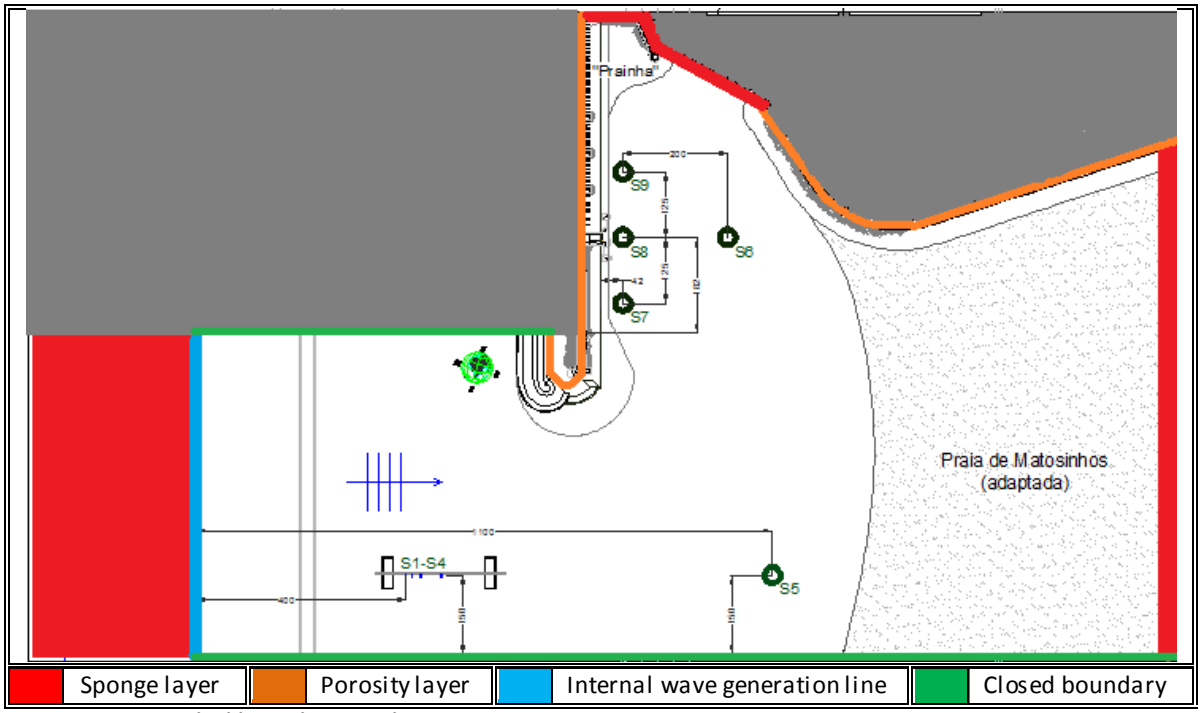

Figure 5-1: Applied boundary conditions in MIKE21 BW.

5.1.2 Model results

During the first simulations the sensitivity of the model was investigated. These simulations were short-term simulations with the purpose of defining the porosity and sponge layers such that a good agreement was obtained between measured and simulated wave spectra.
From the first simulations the following was noticed:

- Shortage of primary wave energy at especially wave gauge 6 and 8 (in the vicinity of the ship).
- Shortage of low frequency energy at all wave gauges.

Applying alternative sponge layers at the beach did not lead to improvement of results. Decreasing the effectiveness of the sponge layer (in order to achieve more reflection from the beach), resulted in an instable model blow-up. In case larger sponge layers are applied at the beach long waves may be absorbed as well. The recommended sponge layers for beaches, according to DHI (2006A), were therefore applied. Applying alternative porosity layers (in terms of length and porosity value) did not have any noticeable effects on the results. In order to obtain more primary wave energy at wave gauge 6 and 8 the head of the breakwater was decreased in size (red striped line in Figure 5-2). In this way the diffraction losses are less and more primary wave energy was simulated at wave gauge 6 and 8 in the vicinity of the ship. The simulated spectrum still gave an underestimation compared to measurements. Since the low frequency waves are more important to obtain ship motions the focus was shifted to overcome the shortage of wave energy at lower frequencies.

The internal generated waves in MIKE21 BW are based on a standard JONSWAP spectrum with a peak period corresponding to the tested wave condition. During the first simulations a significant shortage of simulated low frequency wave energy was noticed at wave gauge 1 to 4. This shortage is due to the fact that MIKE21 BW does not include the wave set-down compensation, which was used during the performed physical model tests. The wave set-down compensation simulates the so-called second order boundary conditions. The shortage of low frequency energy at the internal wave maker in MIKE21 BW was compensated by an extra time-serie which was accompanied with the time-serie of the primary waves. The additional time-serie was based on the measured low frequency spectrum, but contains free long wave energy (blue dashed striped line in Figure 5-2). The additional time-serie may be in phase with the propagating wave groups (instead of out of phase as with a bound long wave).

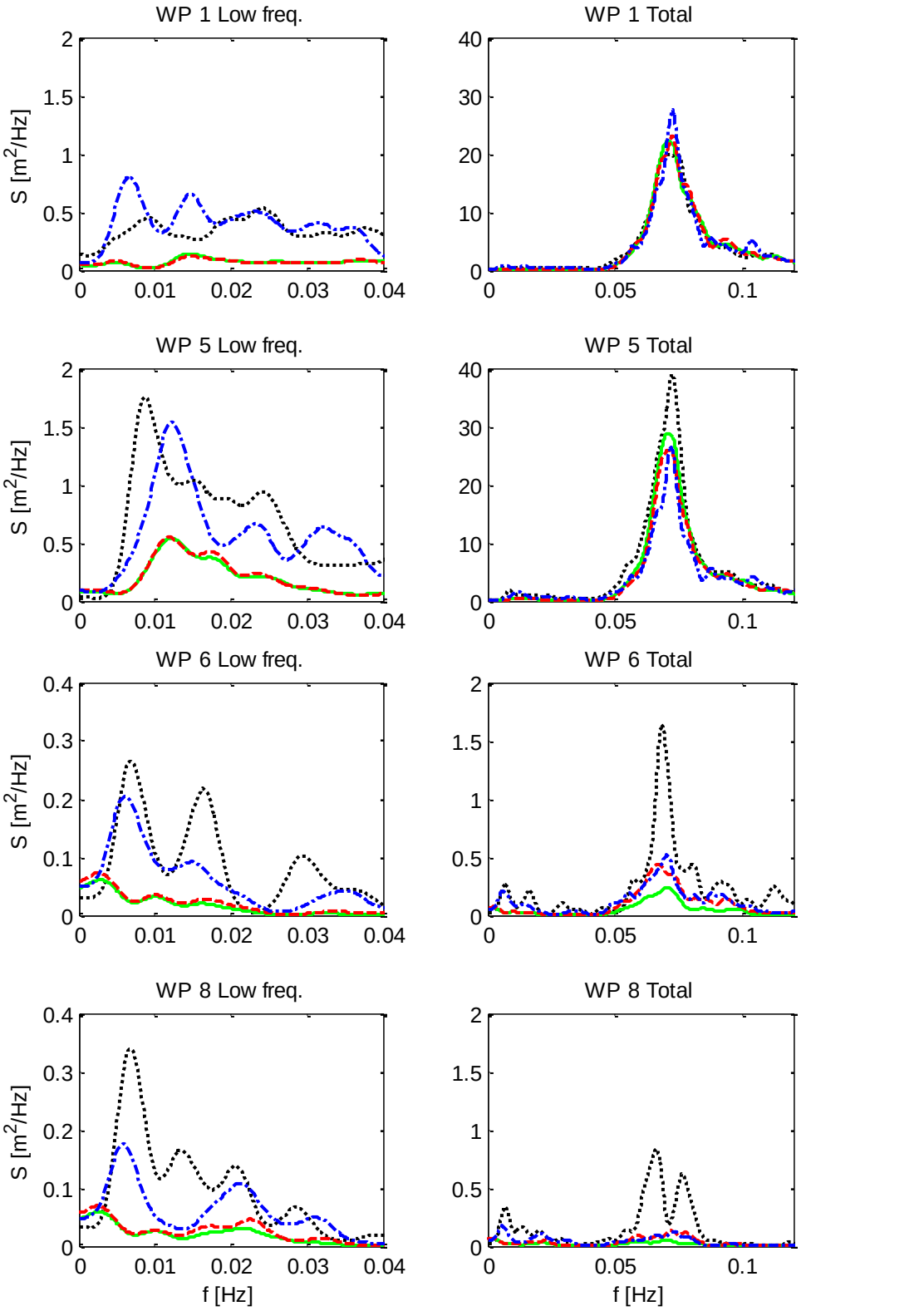

Figure 5-2: Simulated wave spectra with MIKE21 BW.
Tidal level: d=20 [m].
Peak period: T_p=14 [sec].
Low frequency wave spectra: left.
Total wave spectra: right.

The wave spectra as presented in Figure 5-2, are representative for all simulated wave spectra after simulations with MIKE21 BW. A good agreement is achieved for the primary wave spectra at wave gauge 1 and 5, whereas the simulated primary wave height at wave gauge 6 and 8 is clearly underestimated. Some improvement in the simulations were obtained by adapting the head of the breakwater. Improvements due to applying alternative sponge or porosity layers were not noticed (results not presented in this thesis).
MIKE21 BW underestimates the measured wave energy at lower frequencies, if low frequency calibration for the performed simulation is absent. The peaks in the low frequency spectrum of wave gauge 1 are probably due to the fact that both bound and free long waves are simulated with the same frequency or as a consequence of calibration. A fairly good agreement in low frequency energy between measurements and simulations is achieved at wave gauge 5, 6 and 8. At wave gauge 6 both measured peaks in the low frequency spectrum are simulated. At wave probe 8 the first measured peak is well simulated, but the second peak is not.

The spectrum characteristics are calculated for the simulation with an adapted head of the breakwater and including low frequency calibration. Formulas to calculate these characteristics can be found in Holthuijsen (2007) and will not be represented. A relative error is calculated according to Eq. 5-1. The spectrum characteristics are calculated for:

- The total wave spectrum including all frequencies, see Table 5-1.
- The primary wave spectrum, only including frequencies >0.04Hz, see Table 5-2.
- The low frequency wave spectrum, only including frequencies <0.04Hz, see Table 5-3.

The simulated spectral periods (see Table 5-1 to Table 5-3) are higher than the measured spectral periods, although this becomes not clear from the wave spectra as presented in Figure 5-2. A possible cause is that during the physical model tests more wave energy is transferred into super-harmonics, with higher frequencies. These super-harmonics are not accurately described within MIKE21 BW, since the spatial grid size is large. Super-harmonics are less relevant for moored ship computations, since their frequency is not close to the eigen period of ship and mooring system.
Although the wave spectra are not totally satisfactory, the simulations from MIKE21 BW were used for further processing with Harberth and Quaysim. For further processing with these successive models long periods of simulation, including a sufficient number of low frequency waves, are necessary to achieve statistical reliable results. During these long period simulations (of approximately 1.5 hour in prototype) an eddy was noticed in the computational domain of MIKE21 BW. The size and magnitude in terms of velocity of this eddy grew in time. A more detailed explanation and the consequences of this eddy will be explained in section 5.4.

$$\text{Relative Error} = \frac{\text{Simulated} - \text{Measured}}{\text{Measured}} \cdot 100\% \qquad \textit{Eq. 5-1}$$

	W1 M	*W1 S*	Err %	W5 M	*W5 S*	Err %	W6 M	*W6 S*	Err %	W8 M	*W8 S*	Err %
H_{m0} [m]	3.09	*2.92*	-5.4	3.63	*2.90*	-20.2	0.78	*0.51*	-34.5	0.59	*0.31*	-47.8
T_{m01} [s]	11.39	*12.71*	+11.7	12.27	*12.96*	+5.4	10.69	*15.13*	+41.3	12.61	*24.24*	+91.9
T_{m02} [s]	10.50	*12.19*	+16.1	11.35	*12.37*	+8.8	9.26	*13.28*	+43.4	10.39	*18.44*	+77.3

Table 5-1: Calculated total wave spectrum characteristics.
Based on simulations with MIKE21 BW including low-frequency calibration. Cursive=Simulated.

	W1 M	*W1 S*	Err %	W5 M	*W5 S*	Err %	W6 M	*W6 S*	Err %	W8 M	*W8 S*	Err %
H_{m0} [m]	3.05	*2.87*	-5.9	3.57	*2.83*	-20.7	0.74	*0.46*	-38.3	0.54	*0.21*	-60.6
T_{m01} [s]	11.19	*12.36*	+10.5	11.96	*12.48*	+4.4	9.84	*12.51*	+27.1	10.72	*13.49*	+25.8
T_{m02} [s]	10.38	*11.99*	+15.4	11.17	*12.09*	+8.2	8.82	*11.93*	+35.3	9.45	*12.97*	+37.2

Table 5-2: Calculated primary wave spectrum characteristics.
Based on simulations with MIKE21 BW including low-frequency calibration. Cursive=Simulated.

	W1 M	*W1 S*	Err %	W5 M	*W5 S*	Err %	W6 M	*W6 S*	Err %	W8 M	*W8 S*	Err %
H_{m0} [m]	0.47	*0.54*	+16.1	0.66	*0.63*	-6.9	0.24	*0.23*	-5.8	0.25	*0.22*	-9.7
T_{m01} [s]	47.24	*58.62*	+23.8	55.48	*55.49*	-6.2	62.30	*97.55*	+53.2	71.95	*84.37*	+16.2
T_{m02} [s]	42.18	*48.74*	+15.4	49.90	*47.93*	-4.0	52.89	*68.80*	+30.8	61.79	*62.68*	+1.0

Table 5-3: Calculated low frequency wave spectrum characteristics.
Based on simulations with MIKE21 BW including low-frequency calibration. Cursive=Simulated.

5.2 Wave force calculations

5.2.1 Model set-up

The ship is described by 676 panels (see Figure 2-10) and has the characteristics according to Table 2-1. The reflection coefficient for the scattered waves from the breakwater was defined as 40%. The retardation functions were obtained from a run with Quaysim in still water taking the non-linear characteristics of the mooring arrangement into account.

5.2.2 Model results

The calculated wave forces by Harberth are presented as time-series of wave forces in Figure 5-3 to Figure 5-8. The presented time-series are representative for all other simulations with Harberth based on MIKE21 BW computations, which showed similar trends. The calculation of the wave forces on the ship showed unexpected results:

- In the calculated total wave forces and moments an upward trend is noticed, see Figure 5-3 and Figure 5-4.
- This upward trend is caused by increasing second order effects, see Figure 5-7 and Figure 5-8.
- The second order forces consists of four contributions. Only the contribution due to the second order pressure increased significantly, see Figure 5-7 and Figure 5-8.
- The second order forces and moments are finally dominant over the first order wave forces and moments, see Figure 5-5 to Figure 5-8.

The 2nd order wave force due to second order pressure is depending on the velocity potential, $\left(\nabla\Phi\right)^2$, see Eq. A-11 and section 4.3. In case of only waves the second order pressure wave force should vary around an equilibrium value. If an increasing current is acting on the body the second error pressure increases significantly in time. If an increasing current is acting on the body the second order wave forces due to the relative wave height and the first order rotations and first order inertia forces (respectively the third and fourth contribution of the second order wave forces) will not increase, since these contributions are not depending on the flow potential. The second order wave contribution due to first order pressure and body motions (second contribution of the second order wave forces) is depending on the time derivative of the flow potential and therefore less sensitive to increasing currents. If a constant current is acting on the body, the time derivative of the flow potential is zero and hence the second order pressure force constant.

The increasing current acting on the ship is caused by the eddy created in MIKE21 BW. A small numerical instability in the flux field caused the eddy, which in time grew in both size as well as velocity magnitude. Due to the eddy the fluxes in the vicinity of the ship did not behave according to an orbital wave motion, but instead as an orbital wave + current motion. It should be noticed that besides the fluxes grew continuously in time, a spatial gradient in the flux field in the area of interest is noticed as well. The spatial gradient in the flux field also contributes to excessive wave forces on the ship due to disturbances in the calculated potential flow, this will be explained in section 5.4

As a consequence of disturbances in the simulated flux field the calculated wave forces on the ship are not reliable. Within the 3D panel model Harberth the simulated fluxes from MIKE21 BW are converted into orbital velocities of the waves, which serve as a boundary condition to calculate the diffraction force due to the presence of the ship. Due to the increasing current in the flux field the 1st general principle of Harberth no longer holds (see section 4.3). The 1st principle is based on the assumption that a still ship in a current is equal to a ship sailing in still water.

The 1st general principle yields (see section 4.3):

- The 3D panel model Harberth can be applied on arbitrarily shaped bodies, with a zero mean forward speed.

Or equivalently:

- The 3D panel model Harberth can be applied on arbitrarily shaped bodies in waves only.

The calculated first order wave forces, due to both incident and scattered waves, follow from integration of the first order pressures over the mean submerged hull. The first order pressure p is obtained after applying the Bernoulli equation (see Appendix A):

$$-\frac{p-p_0}{\rho} = gz + \frac{\partial \Phi}{\partial t} + \frac{1}{2}\nabla\Phi \cdot \nabla\Phi + \text{constant} \qquad \textit{Eq. 5-2}$$

The first order pressure contains the non-linearity of the waves, but is calculated by assuming potential flow (second and third term RHS Eq. 5-1). From the calculation of the second order forces it is noticed that the second order pressure increased continuously. The continuous increase in second order wave forces is due to spatial and temporal disturbances in the horizontal fluxes, as simulated with MIKE21 BW. Due to temporal and spatial disturbances an increasing current is acting on the ship, which is most pronounced for terms depending on $\left(\nabla\Phi\right)^2$.

As analysed above the second order forces are not reliable due to the increasing current on the ship. In the calculation of the first order wave forces, potential flow is used as well (third term RHS Eq. 5-2). The quadratic pressure related to the second order pressure (third term RHS Eq. 5-2) in the calculation of the first order wave forces on the ship is now dominated by other terms (e.g. hydrostatic pressure). The increase in first order waves is therefore less pronounced compared to the increase in the second order wave forces. For longer period of calculations an increase in the first order wave forces is expected as well. Due to both spatial and temporal disturbances in the flux field, both calculated first order as well as second order wave forces on the ship are not reliable.

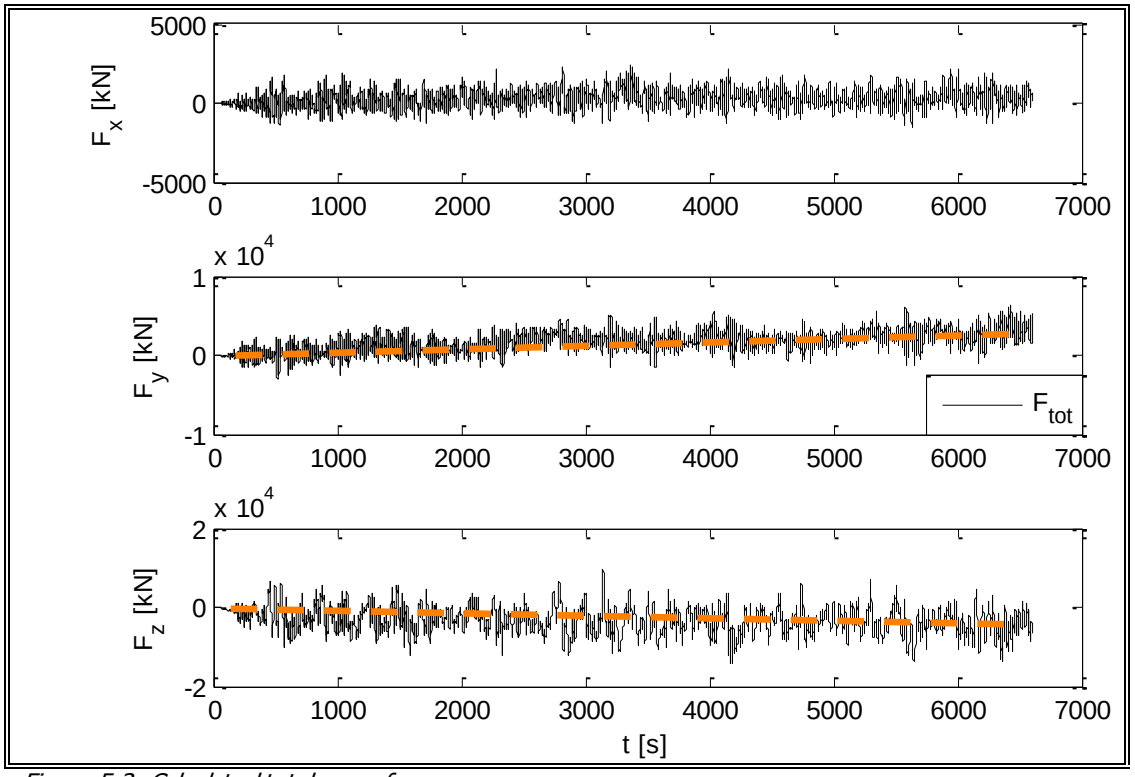

Figure 5-3: Calculated total wave forces

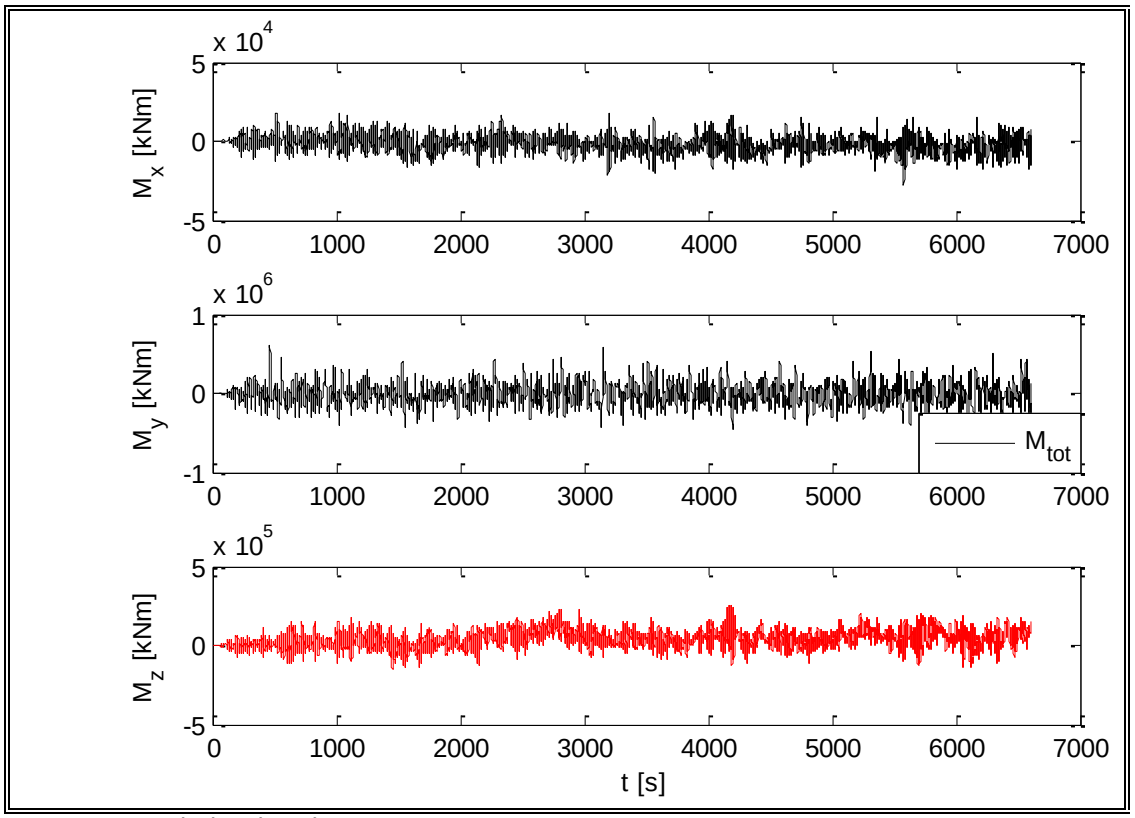

Figure 5-4: Calculated total wave moments

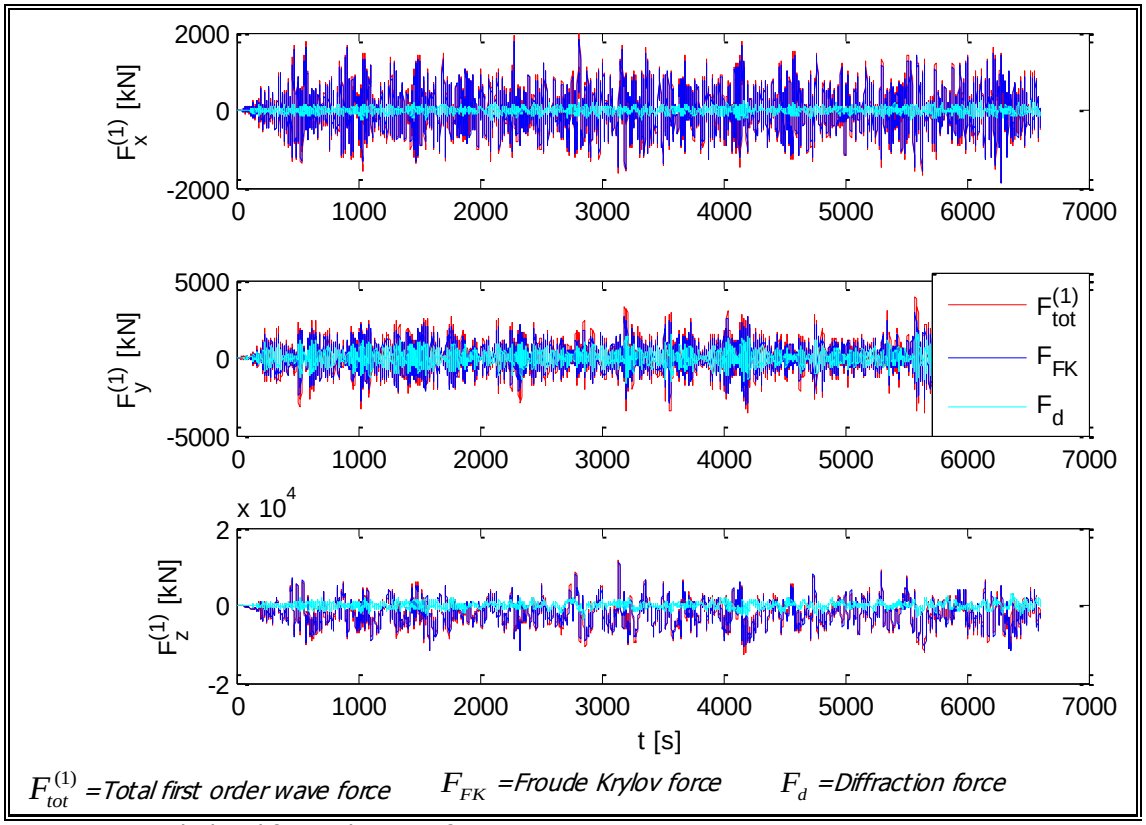

$F_{tot}^{(1)}$ =Total first order wave force F_{FK} =Froude Krylov force F_d =Diffraction force

Figure 5-5: Calculated first order wave forces

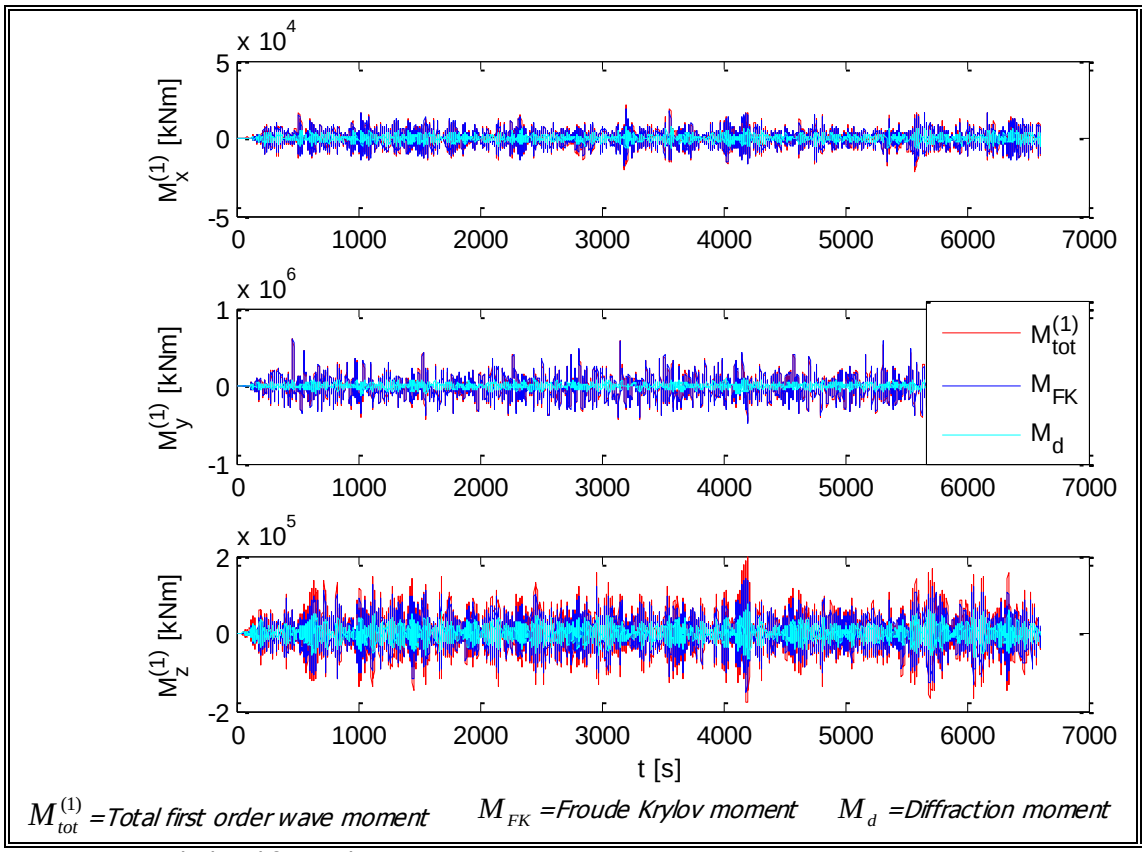

$M_{tot}^{(1)}$ =Total first order wave moment M_{FK} =Froude Krylov moment M_d =Diffraction moment

Figure 5-6: Calculated first order wave moments

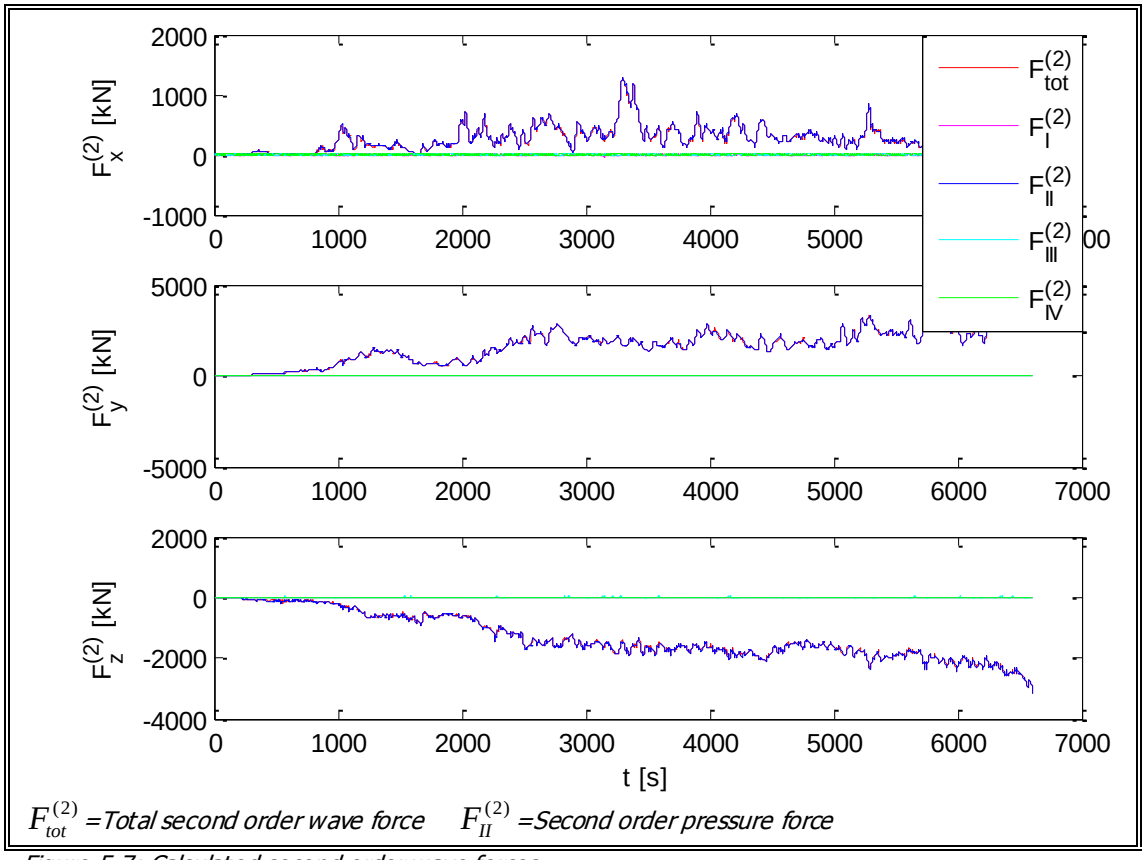

$F_{tot}^{(2)}$ =Total second order wave force $F_{II}^{(2)}$ =Second order pressure force

Figure 5-7: Calculated second order wave forces

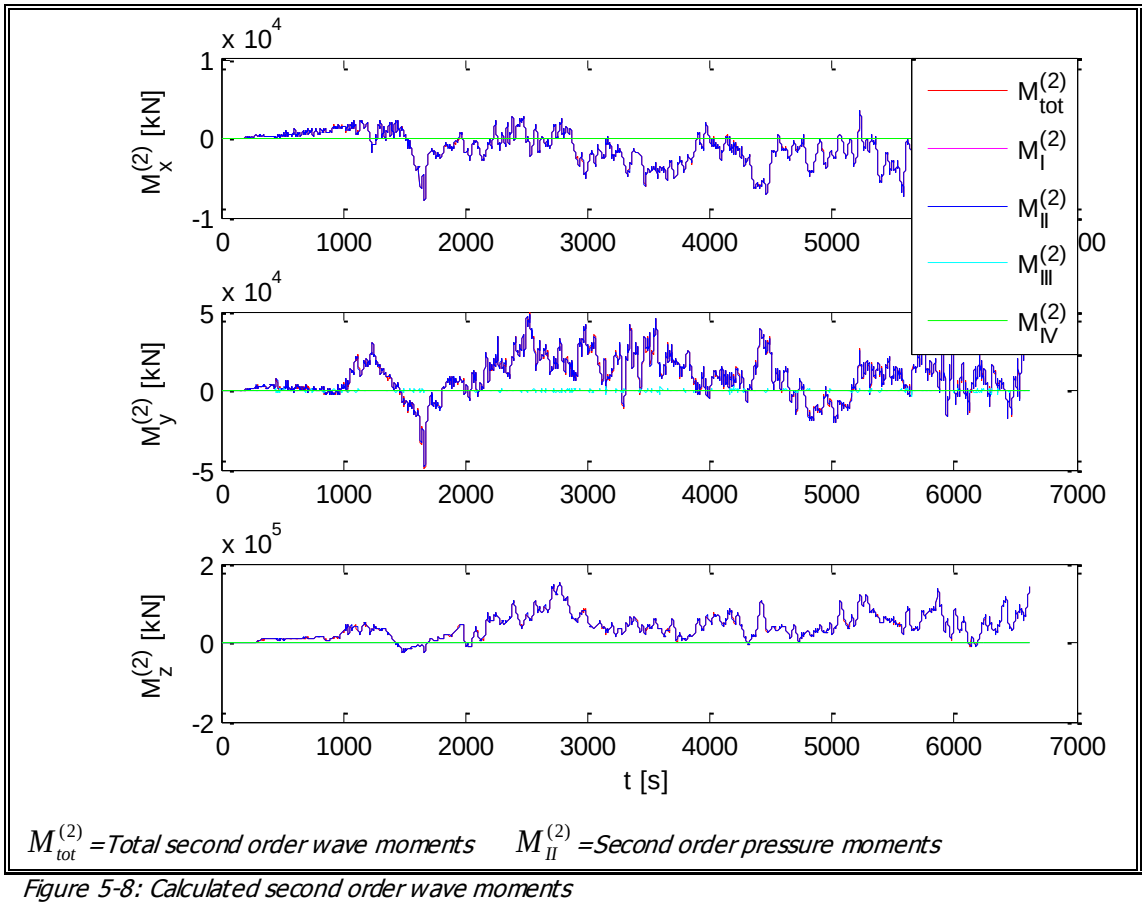

$M_{tot}^{(2)}$ =Total second order wave moments $M_{II}^{(2)}$ =Second order pressure moments

Figure 5-8: Calculated second order wave moments

5.3 Ship simulations

5.3.1 Model set-up

The mooring arrangement is described taking into account the mooring lay-out (see Figure 2-4) and the characteristics of both mooring lines and fenders (see Table 2-2). The ship motions were simulated applying only the calculated first order wave forces, since it was noticed that the second order wave forces increased significantly (which was thought to be unrealistic). The realistic oscillatory part of the second order wave forces was such small that it could be neglected.

5.3.2 Model results

A representative example of the obtained ship motions simulations is given in Figure 5-9. The ship motions are obtained after a run through all three successive numerical models. In the ship motions simulations only the calculated first order wave forces are applied. From the analysis made in section 5.2.2 it is already remarked that the first order wave forces are not reliable. The obtained ship motions are therefore not reliable, but caused by a succession of errors due to increasing horizontal fluxes in MIKE21 BW. It is also possible that there is too much wave reflection from the breakwater and/or beach in MIKE21 BW. Due to high wave reflection the ship makes a sway motion, releases from the fenders and finally starts to surge. Since it is released from the fenders there is no friction to resist the surge motion of the ship.

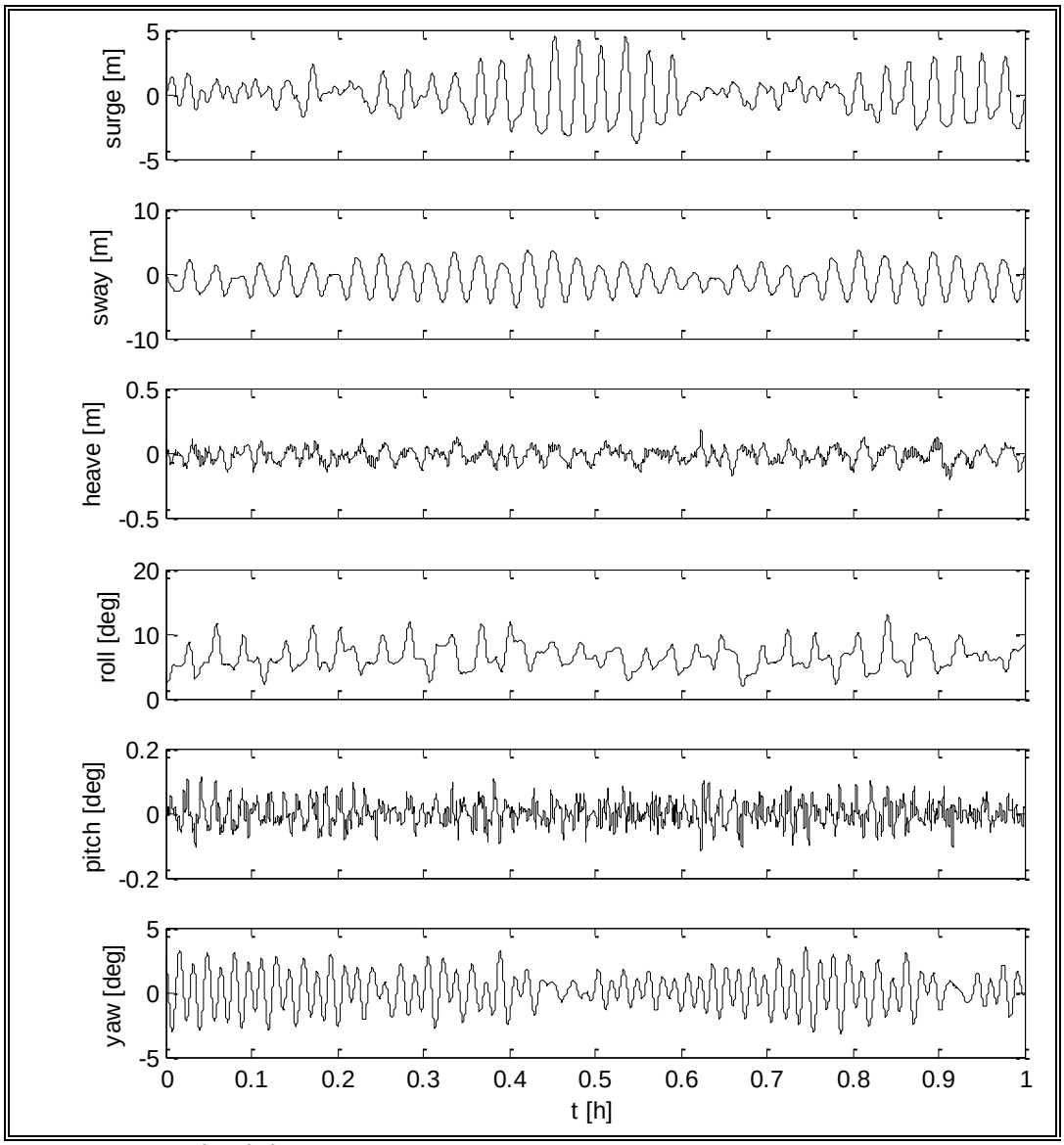

Figure 5-9: Simulated ship motions

5.4 Discussion of model results

During the performed simulations with MIKE21 BW a circulation cell of fluxes is formed within the computational domain at deep water. Physically a circulation cell of fluxes is an eddy, which may exist in the physical model as well. The fluxes of the simulated circulation cell grew in time, with respect to both size as well as magnitude. Before the end of the abandoned simulation duration the total velocity field was dominated by the eddy.

Why the circulation cell grew in time in both size as well as velocity magnitude is not understood. The most obvious reason is that a small numerical instability occurred in a certain grid point, after which surrounding grid points became instable as well. When the model finally blows-up almost the full computational domain showed instable fluxes. The final blow-up of the model takes place at the internal wave generation line, which should generate unidirectional waves. At the beginning of the simulation the fluxes of the generated waves are indeed unidirectional. During the simulation the fluxes most close to the wave guiding wall at the internal wave generation line started to show some directional spreading. Most likely an oblique reflected wave is not well absorbed by the sponge layer after the internal wave generation line. Before the imposed simulation duration the fluxes at the wave generation line increased significant in size and more directional spreading was noticed. At the end of the computation a negative water depth (at 20m water depth) is calculated. The calculated negative water depth is not caused by an inconsistency in the generation of waves, but due to a numerical instability in the computation of the flux field.

As a consequence of an unstable internal wave generation line, some high frequency waves may be generated. According to DHI (2006A) the high frequency "noise" can be avoided by decreasing the selected time step to ensure numerical stability at the internal wave generation line. The selected time-step, as described in section 5.1.1, was already decreased several times without any effect on the obtained results. It should be noticed that the generation of high frequency "noise" was only noticed for the simulations over longer period of time (i.e. couple of hours). It is remarkable that high frequency "noise" is only noticed outside the designed porosity layer, whereas the grid points inside the porosity layer do not show instabilities in the computation of the flux field. The porosity layer works effective for waves that propagate along the boundary, but information from waves perpendicular to the area of interest is lacking.

The screenshots and time-series in Figure 5-10 are a visualization of the fluxes and surface elevations in the area of interest (vicinity of the ship). It should be remarked that along other boundaries instabilities were noticed as well. A numerical instability in the fluxes is clearly noticed, which grew in time in both size and magnitude. The location of the instability, in the area of interest, is located at the separation between a porosity layer and the rest of the computational domain. During the simulation surrounding grid points became unstable as well. The numerical instability finally resulted in excessive fluxes in the computational grid just outside the porosity layer (see plotted time-series in Figure 5-10). It should be remarked that the ship is located in the middle of the plotted areas, which confirms that the calculated wave forces on the ship are obtained due to a numerical instability in the simulated fluxes in MIKE21 BW. Two important aspects can be defined that explain the excessive wave forces on the ship and the resulting unreliable simulated ship motions:

- A spatial gradient in the fluxes at the location of the ship.
- An increase of the simulated fluxes throughout the simulation.

Many attempts were made to make the model stable. These simulations included e.g. the application of time-extrapolation factors, a smaller time step, alternative sponge and/or porosity layers, smoothing of bathymetry and an increasing minimal water depth. These attempts where however not successful, while as a result of adapting parameters in MIKE21 BW the results may not represent true physics. Most noticeable was that simulations with alternative seed numbers could result in longer simulation durations. An alternative seed number is nothing else than an alternative realization of the same spectrum by defining randomly different phases for the primary waves. The random seed number should not have influence on the final results. If the seed number does have influence on the final model results, the simulation duration is too short to obtain a wave-spectrum independent of the incoming time-serie. The questions where and why the model became unstable were not solved during this study.

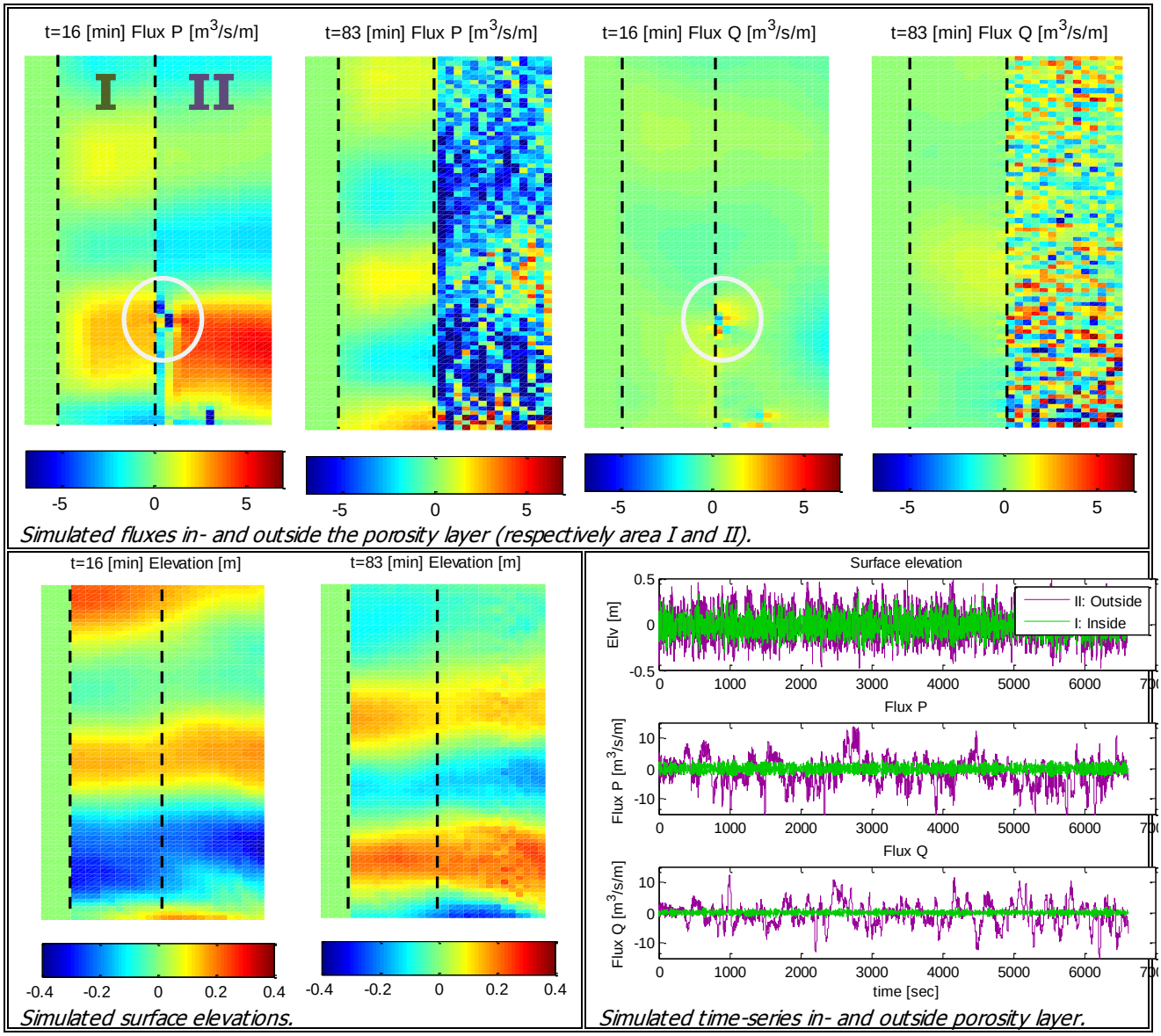

Figure 5-10: Snapshots and time-series in vicinity of the ship simulated with MIKE21 BW.

Other studies performed with MIKE21BW found instabilities within the computational domain as well. Apart from numerical instabilities no convincing reasons were found which could explain instabilities and/or model blow up. Two examples of vulnerability of numerical instabilities in MIKE21 BW will be given here:

Brandi Mortensen (2006) showed that the rip current, which was simulated originally by Sorensen *et al.* (1998), finally became asymmetrical after reaching a steady state and apart from suggesting that this was due to small numerical instabilities, no explanations were given (both bathymetry and computational domain were symmetrical). Brandi Mortensen (2006) found after a longer period of simulation an excessive increase of wave energy within a bay. This finally resulted in a blow-up of the model in deeper water. Extra attempts to obtain longer simulations periods failed.

Mahmoodian (2009), concluded that the application of sponge layers may not work optimal if the direction of the wave is not perpendicular to the direction of the sponge layer. In the case of oblique incident waves on a sponge layer unwanted reflections can be generated. Increasing the width of the sponge layer did not lead to improvements of results in case of oblique incident waves. In order to avoid the unwanted reflections the sponge layer was removed, which yields that full reflection is imposed along lateral boundaries.

Although the details of both studies are not known, corresponding experiences are found with simulations in MIKE21 BW during this study. A build-up of fluxes was noticed in the computational domain, for which the cause could not be discovered. A non-optimal working sponge layer subjected to oblique incident fluxes may be the reason why at the end of the simulation the fluxes most close to the wave guide wall increased significantly in magnitude and showed directional spreading.

Although the input signal in MIKE21 BW could be even more optimized by the inclusion of a theoretical defined bound long wave signal, a fair comparison between the simulated and measured spectra is not possible. After a long period of simulation, the numerical model becomes unstable and finally stops. The numerical simulated duration is much shorter than the duration of the physical model tests (about 1.5 hour numerical simulations compared to 3 hours of physical model tests). To compare the numerical simulations and the physical model tests in a fair way the simulation duration should be equal. If the simulation time is too short the width of the frequency bins is too large to obtain a good representation of the distribution of energy density (especially for the low frequency waves). The statistical variability of the simulated low frequency spectrum is relatively high to make a fair comparison between spectrum characteristics. The number of waves necessary to obtain a representative spectrum differs in literature. As a rule of thumb the number of waves should be persisted as at least $N_{waves} \approx 400$. With a test duration of 3 hours and a representative long wave period of 60 seconds the number of waves becomes $N_{waves} \approx 180$. For the simulated period within MIKE21 BW the number of waves is only $N_{waves} \approx 90$.

A switch to an alternative Boussinesq-type wave model was made due to the following reasons:

- As a consequence of numerical instabilities unreliable horizontal fluxes were obtained.
- The cause of increasing horizontal flues in the computational domain of MIKE21 BW could not be discovered during this study.
- Since the horizontal fluxes from MIKE21 BW were not reliable, the successive computations with Harberth and Quaysim are not reliable as well, see section 5.2.2 and 5.3.2.
- Simulations over longer periods of time could not be made in MIKE21 BW, since the cause of the instabilities was not discovered during this study.
- Long period of simulations are required to obtain statistical reliable ship motions.

Remark

In both Harberth and Quaysim numerical errors can be made as well. These errors may be as a consequence of several factors: irregular frequencies, insufficient low frequency damping in the retardation functions, other numerical errors etc.. Since already incorrect horizontal fluxes in MIKE21 BW were simulated a sequence of mistakes followed, see Figure 5-11.

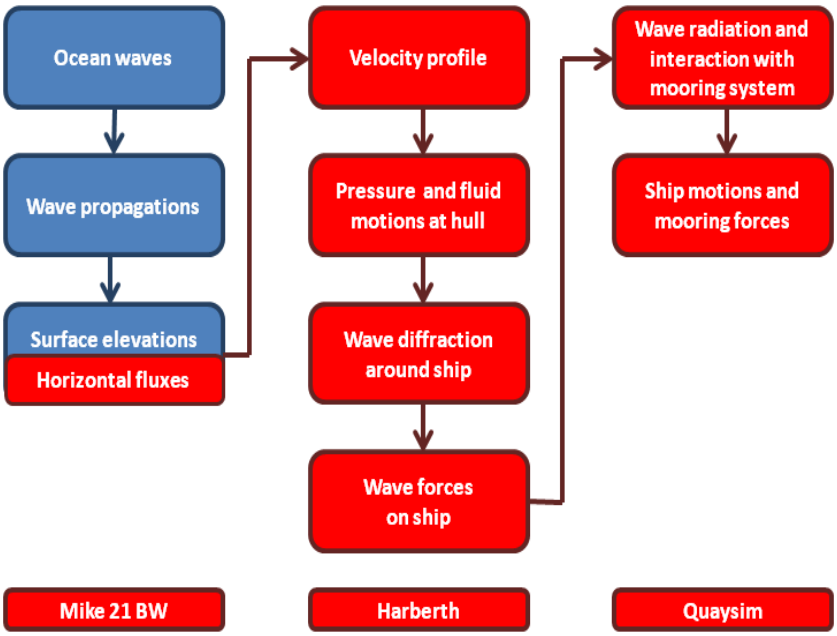

Figure 5-11: Feedback to coupled numerical model scheme.

6 Numerical simulations with TRITON

6.1 Model set-up

6.1.1 General settings

The spatial grid cell size in TRITON was selected as Δx=4meter. The considerations to select this spatial grid cell size are the same as described in section 5.1.1. A time step of Δt=0.1 seconds was selected to ensure numerical stability based on the CFL condition. The selected time step is chosen conservatively. As a consequence the total simulation duration in terms of total computational time can be optimized by selecting a larger time step that still fulfills the CFL condition and for which the waves are described with sufficient accuracy.

6.1.2 Boundary conditions

The first step in the model set-up of TRITON is to determine which boundary conditions should be applied. For the model set-up four types of boundary conditions can be distinguished:

- Wave generation line.
- Closed boundary conditions.
- Partial reflecting boundary condition for beaches.
- Partial reflecting boundary condition for breakwaters.

The used model set-up is visualized in Figure 6-1. Notice that the location of the wave generation line is not equal to the location of the wave paddles in the physical model. The wave generation line is placed at the location of wave gauge 1, which will be explained in section 6.3.2.

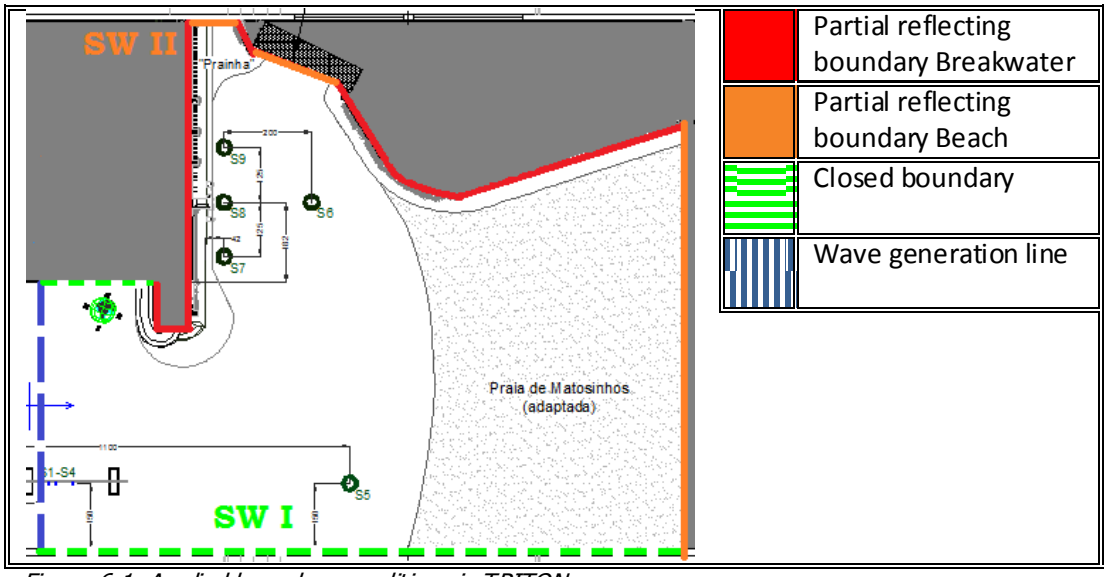

Figure 6-1: Applied boundary conditions in TRITON.

6.2 Program of simulations

A general overview of the performed simulations is given in this section. For more detail about the applied boundaries conditions in TRITON, one is referred to section 6.1.2 and section 6.3. All simulations in TRITON are performed for a tidal level of d=20 meters. The numerical simulation duration in TRITON is equal to the duration of the physical model tests, see Table 6-1. Wave breaking and moving shoreline (run-up and run-down) are excluded during all simulations.

T_p [sec]	Total simulation duration
10	106 minutes
14	149 minutes
18	193 minutes

Table 6-1: Total simulation duration physical model tests and TRITON.

Partial boundary conditions breakwaters and beaches

During the first four simulations in TRITON the partial reflecting boundaries along the beaches and breakwaters are varied according to Table 6-2. These simulations are performed to investigate the sensitivity of the obtained primary wave spectra from the simulations for different applied reflection coefficients. An explanation of the selected reflection coefficients will be given in section 6.3.1.

Run-id	T_p [sec]	Generated waves	C_r Breakwater	C_r Beach
01	14	Measured surface elevations	30%	2%
02	14	Measured surface elevations	40%	2%
03	14	Measured surface elevations	50%	2%
04	14	Measured surface elevations	40%	10%

Table 6-2: Variation of partial reflecting boundaries.

Wave conditions with different peak periods

Two alternative wave conditions are simulated in TRITON. One wave condition with a peak period of T_p=10 seconds and a second wave condition with a peak period of T_p=18 seconds, see Table 6-3. These runs are used to verify that other wave conditions in TRITON can be simulated accurately as well.

Run-id	T_p [sec]	Generated waves	C_r Breakwater	C_r Beach
05	10	Measured surface elevations	40%	2%
06	18	Measured surface elevations	40%	2%

Table 6-3: Variation of primary peak wave period.

Wave generating boundary

Within TRITON it is possible to directly apply the measured surface elevations from the physical model tests at the wave generation boundary. The measured surface elevations at the first wave probe in front of the wave maker of the physical model were used as an incoming wave boundary for runs 01 to 06. In runs 07 to 09 different techniques to generate incoming waves are applied according to Table 6-4. The applied techniques will be explained in more detail in section 6.3.2.

Run-id	T_p [sec]	Generated waves	C_r Breakwater	C_r Beach
07	14	First order wave generation	40%	2%
08	14	Second order wave generation method 1	40%	2%
09	14	Second order wave generation method 2	40%	2%

Table 6-4: Variation of wave generation.

Additional simulations

Three additional simulations are carried out with TRITON. These additional simulations are carried out for the following reasons:

Run 10: The breakwaterhead initially simulated in TRITON is based on the adapted breakwaterhead which was used performing simulations with MIKE21 BW. This breakwaterhead is shorter than the breakwaterhead applied in the physical model. As a consequence too much high frequency energy in the area of interest may be simulated.

Run 11: Low frequency waves that diffract behind the North breakwater (IV in Figure 2-8), may reflect and cause standing wave patterns between the physical model side walls. These standing wave patterns are due to the finite physical model basin sizes. Side wall I (see Figure 6-1) is schematized as a partial reflecting boundary with a low reflection coefficient to investigate the effect of the side wall on possibly standing waves.

Run 12: The partial reflecting boundaries applied at side wall II (see Figure 6-1) have a low reflection coefficient of 2% in Run 01 to Run 11. Small partial reflection from this boundary is expected for the high frequency waves, but waves with low frequencies may reflect full from the boundary. As a consequence, the energy of especially the long waves in the numerical model may be underestimated.

Run 13: The porous absorbent beach (detail Figure 2-8) is removed and a closed boundary condition is applied at the entrance to the port basin and side wall II. The expectation was that the short waves will break on the porous beach installed at the entrance of the harbour basin (see detail Figure 2-8) and small wave reflection from the porous beach was expected. The entrance to the harbour basin was therefore schematized as a partial reflecting boundary with a low reflection coefficient (Run 01 to Run 11). The hypotheses is that the porous beach is probably effective in absorbing high frequency waves, but is less effective in case of low frequency waves.

Run 14: A basin is added and the absorbent beach installed at the entrance is removed. The boundaries of the basin are full reflecting, see Figure 6-2. The entrance of the basin is equal to the physical model basin, but the basin itself is a smaller reproduction of the basin within the physical model.

Remark

Measurements of velocities and/or surface elevations in the harbour basin are not carried out. The hypotheses cannot be verified by physical model measurements.

Run-id	T_p [sec]	Generated waves	Remark:
10	14	Measured surface elevations	Adapted breakwaterhead
11	14	Measured surface elevations	Partial reflecting BC side wall I
12	14	Measured surface elevations	Full reflecting BC beaches side wall II
13	14	Measured surface elevations	Closed boundary at basin entrance
14	14	Measured surface elevations	Basin added with full reflecting boundaries

Table 6-5: Variation of other boundary conditions.

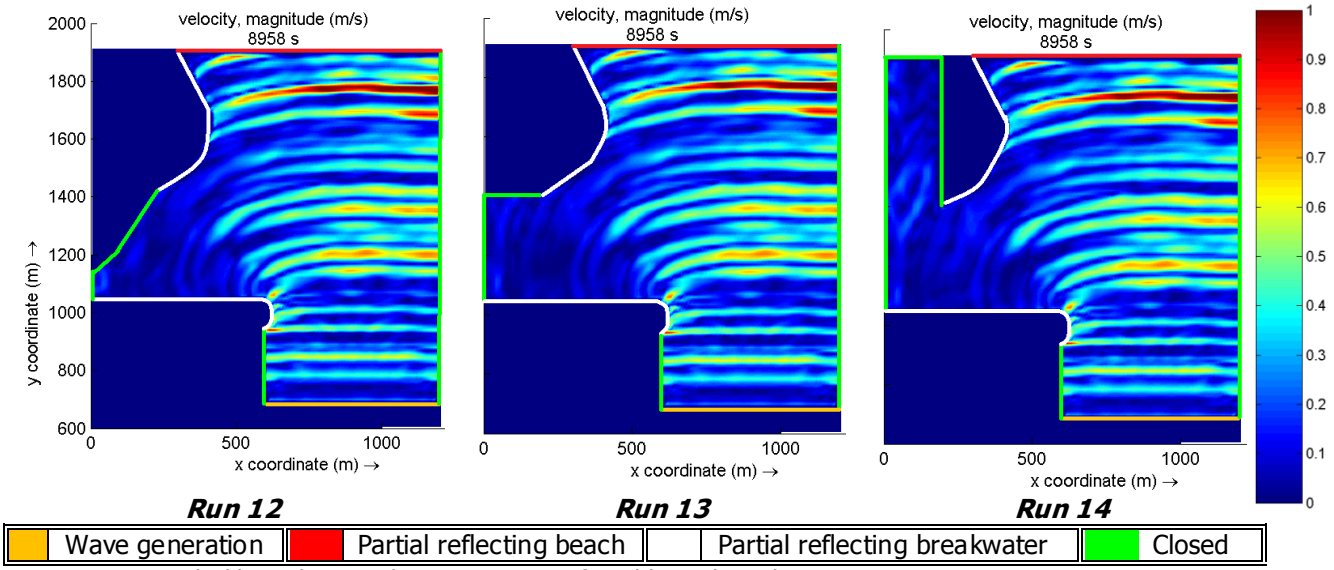

Figure 6-2: Applied boundary conditions in TRITON for additional simulations. Run 12 to 14.

6.2.1 Summary of simulations

An overview of the simulations carried out with TRITON is given in Table 6-6.

Run-id	T_p [sec]	Incoming wave	C_r Br Wat	C_r Beach	Remark:
01	14	Measured	30%	2%	
02	14	Measured	40%	2%	
03	14	Measured	50%	2%	
04	14	Measured	40%	10%	
05	10	Measured	40%	2%	
06	18	Measured	40%	2%	
07	14	1st order BC	40%	2%	
08	14	2nd order BC 1	40%	2%	
09	14	2nd order BC 2	40%	2%	
10	14	Measured	40%	2%	Adapted breakwaterhead
11	14	Measured	40%	2%	Partial reflecting BC SW I
12	14	Measured	40%	2%	Full reflecting BC SWII
13	14	Measured	40%	2%	Closed basin entrance
14	14	Measured	40%	2%	Open basin entrance

Table 6-6: Overview of simulations with TRITON.

6.3 Explanation of boundary conditions

6.3.1 Partial reflecting boundaries

The partial reflecting boundaries in TRITON are depending on the reflection coefficient and the peak period of the primary waves. In order to determine the reflection coefficients for the rubble mound breakwater and the beach two different equations are presented.
The reflection coefficient of a rubble mound breakwater can be approximated using the empirical relationship of Muttray *et al.* (2006):

$$C_R = \left(1{,}3 + 3d \cdot \frac{2\pi}{L_0}\right)^{-1} \qquad \textit{Eq. 6-1}$$

In which:

C_R = Reflection coefficient [-]
d = Still water depth [m]
L_0 = Deep water wave length [m]

T_p [sec]	L_0 [m]	d [m]	C_R [-]
10	156	16~20	0.30~0.27
14	306	16~20	0.44~0.40
18	506	16~20	0.53~0.49

Table 6-7: Reflection coefficients of a rubble mound breakwater for different wave conditions.

For a beach the reflection coefficient mainly depends on the beach slope and the type of breaking. The slope of the beach during the physical model tests is approximated and assumed to be uniform alongshore. The reflection coefficient of a beach is, according to Battjes (1974), given by:

$$C_R = 0{,}1\xi^2 \text{ with: } \xi = \frac{\tan\beta}{\sqrt{H / L_0}} \qquad \textit{Eq. 6-2}$$

In which:

$\tan\beta$ = Beach slope angle [-]
ξ = Iribarren number [-]
H = Wave height [m]

T_p [sec]	L_0 [m]	H [m]	$\tan\beta$ [-]	ξ [-]	C_R [-]
10	156	3	1/25=0,04	0.29	0.008
14	306	3	0,04	0.40	0.016
18	506	3	0,04	0.52	0.027

Table 6-8: Reflection coefficients of a beach for different wave conditions

The calculated reflection coefficients agree well with the range of reflection coefficients which were obtained by breakwaters tests at FEUP ($0.25<C_r<0.45$), see Table 6-7. The sensitivity of the reflection coefficients for partial reflecting breakwaters within TRITON is tested in run 01 to run 03, see section 6.2. Minimal wave reflection is expected from the absorbent beach at the end of the physical model opposing the wave generators (see V in Figure 2-8). The applied reflection coefficient from the beach in TRITON is set to 2% for runs 01 to 03, but was increased in run 04 to 10% in order to investigate the effect of more wave reflection from the beach, see section 6.2.

6.3.2 Generated waves

The measured surface elevations at the first wave probe of the physical model tests serve directly input for the generation of waves in TRITON. TRITON calculates the corresponding velocities of the waves. Both surface elevations and velocities at the incoming wave boundary are controlled by the adaptive boundary procedure. It should be noticed that a linear interpolation technique is used to define the generated waves for TRITON. Application of an interpolation technique was required due to the fact that the sample period of the surface elevations during the physical model tests is not equal to the time-step defined in TRITON. The sample frequency during the physical model tests was 10/24 Hz (prototype value), whereas the generated waves in TRITON are defined with a sample frequency of 1/10 Hz. Effects due to application of the applied interpolation technique are expected to be minimal and non-appreciable for the results.

Directly applying the measured surface elevations as an input for TRITON has disadvantages. The measured surface elevations at the wave probes in front of the wave maker in the physical model contains the generated waves, but also reflected waves (and possibly re-reflected waves). Free reflected waves can be generated by several basin effects, see Voogt *et al.* (2005):

- Reflections due to the finite size of the basin.
- Mismatch in velocities at the wave maker compared with ocean waves, if no second order correction is made at the wave maker.
- Release of set-down waves after shoaling resulting in free waves.

Dissipation of reflected free long waves in the physical model basin is minimal since the efficiency of the dynamic wave absorption unit of the wave maker is minimal for low frequency waves, see Figure 2-9. As a consequence the measured free (re-) reflected long waves are included in the incoming signal of TRITON. The outgoing waves measured at wave gauge 1 are now generated in TRITON as well.

In run 07 a so-called 1st order boundary condition is imposed at the wave generation line in TRITON. This incoming wave signal is based on the measured surface elevations, but waves with periods higher than 25 seconds are excluded. A bound long wave at the incoming wave boundary associated with the primary waves is not imposed, but will be generated within the computational domain of TRITON in combination with possible spurious free waves.

A theoretical bound long wave can be included in the incoming wave signal of TRITON. In that case a 2nd order boundary condition is imposed at the wave generation line. This is done by adding a theoretical derived bound long wave signal with the incoming primary waves, in which the latter is the generated time-serie of run 07. Two methods to derive a theoretical bound long wave are distinguished:

- A theoretical bound long wave signal based on the conservation of radiation stress as proposed by Longuet-Higgins and Stewart (1962) $\rightarrow$ Run 08.
- A theoretical bound long wave based on interaction between pairs of primary waves in a wave group, see Herbers *et al.* (1994) $\rightarrow$ Run 09.

The first method calculates a bound long wave based on the wave envelope in which a constant interaction coefficient is applied between the amplitude of the bound long wave and the wave group. The second method is based on interaction between pairs of primary waves in wave group each having their own interaction coefficient. Summation over all the components of pairs of primary waves gives the total bound long wave. In TRITON the incoming time-serie of waves needs to be defined in surface-elevations. The original expressions of Herbers *et al.* (1994) are valid for bottom pressures. Adjustments to rewrite the transfer functions in surface elevations can be found in Van Dongeren *et al.* (2003).

Within the second method a threshold need to be defined to determine the interaction pairs of primary waves. This is done according to the following methodology:

- The measured surface elevations are converted in a wave spectrum via FFT analysis.
- Waves with a period larger than 25 seconds are removed from the wave spectrum.
- A threshold is defined as 95% of the most energetic primary waves.
- For each possible pair of primary waves in the defined threshold the contribution to the bound long wave is calculated.

Defining a theoretical bound long wave including more than 95% of the most energetic primary waves did not lead to noticeable differences in the defined time-serie. It can therefore be concluded that the theoretical bound long wave based on the 95% criteria is accurately described.

Remark

Wave splitting, see Voogt *et al.* (2005) and Waals (2009), was not performed during the physical model tests. Wave splitting tools decompose measured waves into:

- Incident free waves
- Incident bound waves
- Reflected waves

Wave splitting tools can be used to indentify spurious free waves and reflected waves in the model basin. Incorporating these waves in the numerical simulations may further improve the agreement between measurements and simulations.

7 Comparison physical model results and TRITON

Within this section references are made to figures which can be found in Appendix C: TRITON simulations. For the location of the different wave gauges one is referred to Figure 2-12.

For the calculation of spectrum characteristics a distinction is made between:

- The full wave spectrum: including all frequencies.
- The primary wave spectrum: only including frequencies > 0.04 Hz.
- The low frequency wave spectrum: only including frequencies < 0.04 Hz.

Partial boundary conditions breakwaters and beaches

In run 01 to run 04 different reflection coefficients are defined for the breakwaters and beaches along the model boundaries. A good overall agreement between the simulated and measured wave spectra for the primary waves in terms of spectrum characteristics and spectral shape is obtained, see Figure 7-1 and Figure C- 1. At wave gauge 5 the simulations give an underestimation compared to measurements. This difference may be due to more reflection of the most energetic waves from the beach. Despite the increase of the reflection coefficient of the beach in run 04 higher energetic waves at wave gauge 5 were not noticed. A possible reason is that the beach slope in the physical model basin is steeper than the beach slope applied in the numerical simulations. If the beach slope is not modelled correctly this mainly affects the amplitude of free reflected waves from the beach, since the amplitude of free reflected waves increases for increasing beach slopes, see Baldock (2000).

From the simulated low frequency wave spectra at wave gauge 1 and 5 it is observed that the increase in spectral density magnitude is well simulated for frequencies around 0.02Hz (although a slight underestimation is noticed). The underestimation of primary wave energy at wave gauge 5 for the most energetic waves is only noticed for the tested wave conditions of T_p=14 and 18 seconds. For the tested wave condition of T_p=10 seconds there is no underestimation of primary wave energy, see Figure 7-2 and Figure C- 2.

The simulated wave height for the low frequency waves equals the measured low frequency wave height, but the spectral shape at low frequencies is not satisfactory. Wave energy is simulated at lower frequencies compared to measurements. As a consequence a deviation in both $T_{m01;low}$ and $T_{m02;low}$ compared to measurements is calculated. The largest deviation between measurements and simulations is noticed for $T_{m01;low}$ at wave probe 6 and 8. This deviation is due to the simulated wave energy at very low frequencies (<0.005Hz), since the calculated spectral period is most sensitive for wave energy at these very low frequencies. Although the simulated wave height at low frequencies is in the same order of magnitude as measurements, wave energy is predicted at different frequencies.

From run 01 to 04 the following can be concluded:

- The reflections coefficients for the partial reflecting boundaries in TRITON are well selected.
- Selecting alternative reflection coefficients for partial reflecting boundaries mainly affects the simulated primary wave energy, but has negligible effects on the low frequency waves.
- The reflection coefficients as applied in run 02 gave the best agreement between measurements and simulations for the most energetic primary waves in the vicinity of the ship (see wave spectrum at wave gauge 8 in Figure C- 1).

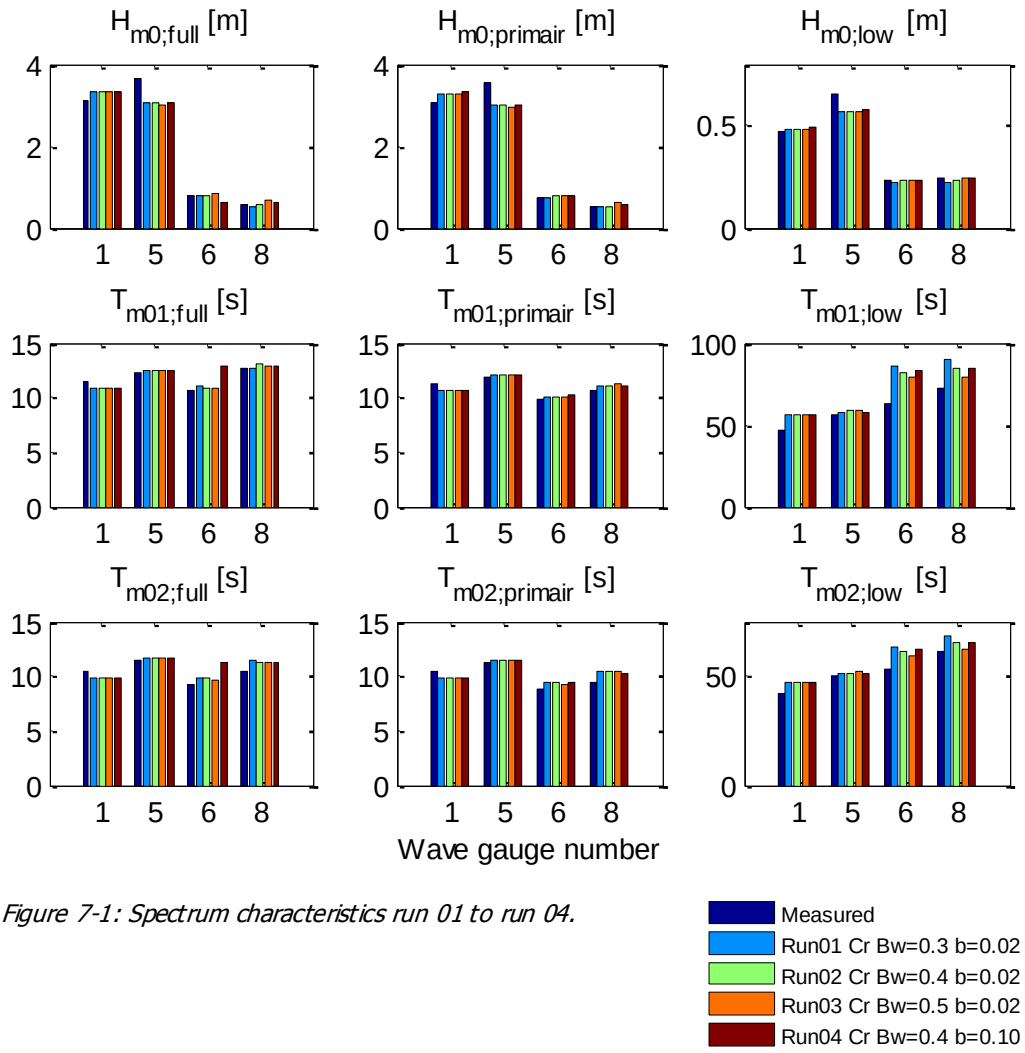

Figure 7-1: Spectrum characteristics run 01 to run 04.

Wave conditions with different peak periods

Runs for other tested wave periods (T_p=10 [sec] and T_p=18 [sec] in run 05 and run 06 respectively), showed that these wave conditions can be well simulated in TRITON, see Figure 7-2 and Figure C- 2. As noticed in the section before the primary wave height at wave gauge 5 is underestimated, but the primary waves in the vicinity of the ship are well simulated. The expected trend of increasing low frequency energy with the incoming peak period of the primary waves is clearly visible in Figure C- 2. The increase of low frequency energy with increasing period was expected, since the surface elevations of each of the infra-gravity components increases with increasing peak period of incoming swell (which can be derived based on the conservation of radiation stress for a flat bottom, see e.g. Van Noorloos (2003)). In the vicinity of the ship enhancement of low frequency wave energy is noticed for increasing peak period. It should be remarked that in the vicinity of the ship the frequencies corresponding to the enhanced low frequency wave energy peaks are not predicted well.

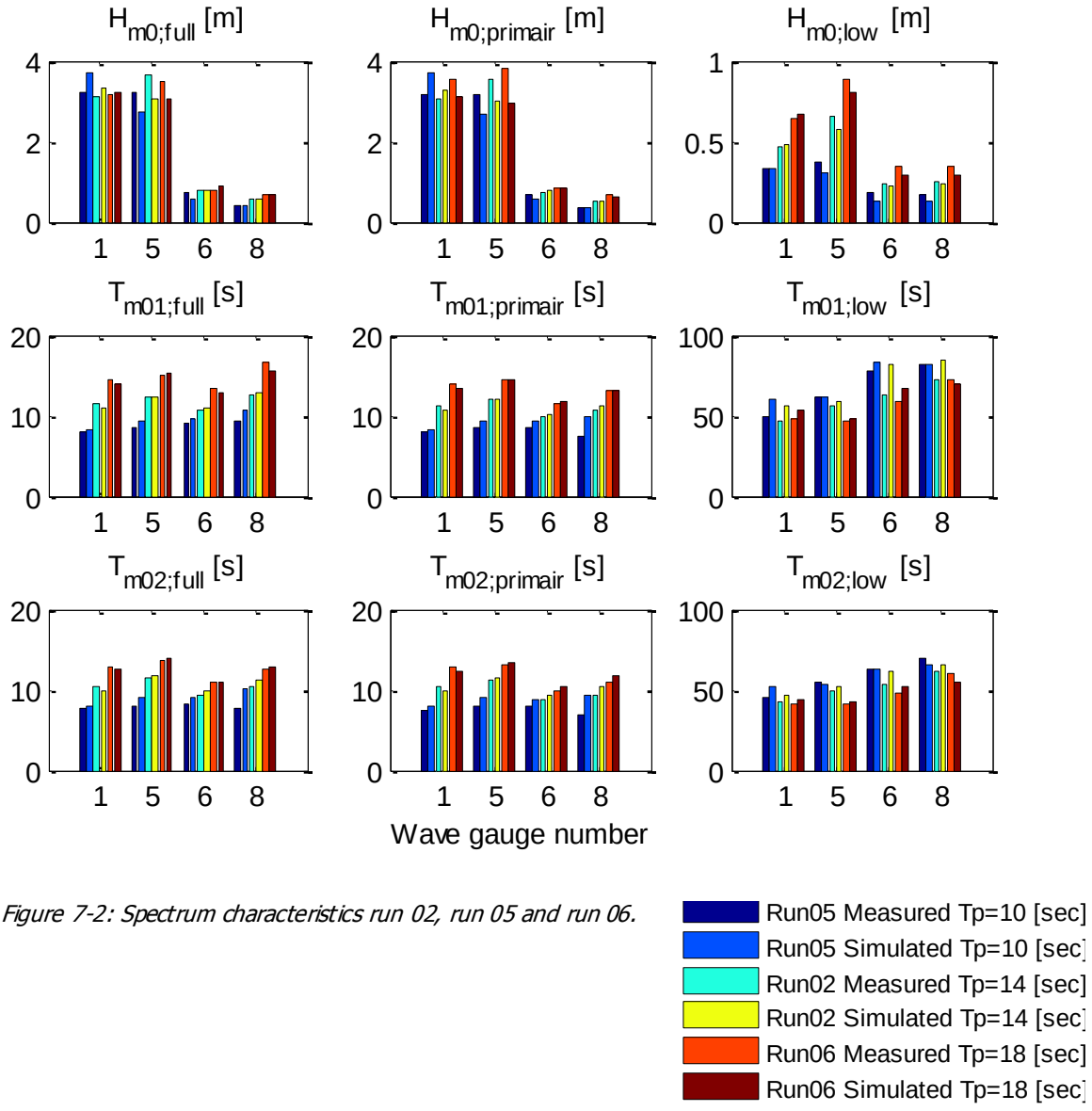

Figure 7-2: Spectrum characteristics run 02, run 05 and run 06.

Wave generating boundary

In run 07 to 09 the generated waves in TRITON are varied, see Figure C- 3 and Figure 7-3. In run 07 only primary waves are generated. The incoming bound long wave associated with the primary waves groups is now generated within the computational domain of TRITON in combination with spurious free waves. Not imposing a bound long wave already in the incoming time-serie led to a significant underestimation of the total amount of low frequency energy compared to measurements. The calculated low frequency wave height ($H_{m0;low}$) is decreased with a factor two.

An improvement in the agreement between measurements and simulations is made by defining a second order boundary condition for the generated waves. Instead of only generating primary waves a theoretical bound long waves associated with the primary waves is now imposed in the incoming time-serie. Although the amount of wave energy at the lower frequencies is increased there is an underestimation of low frequency wave energy noticed at wave gauge 1 and 5. At wave gauge 6 and 8 the simulated low frequency wave height is slightly underestimated compared to measurements. Although the simulated low frequency wave height is almost equal to the measured low frequency wave height, the distribution over the corresponding frequencies is not well predicted. From the wave spectrum and the calculation of the spectral periods it is observed that there is an accumulation of wave energy for the very low frequencies (<0.005Hz), which does not correspond with a peak in the measured wave spectrum. An explanation for this accumulation of wave energy at these very low frequencies cannot be given. The expected ship response for these energetic very low frequency waves is however low, see Figure 3-6.

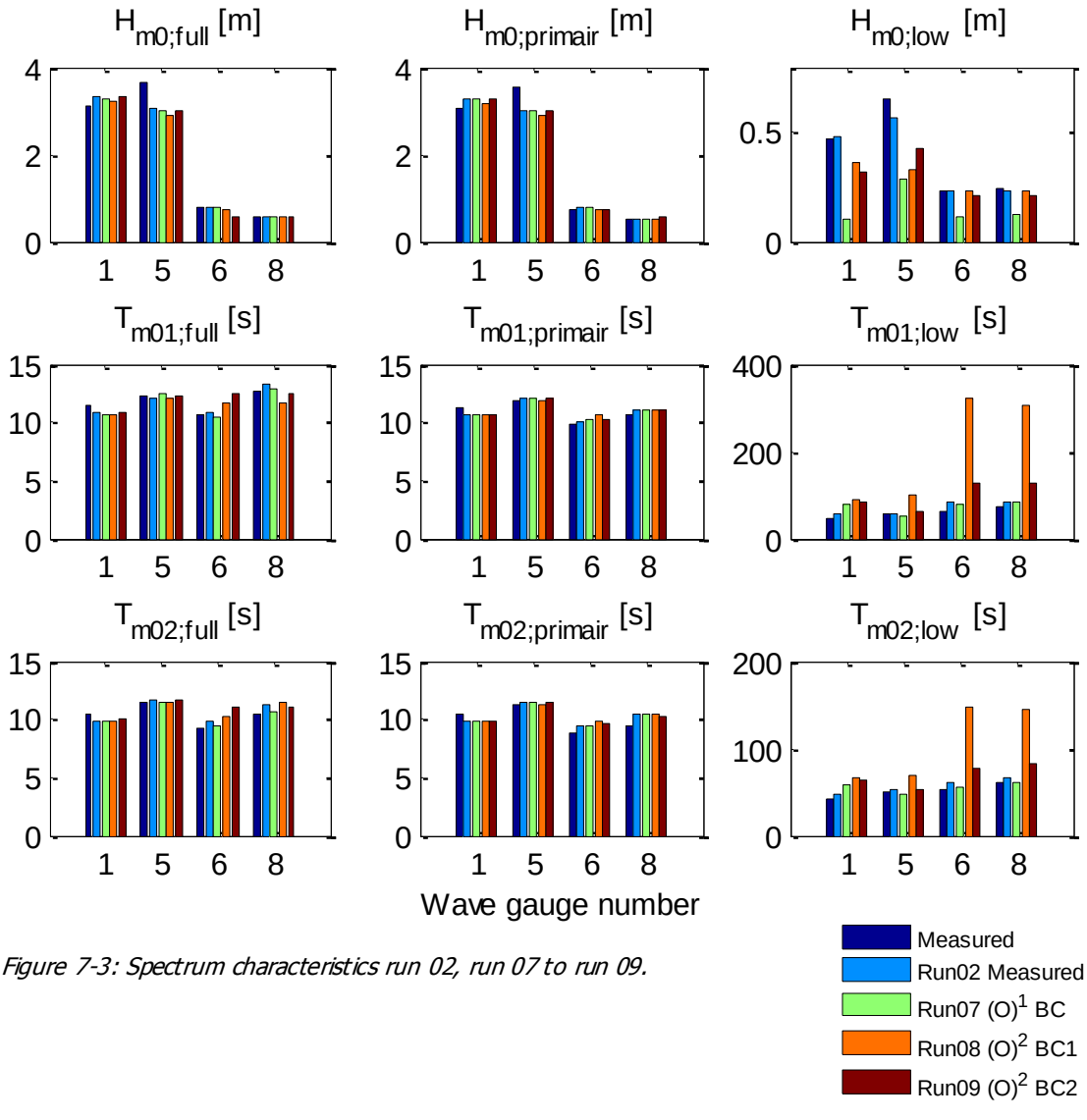

Figure 7-3: Spectrum characteristics run 02, run 07 to run 09.

A better agreement between simulations and measurements by imposing a bound long wave was expected, since during physical model tests second order wave steering was used. In case of second order wave steering in the simulations within TRITON it is remarkable that especially the energy density in the range 0.02~0.04Hz is less compared to measurements. Since a wave spectrum does not include directional information only possible explanations can be given for this shortage.

This shortage may be due to:

- Shortcomings in the description of the theoretical bound long wave.
- Possible measured (re-)reflected free waves from the wave maker, which are not absorbed.
- Transverse measured waves standing between the guide wall and the side wall of the physical model basin. These waves are not or partly absorbed, since the absorption of the wave maker mainly absorbs normal incident waves.
- Scattering of primary waves from the breakwaterhead, which interact with generated incident waves resulting in radiated free long waves
- Free long waves which are released due to diffraction of the primary waves.
- More energetic waves reflecting from the beach (V in Figure 2-8).

Since negligible moored ship response for waves with these frequencies (0.02~0.04Hz) is measured, see Figure 3-6, this shortage will not be investigated further.

Additional simulations

For the wave spectra for run 10 and 11 one is referred to Figure C- 4, whereas the spectrum characteristics can be found in Figure 7-5. In run 10 the head of the breakwater is enlarged by replacing the partial boundaries of the head of the breakwater. The adaptation mainly influences the simulated primary waves at wave probe 6 and 8. The breakwaterhead as modelled in run 02 gave an small underestimation of the most energetic primary waves at wave probe 6, whereas in simulation 10 the underestimation of the most energetic waves is more significant. Adaptation of the breakwaterhead did not lead to major changes in the low frequency spectrum, but less energy is transferred to frequencies around 0.02 Hz in the vicinity of the ship.

The reason why less wave energy is transferred to sub-harmonics is the following:
The breakwaterhead is a discontinuity in the bathymetry at which free long waves are released, see Figure 2-17. By replacing the partial reflecting boundaries of the breakwaterhead bathymetrical information is missing. Due to the adaptation of the breakwaterhead primary wave shoaling and the generation of sub-harmonics at the harbour entrance is taken less into account, see Figure 7-4.

The resulting effects on the waves due to adaptations of the breakwaterhead are small, but less wave energy is transferred to the sub-harmonics with frequencies around 0.02 Hz. As stated in the section above the moored ship response for these wave frequencies is low and therefore less important.

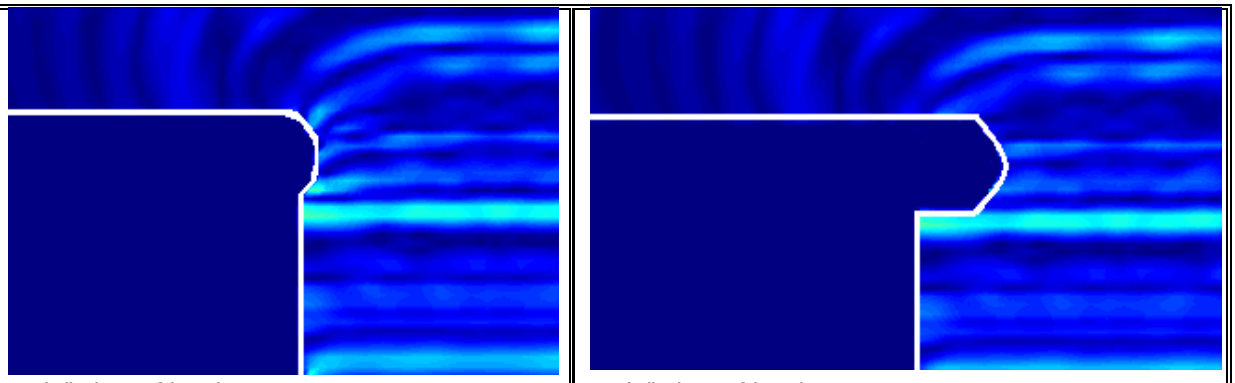

Figure 7-4: Schematization tip of breakwater in TRITON.

After run 11 some remarkable results are obtained:

- A lower primary wave height at wave gauge 1 and 5 compared with the base run.
- A higher primary wave height at wave gauge 6 and 8 compared with the base run.
- Significant less low frequency energy at wave probe 5 compared to the base run.

The differences in calculated wave heights are small, see Figure 7-5. The wave spectrum however significantly changed in spectral shape, see Figure C- 4. Possibly more wave energy is transferred into super-harmonics. These super-harmonics have high frequencies and are for moored ship responses less relevant.

The obtained results are influenced by some numerical imperfections. Partial reflecting boundaries in TRITON are not designed for waves that propagate along the model boundary. As a result the generated waves that propagate along the model boundary are affected. This results in a distorted view in the surface elevations as well as the flow field. This distorted view is due to diffraction losses as well as numerical imperfections, see Figure 7-6. The boundary condition at the side wall is open for all outgoing waves, but since the generated incoming waves are affected as well the final results are not representative.

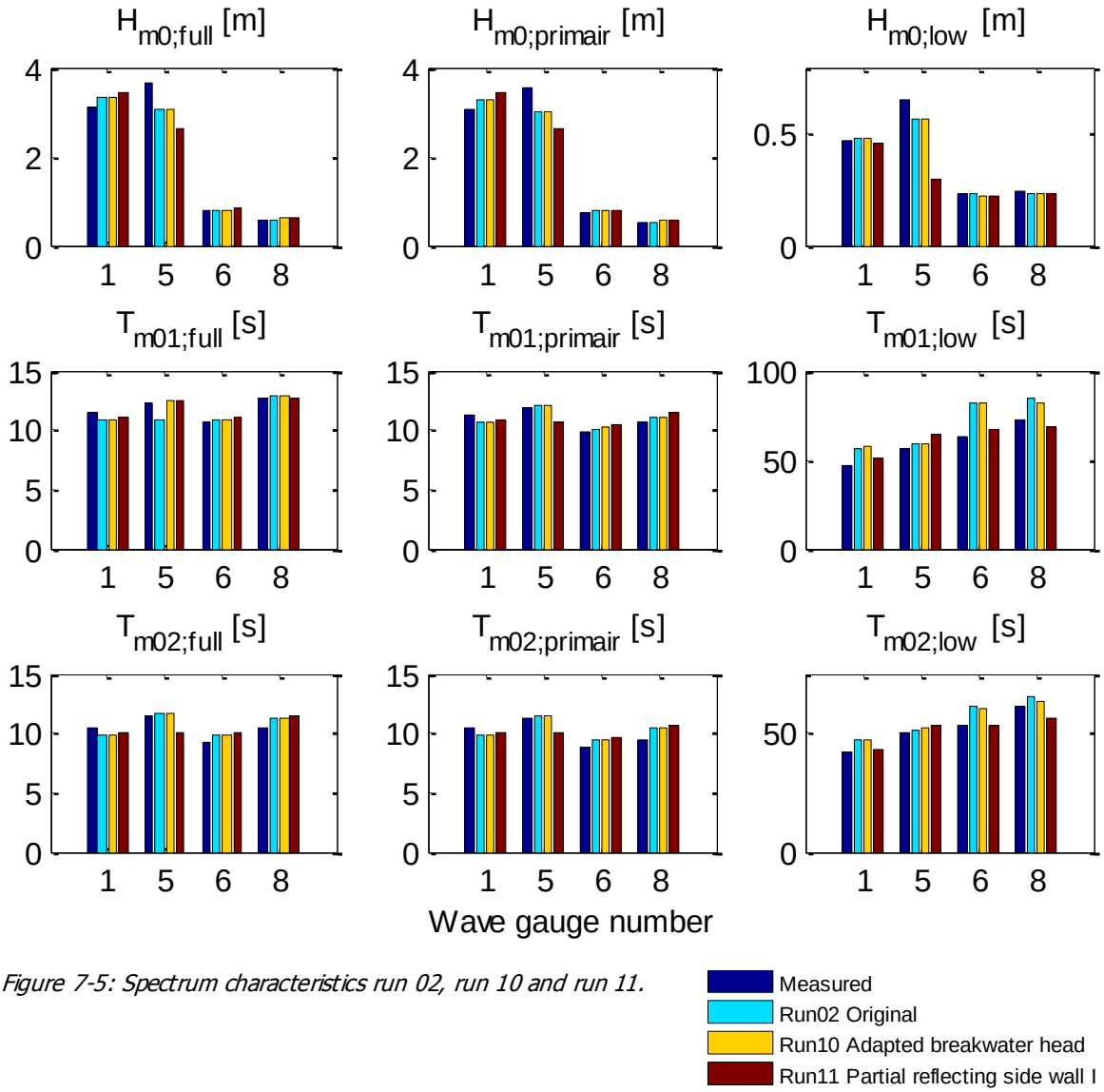

Figure 7-5: Spectrum characteristics run 02, run 10 and run 11.

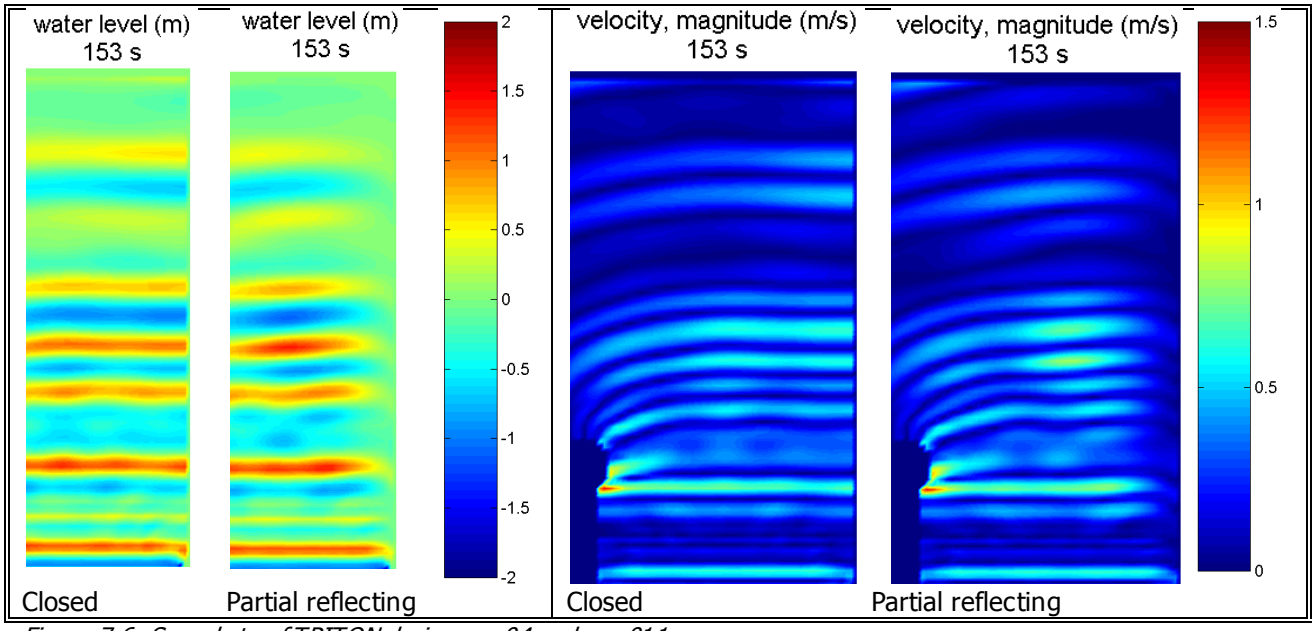

Figure 7-6: Snapshots of TRITON during run 04 and run 011.

Remarks

After run 01 to run 11 the following should be remarked:

- There is a difference in wave energy at wave gauge 1 for very low frequencies around 0.005Hz.
- In the vicinity of the ship (at wave gauge 6 and 8) the amount of low frequency wave energy is well predicted, but the distribution of energy over the corresponding frequencies is not well predicted. TRITON overestimates the amount of low frequency energy at very low frequencies compared to measurements. The measured peaks in the wave spectra are not simulated in TRITON.

The difference in wave energy at wave probe 1 for the very low frequencies around 0.005Hz, may be a consequence of the following reasons:

- The distance between the beach and wave maker in the physical model differs from the numerical model since the wave are generated at the location of the first wave probe instead of the wave maker.
- The generation line in the numerical model reflects wave energy for these very low frequencies. An improvement in TRITON at the wave generation line can be made by decreasing the reflection of the generation line (in this case $\omega_{explicit}$ instead of C_r).
- Generation of a so called evanescent wave, for which the amplitude decays exponentially from the boundary.

Since the difference in wave energy at very low frequencies (around 0.005Hz) is only noticed at wave gauge 1 and not at wave gauge 5 it is most likely the latter reason. This evanescent wave is a local numerical spurious wave with a small amplitude which decays exponentially from the boundary. The evanescent wave is thus a local disturbance and will not have any effects on a global scale (locations of the other wave gauges).

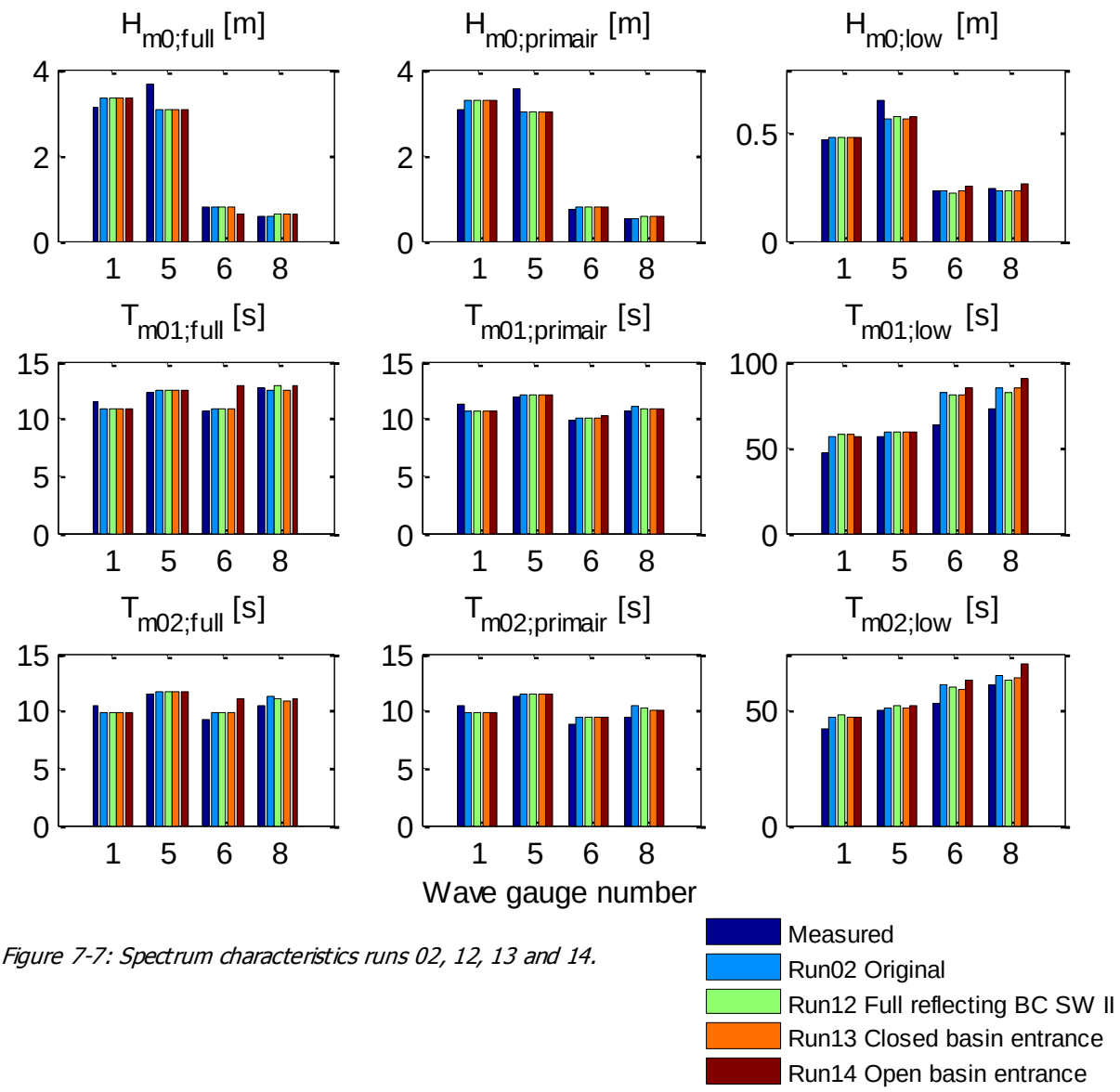

Figure 7-7: Spectrum characteristics runs 02, 12, 13 and 14.

In run 12 the reflection coefficient of the beach and the porous beach at sidewall II are higher, see Figure 6-1. Adaptation of this reflection coefficient has no effect on the primary wave spectrum, but does affect the spectral density around 0.01Hz at wave probes 6 and 8. Taking the changes in simulated spectral density into account as well as the combined measured spectra of waves and surge motion (see Figure 3-6) it supports that the wave direction of the generated sub-harmonics is mainly parallel relative to the North breakwater.

Although the reflection coefficient of the model boundary is increased for the porous absorbent beach the simulated spectral density decreased. Two possible explanations can be given:

- Physical: a standing wave pattern is formed and the output location is placed in a node.
- Numerical: spurious free waves due to a deviated reflection coefficient of the model boundary.

For waves with a frequency of 0.01Hz all structures will fully reflect and physically the same standing wave patterns will be generated compared to the original run (run 02). Since the conditions for both runs were constant, except for the reflection coefficient of the model boundaries, a numerical reason must be the underlying reason.

The numerical reason will be explained with an example for which a typical wave period of 14 seconds is assumed. The performance of the partial boundary condition procedure in TRITON is depending on a typical period (usually chosen as T_p), which is defined in the input. The model boundary is expecting waves with the typical wave period and the partial reflection coefficient is valid for those waves. For waves with periods close to the typical period (e.g. 10~18 seconds) the reflected wave is correctly calculated as well. If the difference between the typical period and the wave period is very large (e.g. typical wave period of 14 seconds versus an incoming wave period of 100 seconds) the amplitude of the reflected wave may be different than expected based on the reflection coefficient. Although this effect may be small in absolute terms (amplitude), for the small amplitude waves as considered here this effect may be relative large (in terms of spectral density, which is quadratic depending on the wave amplitude). The performance of partial boundary conditions in TRITON is subjected to further research and outside the scope of this thesis. The difference between run 02 and run 12 is expected to be so small that it would not have any effect on the response of the moored ship.

In simulations 13 and 14 a modification is made in the harbour configuration. In the original simulations the bathymetry as well as the boundary conditions were represented as accurate as possible. The configuration did however not include the harbour basin, which was reproduced in the physical model, see Figure 6-1. The expectation was that the short waves will break on the porous beach installed at the entrance of the harbour basin (see detail Figure 2-8) and small reflection from the porous beach was expected. The entrance to the harbour basin was therefore initially schematized as a partial reflecting boundary with a low reflection coefficient. By increasing the reflection coefficient of the porous beach contradicting results were obtained, see discussion run 12.

After simulation 13 the peak at a frequency of 0.015Hz at wave probe 6 becomes more pronounced (see Figure 7-8), which is possibly due to a simulated standing wave (see both measured and simulated peaks in wave spectra). The resulting effect is small and only some specific simulated wave amplitudes differ, which causes the differences in the simulated spectral density.

In run 14 an arbitrary basin is added. Due to the arbitrary basin an shift towards the frequency of 0.005 Hz is noticed compared to previous simulations (see also calculated spectral period in Figure 7-7). The first measured peak in the vicinity of the ship becomes more pronounced and is now simulated (see Figure C- 5). The effect of the added basin becomes more pronounced when less smoothing is applied to the presented wave spectrum, see Figure 7-8. It should be noticed that the number of frequency bins for both simulations and measurements are equal and constant smoothing is applied.

TRITON did not simulate the peak at a wave frequency of 0.006Hz during all simulations, whereas a peak for these frequencies is measured. After inclusion of a basin in run 14 a peak appears at a frequency of 0.007Hz in the simulated wave spectrum. An increase in wave energy, due to a standing wave, at the correct corresponding frequencies is indentified and an improvement in the agreement between measurements and simulations is obtained.

Possibly long wave transmission took place through the designed porous beach installed at the entrance of the basin (VII in Figure 2-8). Since there is no damping installed in the physical model basin, the generated free long waves may amplify and as a result a standing wave is formed in the physical model basin. Although the response amplitude is not correctly scaled, the corresponding frequencies at which resonant amplification occurred is correctly simulated. The measured peak at a frequency of 0.016Hz at wave gauge 6 is still not simulated, but this peak may very well correspond to the second mode of the standing wave.

The mismatch in amplitude between measurements and simulations at frequencies around 0.005Hz for runs 01 to 13 is possibly caused by spurious free reflected waves, due to the finite sizes of the physical model basin. A transverse standing wave was already suggested to be a possible cause for the found local peaks in the wave spectra, see chapter 3. The assumption was endorsed by the measured surge motion and wave spectra, see Figure 3-6. The simulated basin in TRITON is smaller than the harbour basin build in the physical model. Due to space limitations the represented harbour basin in the physical model is a smaller reproduction of the total harbour basin (i.e. the total harbour of Leixões).

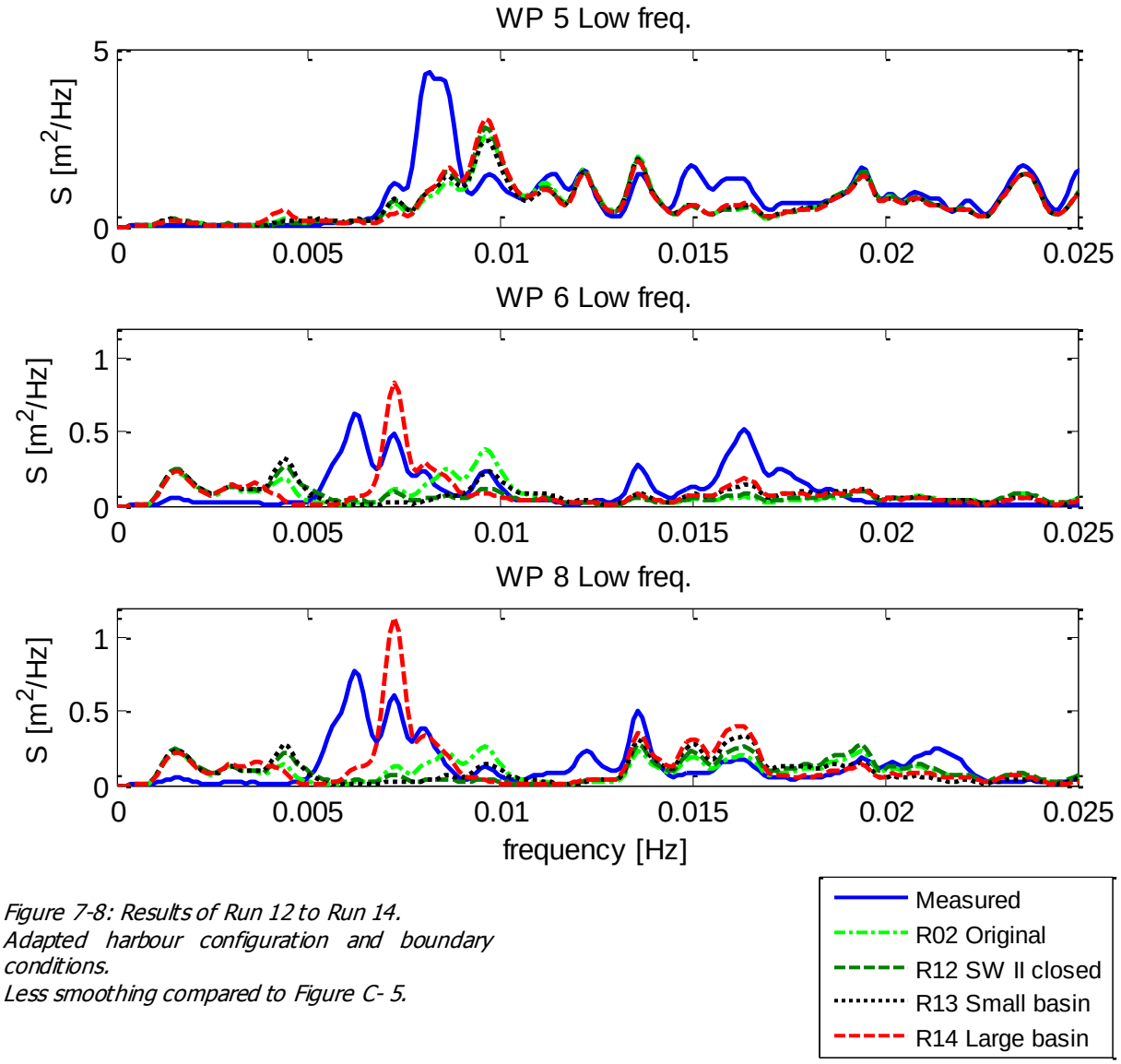

Figure 7-8: Results of Run 12 to Run 14.
Adapted harbour configuration and boundary conditions.
Less smoothing compared to Figure C- 5.

7.1 Summary of simulations

After the performed simulations in TRITON the following can be concluded:

- The harbour configuration is important to obtain standing waves with the corresponding low frequencies.
- Changes in reflection coefficients for partial reflecting boundaries had a minor effect on the obtained wave spectrum.
- Whether or not imposing a bound long wave in the generation of waves had a major effect on the obtained low frequency spectrum.
- Increasing the spectral peak period of the primary waves resulted in an increase of the amplitudes of the low frequency waves.

Based on the simulations carried out during this study some important factors for correctly modelling the waves for a port can be qualitatively judged, see Table 7-1.

	High frequency waves	Low frequency waves
Lay-out of the port	++	++
Reflection coefficients of port structures	+	+/-
Imposing a bound long wave in generated waves	-	+

Table 7-1: Qualitative judgement of sensitivity TRITON.

8 Discussion of Boussinesq-type wave model results

The simulations of MIKE21 BW and TRITON cannot be compared directly. This is due to the fact that alternative model set-ups and alternative numerical techniques are applied during simulations with both models. The final results of the simulations carried out with MIKE21 BW and the results of unstable TRITON simulations show similarities. In both cases eddies are observed in the computational domain. The eddies grew in both size as well as velocity magnitude during the simulations. Finally, the velocities of these eddies became dominant over the wave induced fluxes. Both velocity and magnitude of the generated eddies are thought to be physically unrealistic, but purely a consequence of numerical instabilities. Apart from suggesting that a numerical instability is the cause of excessive eddies within MIKE21BW as well as in TRITON, no evidence can be given.

MIKE21BW can become numerical unstable for various reasons, see DHI (2006A). Why MIKE21 BW became numerical unstable during this study is unknown. Attempts to stabilize MIKE21 BW in order to obtain longer periods of simulations did not work out. By altering the model set-up in TRITON stable model results were obtained for long period simulations. The effects of avoiding numerical instable boundaries are clearly visible after long time of simulation, see Appendix D.

It should be remarked that the major aspects (e.g. bathymetry, grid spacing and time-step) to set-up simulations in both Boussinesq-type wave models were kept constant. The main difference between both models is the inclusion of the boundary conditions (e.g. partial reflecting structures and wave generation) and alternative numerical schemes.

Based on the work in this study it cannot be concluded that either TRITON or MIKE21 BW is a better numerical model. Both numerical models have their strengths and weaknesses. The switch from MIKE21 BW to TRITON was made due to problems within MIKE21 BW. The switch to an alternative Boussinesq-type wave model was made, since the causes of numerical instabilities after long periods of simulation in MIKE21 BW could not be discovered by the model-user. Since long period simulations are required for the final goals e.g. obtaining ship motions, the switch to TRITON was logical and finally successful for the purposes of this study. From the analysis made in chapter 5 it was concluded that the obtained ship motions, based on computations with MIKE21 BW, due to numerical instabilities in the simulated fluxes were not reliable.

9 Conclusions and recommendations

9.1 Conclusions

The original objective of this study was to simulate the moored ship motions at berth "A" in the Port of Leixões by applying a sequence of numerical models:

- In order to predict the wave motions at berth "A" in the Port of Leixões the effects of diffraction, partial reflection and non-linear wave interaction are relevant hydrodynamic processes. To include the relevant hydrodynamic processes an appropriate Boussinesq-type wave model was selected.
- It is possible to simulate ship motions based on the output of Boussinesq-type wave models which serve as an input for a panel model. The calculated wave forces from the panel model serve as an input for a ship simulation model.
- To obtain statistical reliable ship motions the applied Boussinesq-type wave model should be robust enough to simulate waves over several hours, meanwhile describing the relevant hydrodynamic processes in an accurate way.

In the initial approach the Boussinesq-type wave model MIKE21 BW was applied, which became numerical unstable. The cause for these numerical instabilities within MIKE21 BW could not be discovered during this study, but based on the performed simulations the following can be concluded:

- Numerical instabilities may cause unwanted effects expressed in the velocity field of a Boussinesq-type wave model.
- Numerical instabilities in the velocity field of the Boussinesq-type wave model resulting in eddies with high velocities magnitudes will cause an increase in calculated second order wave forces on the ship, if these eddies are located in the vicinity of the ship.
- As a consequence of numerical instabilities in the simulated velocity field the wave forces on the ship and thus the obtained ship motions are not reliable.

A switch was made during this study to the Boussinesq-type wave model TRITON and the original objective adjusted. The focus of this study is shifted to simulate the low frequency waves that caused the ship motions during the physical model tests. From the simulations carried out with the Boussinesq-type wave model TRITON the following can be concluded:

- Not imposing 2nd order boundary conditions in TRITON may lead to an underestimation of low frequency energy compared to measurements if 2nd order boundary are simulated during physical model tests.
- TRITON is well able to predict possible basin oscillations.
- A measured standing wave in the physical model is the main cause of the measured surge responses of the moored vessel.
- The wave simulations as performed with TRITON are expected to be sufficiently accurate to serve as an input for vessel response computations.
- The wave simulations as performed with TRITON may serve as a base for further research.

9.2 Recommendations

Numerical modelling:

- Modelling of the total Port of Leixões with a Boussinesq-type wave model (or equivalent), taking into account all relevant hydrodynamic processes for moored vessel response.
- Further investigation of the moored ship motions based on simulations with the Boussinesq-type wave model TRITON or equivalent model. The wave forces on the ship should be calculated with the panel model Harberth or equivalent model.

Physical modelling (in case of additional tests):

- Place wave gauges in the corners of the physical model basin to discover possible spurious basin resonance.
- Consider the options of wave splitting, since this may provide more insight in the origin of the generated free waves in the physical model.

DOLPHIN project:

- Perform wave measurements inside and outside the Port of Leixões to calibrate and validate both physical and numerical models.
- Perform local ship motion measurements to calibrate and validate both physical and numerical models.
- Long wave transmission through the permeable core of the North breakwater may result in sway motions of the moored vessel. It is recommended to take this mechanism into account when analysing prototype measurements.

Bibliography

Baldock, T.E., Huntley, D.A., Bird, P.A.D., O'Hare, T.O. and Bullock, G.N. (2000). Breakpoint generated surf beat induced by bichromatic wave groups. *Coastal Engineering, 39, p.213-242.*

Baldock, T.E., and Huntley, D.A. (2002). Long-wave forcing by the breaking of random gravity waves on a beach. *Proceedings Royal Society Londen, serie A 458, p.2177-2201.*

Battjes, J.A. (1974). Surf similarity. *14th International conference on Coastal Engingeering, ASCE, p.466-480.*

Battjes, J.A., Bakkenes, H.J., Janssen, T.T., and Van Dongeren, A. (2004). Shoaling of subharmonic gravity waves. *Journal Geophysical Research, 109, C02009.*

Beck, R.F. (1994). Time-domain computations for floating bodies. *Applied Ocean Research, 16, p.267-282.*

Bingham, H.B. (2000). A hybrid Boussinesq-panel method for predicting the motion of a moored ship. *Coastal Engineering, 40, p. 21-38.*

Borsboom, M.J.A., Doorn, N., Groeneweg, J., and Van Gent, M.R.A. (2000). A Boussinesq-type wave model that conserves both mass and momentum. *Proceedings 27th ICCE Conference, Sydney, p. 148-161.*

Borsboom, M.J.A., Groeneweg, J., Doorn, N., and Van Gent, M.R.A. (2001). Flexible boundary conditions for a Boussinesq-type wave model. *Waves Conference, San Fransisco, United States of America.*

Bosboom, J. and Stive, M.J.F. (2010). Coastal dynamics 1. Lecture notes CT4305 Part 1, Delft University of Technology, The Netherlands.

Bowers, E.C. (1977). Harbour resonance due to set-down beneath wave groups. *Journal Fluid Mechanics, 79, p.71-92.*

Brandi Mortensen, S. (2006). Numerical modeling of the surf zone dynamics in Waimea Bay. Msc. Thesis, Technical University of Denmark, Denmark.

Cummins, W.E. (1962). The impulse response function and ship motions. *International Symposium on Ship Theory, Hamburg, Germany, nr. 8.*

De Bont, J., (2009). Validation of a numerical model for motions of ships moored with MoorMaster™ units, in a harbour under influence of ocean waves. Msc. Thesis, Delft University of Technology, The Netherlands.

De Girolamo, P, (1996). An experiment on harbour resonance induced by incident regular waves and irregular short waves. *Coastal Engineering, 27, p.47-66.*

De Jong, M.P.C., Borsboom, M.J.A. and Dekker J. (2009). Calculation of low-frequency waves in shallow water and comparison to common practice in diffraction methods. *Proceedings of the 28th International Conference on Ocean, Offshore and Arctic Engineering, Honolulu, Hawaii, USA.*

De Jong, M.P.C., Borsboom, M.J.A., De Bont, J.A.M, and Van Vossen, B. (2011). Evaluation of an extended operational Boussinesq-type wave model for calculating low-frequency waves in intermediate depths. *Accepted for presentation at the ASME 2011 30th International Conference on Ocean, Offshore and Arctic Engineering OMAE2011, June 19-24, 2011, Rotterdam, The Netherlands.*

Deltares (2008). Triton 1.0: User and technical manual. Delft, The Netherlands.

DHI (2005). Mike21 Boussinesq wave module: Short description. Hørsholm, Denmark.

DHI (2006A). Mike21 Boussinesq wave module: User guide. Hørsholm, Denmark.

DHI (2006B). Mike21 Toolbox: User guide. Hørsholm, Denmark.

Gallagher, B. (1971). Generation of surfbeats by non-linear wave interactions. *Journal Fluid Mechanics, 49, p.1-20.*

Herbers, T.H.C., Elgar, S., and Guza, R.T. (1994). Infragravity-Frequency (0.005-0.05Hz) Motions on the shelf. Part I: Forced waves. *Journal of Physical Oceanography, 24, p.917-927.*

Herbers, T.H.C, Elgar, S., and Guza, R.T. (1995A). Generation and propagation of infragravity waves. *Journal Geophysical Research, 100, p.24863-24872.*

Herbers, T.H.C, Elgar, S., Guza, R.T., and O'Reilly, W.C. (1995B). Infragravity-Frequency (0.005-0.05Hz) Motions on the shelf. Part II: Free waves. *Journal of Physical Oceanography, 25, p.1063-1079.*

Holthuijsen, L. (2007). Waves in oceanic and coastal waters. Cambridge University Press.

Huntley, D.A., Guza, R.T., and Thornton, E.B. (1981). Field observations of surf beats Part 1: Progressive edge waves. *Journal Geophysical Research, 86, p.6451-6466.*

Journée, J.M.J., and Massie, W.W. (2001). Offshore hydromechanics, First edition, Delft University of Technology, The Netherlands.

Kofoed-Hansen, H., Kerper, D.R., Sørensen, O.R., and Kirkegaard, J. (2005). Simulation of long wave agitation in ports and harbours using a time-domain Boussinesq model. *Proceedings of Fifth International Symposium on Ocean Wave Measurement and Analysis-Wave, Madrid, Spain.*

Kofoed-Hansen, H., Sloth, P., Sørensen, O.R., and Fuchs, J. (2000). Combined numerical and physical modelling of seiching in exposed new marina. *Proceedings of 27th International Coastal Engineering Conference, Sydney, Australia*

Korsmeyer, F.T, and Sclavounos, P.D., (1989). The large-time asymptotic expansion of the impulse response function for a floating body. *Applied Ocean Research, Vol. 11, No. 2.*

Longuet-Higgings, M.S. and Stewart, R.W. (1962). Radiation stress and mass transport in gravity waves, with application to 'surf beats'. *Journal Fluid Mechanics, 13, p.529-562.*

Madsen, P.A., (1983). Wave reflection from a vertical permeable wave absorber. *Coastal Engineering, 7, p.381-396.*

Madsen, P.A., Murray, R., and Sørensen, O.R., (1991). A new form of Boussinesq equations with improved linear dispersion characteristics. Part 1. *Coastal Engineering, 15, p. 371-388.*

Madsen, P.A., and Sørensen, O.R., (1992). A new form of Boussinesq equations with improved linear dispersion characteristics. Part 2: A slowly-varying bathymetry. *Coastal Engineering, 18, p. 183-204.*

Madsen, P.A., and Sørensen, O.R., (1993). Bound waves and triad interactions in shallow water. *Ocean Engineering, 20, p. 359-388.*

Madsen, P.A., Sørensen, O.R., and Schäffer, H.A, (1997). Surf zone dynamics simulated by a Boussinesq type model. Part I: Model description and cross-shore motion of regular waves. *Coastal Engineering, 32, p. 255-287.*

Madsen, P.A., Sørensen, O.R., and Schäffer, H.A, (1997). Surf zone dynamics simulated by a Boussinesq type model. Part II: Surf beat and swash zone oscillations for wave groups and irregular waves. *Coastal Engineering, 32, p. 289-320.*

Madsen, P.A., Bingham, H.B., and Schäffer, H.A., (2003). Boussinesq-type formulations for fully nonlinear and extremely dispersive water waves: derivation and analysis. *Proceedings of the Royal Society London, Part A, 489, p. 1075-1104*

Mahmoodian, M. (2009). Impact assessment of a new wave energy converter, Anaconda. Msc. Thesis. University of Southampton.

Mei, C.C. and Agnon, Y. (1989). Long-period oscillations in a harbour induced by incident short waves. *Journal Fluid Mechanics, 208, p. 595-608.*

Munk, W.H. (1949). Surfbeats. *Trans. Am. Geophys. Union 30, p.849-854.*

Muttray, M., Oumeraci, H. and Ten Oever, E. (2006). Wave reflection and wave run-up at rubble mound breakwaters. *International Conference on Coastal Engineering, San Diego, 2006.*

OCIMF (1997). Mooring equipments guidelines (Second edition). *Oil Companies International Marine Forum. London: Whiterby Seamanship International.*

OCIMF (2008). Mooring equipments guidelines (Third edition). *Oil Companies International Marine Forum. London: Whiterby Seamanship International.*
Peregrine, D.H. (1967). Long waves on a beach. *Journal Fluid Mechanics, 27, p. 815-827.*

PIANC (1995). Criteria for movements of moored ships in harbours: a practical guide. Supplement to bulletin no. 88. Report of working group PTC II-24.

Pinkster, J.A. (1980). Low frequency second order wave exciting forces on floating structures. PhD. thesis, Delft University of Technology, The Netherlands.

Pinkster J.A. (1995). Hydrodynamic interaction effects in waves. *Proc. 5th Int. Offshore and Polar Engineering, The Hague, Vol III, p.414-419.*

Rabinovich, A.B., (2009). *Handbook of coastal and ocean engineering Kim Y,* World Scientific.

Reniers, A.J.H.M., Roelvink, J.A., and Thornton, E.B. (2004). Morphodynamic modeling of an embayed beach under wave group forcing. *Journal of Geophysical Research, 109, C01030.*

Rosa-Santos, P. Veloso-Gomes, F., Taveira-Pinto, F., Guedes-Soares, C., Fonseca, N., Alfredo Santos, J., Paulo Moreira, A., Costa, P., and Brogueira-Dias, E. (2008A). Physical model study of the behavior of an oil tanker moored at a jetty. *Proc. on the 2nd International Conference on the Application of Physical Modeling to Port and Coastal Protection*, Coastlab 2008, Bari, Italy.

Rosa-Santos, P., Veloso-Gomes, F., Taveira-Pinto, F., Brogueira-Dias, E., and Guedes-Lopes, H. (2008B). Improving operational conditions at Leixões oil terminal, Portugal. *COPEDEC VII*, Dubai, UAE.

Rosa-Santos, P., Veloso-Gomes, F., Taveira-Pinto, F., Guedes-Soares, C., Fonseca, N., Paco, A, Paulo Moreira, A., Costa, P., Malheiros, P., and Brogueira-Dias, E. (2009) Influence of the use of mooring line pre-tension on the behavior of a moored oil tanker. *International Conference in Ocean Engingeering (ICOE2009)*, IIT Madras, Chennai, India.

Rosa-Santos, P., Veloso-Gomes, F., Taveira-Pinto, F., and Brógueira-Dias, E. (2010). Physical Modelling of Leixões Oil Terminal, Portugal. *Port Infrastructure Seminar*, Delft, The Netherlands.

Sand S.E., (1982). Long waves in directional seas. *Coastal Engineering, 6, p.195-208.*

Schäffer, H.A. (1993). Infragravity waves induced by short-wave groups. *Journal Fluid Mechanics, 247, p.551-588.*

Schäffer, H.A. and Sørensen, O.R (2006). On the internal wave generation in Boussinesq and mild-slope equations. *Coastal Engineering 53, p. 319-323*

Sempere, J. M. (2006). Study of the swell conditions affecting the moored ships in Coega Harbour (Cape Town, South-Africa) and proposal for improving the infrastructures. Msc. Thesis, Delft University of Technology, The Netherlands.

Sørensen, O.R., Schäffer, H.A. and Madsen, P.A. (1998). Surf zone dynamics simulated by a Boussinesq type model. III. Wave-induced horizontal nearshore circulations. *Coastal Engineering 33, p. 155-176.*

Symonds, G., Huntly, D.A., and Bowen, A.J. (1982). Two-dimensional surf-beat: long wave generation by a time-varying break point. *Journal Geophysical Research, 87, p.492-498.*

Taveira-Pinto, F., Veloso-Gomes, F., Rosa-Santos, P., Guedes-Soares, C., Fonseca, N., Alfredo Santos, J., Paulo Moreira, A., Costa, P., and Brogueira-Dias, E. (2008). Analysis of the behavior of moored tankers. *International Conference in Ocean Engingeering (OMAE2008)*, Estoril, Portugal.

Tucker, M.J. (1950). Surf beats: sea waves of 1 to 5 min. period. *Proceedings Royal Society Londen, serie A 202, p.565-573.*

Van Dongeren, A., Reniers, A., Battjes, J.A. and Svendsen, J. (2003). Numerical modeling of infragravity wave response during DELILAH. *Journal Geophysical Research, 108, 3288, doi:10.1029/2002JC001332*

Van der Molen, W., Monárdez, P., and Van Dongeren, A., (2006A). Numerical simulation of long-period waves and ship motions in Tomakomai Port. *Japan Coastal Engineering Journal, 48, p. 59-79.*

Van der Molen, W. (2006B). Behaviour of moored ships in harbours. PhD. thesis, Delft University of Technology, The Netherlands.

Van der Molen, W., and Wenneker, I., (2008). Time-domain calculation of moored ship motions in nonlinear waves. *Coastal Engineering, 55, p. 409-422.*

Van der Molen, W., (2009). Mike21-Harberth: Moored ship response modelling in harbours. User guide.

Van der Molen, W. and Moes, H. (2009). General characteristics of South African ports and the safe mooring of ships. *Proceedings of the 28th Southern African Transport Conference p.308-315.*

Van der Molen, W., Rossouw, M., Phelp, D., Tulsi, K., and Terblanche, L. (2010). Innovative technologies to accurately model waves and moored ship motions. *CSIR 3rd Biennial Conference 2010. Science Real and Relevant, CSIR International Convention Centre, Pertoria, South Africa*

Van Noorloos, J.C. (2003). Energy transfer between short wave groups and bound long waves on a plane slope. *MSc Thesis, Delft University of Technology, The Netherlands.*

Van Oortmerssen, G. (1976). The motions of a moored ship in waves. *PhD thesis, Delft University of Technology, The Netherlands.*

Veloso-Gomes, F. Taveira-Pinto, F., Rosa-Santos, P., Brogueira-Dias, E., and Guedes-Lopes, H. (2005). Berthing characteristics and the behavior of the oil terminal of Leixões Harbour, Portugal. *Marine Heritage and Modern Ports Wit-Press.*

Voogt, A., Bunnik, T., and Huijsmans, R.H.M. (2005). Validation of an analytical method to calculate wave setdown on current. *24th International Conference on Ocean, Offshore and Artic Engineering, 2005, Halkidiki, Greece.*

Waals, O.J. (2009). On the application of advanced wave analysis in shallow water model testing (wave splitting). *28th International Conference on Ocean, Offshore and Artic Engineering, 2009, Honolulu, Hawaii, U.S.A..*

Wenneker, I, Borsboom, M, Pinkster, J.A., Weiler, O. (2006). A Boussinesq-type wave model coupled to a diffraction model to simulate wave-induced ship motion. *31th PIANC Congress, Estoril, Portugal.*

Woo, S.B. and Liu, P.L.F. (2004). Finite-Element Model for Modified Boussinesq Equations. II: Applications to Nonlinear Harbor Oscillations. *Journal of Waterway, Port, Coastal and Ocean Engineering, 130, p. 17-28.*

Wu, J.K., and Liu, P.L.F. (1990). Habour excitations by incident wave groups. *Journal Fluid Mechanics, 217, p. 595-613.*

Appendices

Appendix A: Harberth formulations

Appendix B: Physical model results

Appendix C: TRITON simulations

Appendix D: Modification of model set-up boundary conditions in Boussinesq-type wave model TRITON

Appendix E: Alternative resonance mechanism

Appendix A. Harberth formulations

Harberth considers the ship in a fluid that is incompressible, homogeneous and irrotational. A definition sketch of the floating body in the computational domain is given in Figure A- 1. For further description a right-handed coordinate system is used. An explanation of the symbols is given in Table A- 1.

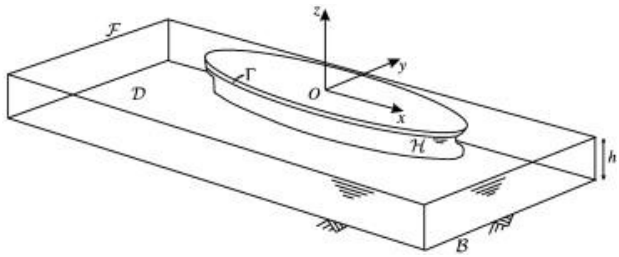

Figure A- 1: Computational domain Harberth

Symbol	Designation
$\mathcal{D}$	Computational model domain
$\mathcal{B}$	Sea floor
$\mathcal{F}$	Fluid surface
$\mathcal{H}$	Wetted surface of ship hull
Γ	Waterline
W	Wetted surface of fixed structures

Table A- 1: Harberth symbols

The fluid flow around the floating body is described by means of a velocity potential. The velocity potential can be described with:

$$\Phi = \phi^I + \phi^S + \sum_{j=1}^{6} \phi^j \qquad \textit{Eq. A- 1}$$

In which:

Φ	=	Total potential	[m^2/s]
ϕ^I	=	Incident wave potential	[m^2/s]
ϕ^S	=	Scattered wave potential	[m^2/s]
ϕ^j	=	Radiation potential in mode j	[m^2/s]

Radiation problem

The hydrodynamic coefficients can be obtained by solving the radiation problem. The radiation problem is treated for the body making an impulsive movement in initially sill water, according to:

$$\dot{X}_j(t) = \delta(t), \quad j = 1,2,...6 \qquad \textit{Eq. A- 2}$$

The radiation potential is decomposed into a impulsive and a time-varying part:

$$\phi^j(\vec{x},t) = \psi^j(\vec{x})\delta(t) + \chi^j(\vec{x},t) \qquad \textit{Eq. A- 3}$$

In which:

ψ^j	=	Impulsive part of the radiation potential	[m^2/s]
χ^j	=	Time-varying part of the radiation potential	[m^2/s]
$\delta(t)$	=	Dirac delta function (unit impulse function)	

The potentials have to fulfill the boundary conditions according to Table A- 2. BC [I] follows from the assumption of incompressible and irrotational flow. The dynamic boundary condition (BC [II]) applied at the free surface ensures that the pressure at the free surface equals the atmospherically pressure. BC [III] follows from the assumption that no water particles may leave the free surface. BC [IV] and [V] are no leak conditions, such that the velocities at the applied boundaries are zero. According to BC [VI] no fluid can cross the ship hull boundary by setting the velocity of the fluid equal to the velocity of the body boundary in the normal direction of the body surface. The radiation conditions (BC [VII] and [VIII]) ensures that the sources radiate waves, instead of absorbing them and that the potentials are outgoing at an infinitely large distance from the oscillating body.

Number:	Boundary condition:	Applied at:	Type of boundary condition:
[I]	$\nabla^2\chi^j = \frac{\partial^2\chi^j}{\partial x^2} + \frac{\partial^2\chi^j}{\partial y^2} + \frac{\partial^2\chi^j}{\partial z^2} = 0$	$\mathcal{D}$	Laplace or continuity condition
[II]	$\psi^j = 0$	$z = 0$	Linearized dynamic free surface condition
[III]	$\frac{\partial^2\chi^j}{\partial t^2} + g\frac{\partial\chi^j}{\partial z} = 0$	$z = 0$	Linearized kinematic free surface or Cauchy Poisson condition
[IV]	$\frac{\partial\chi^j}{\partial n} = 0$	$z = -h$ W and $\mathcal{H}$	Neumann / no leak condition
[V]	$\frac{\partial\psi^j}{\partial n} = 0$	$z = -h$ W	Neumann / no leak condition
[VI]	$\frac{\partial\psi^j}{\partial n} = n^j$	$\mathcal{H}$	Neumann condition
[VII]	$\underset{R\to\infty}{Lim}\left(\chi^j\right) = 0$	$R \to \infty$	Dirichlet or radiation condition
[VIII]	$\underset{R\to\infty}{Lim}\left(\psi^j\right) = 0$	$R \to \infty$	Dirichlet or radiation condition

Table A- 2: Boundary conditions radiation problem.

The applied Green functions will not be presented, for these functions one is referred to Van der Molen (2006B). The hydrodynamic forces can be obtained from pressure integration over the wetted hull. The wetted hull is divided in such a number of panels, that the velocities and pressure at each panel is assumed to be constant. Integration over the impulsive part of the radiation potential provides the added mass coefficients, while integration over the time-varying part of the radiation potential leads to the impulse response functions.

$$\boldsymbol{A}_{kj} = \rho\iint \psi^j n^k dS, \qquad k = 1,2,\ldots 6 \qquad \textit{Eq. A- 4}$$

$$\boldsymbol{K}_{kj}(t) = \rho\iint \frac{\partial\chi^j}{\partial t} n^k dS, \quad k = 1,2,\ldots 6 \qquad \textit{Eq. A- 5}$$

In which:

n^k = Outward pointing normal vector

dS = Surface element

Incident and scattered wave computation

The hull of the ship is described by panels in such a way that the pressure and velocity is assumed to be constant on each panel. Backward transformation of the depth-averaged velocity and pressure is required to find the original incident velocity and pressure distributions over the water depth. The formulations for both the velocities as well as the pressure are given as power series in Table A- 3. The power series are given in the obtained fluxes from Mike21 BW, in which d =still water level and $h = d + \zeta$. Subscripts x,y and t denote partial differentiation to space and time respectively.

The diffraction problem is solved for the scattering of waves around the floating body. Scattering of the incident wave around other fixed structures in the vicinity of the floating body is assumed to be included in the incident wave potential (which is obtained by the backward transformation as described before). The scattered potential have to fulfill the boundary conditions according to Table A- 4. The applied Green functions will not be presented, for these functions one is referred to Van der Molen (2006B).

Taylor expansion of imported data:	With:
$u(z) = u^{(0)} + \frac{1}{2}(z+d)^2 u^{(2)}$	$u^{(0)} = \frac{P}{h} + \frac{1}{6} dP_{xx} - \frac{1}{3} d_x P_x$ $u^{(2)} = -\frac{P_{xx}}{d}$
$v(z) = v^{(0)} + \frac{1}{2}(z+h)^2 v^{(2)}$	$v^{(0)} = \frac{Q}{h} + \frac{1}{6} dQ_{yy} - \frac{1}{3} d_y Q_y$ $v^{(2)} = -\frac{Q_{yy}}{d}$
$w(z) = w^{(0)} + (z+d) w^{(1)} + \frac{1}{6}(z+d)^3 w^{(3)}$	$w^{(0)} = -d_x \frac{P}{h} - d_y \frac{Q}{h}$ $w^{(1)} = -u_x^{(0)} - v_y^{(0)}$ $w^{(3)} = -u_x^{(2)} - v_y^{(2)}$
$p(z) = p^{(0)} + \frac{1}{2}(z+d)^2 p^{(2)}$	$p^{(0)} = \rho g \zeta - \frac{1}{2} d^2 p^{(2)}$ $\frac{p^{(2)}}{\rho} = -\frac{\zeta_{tt}}{d}(1+3B_B) + B_B g(\zeta_{xx} + \zeta_{yy})$ $+ \frac{d_x}{d}(\frac{P_t}{2d} + 3B_B g \zeta_x) + \frac{d_y}{d}(\frac{Q_t}{2d} + 3B_B g \zeta_y)$

Table A- 3: Power series of the imported data from the Boussinesq wave model Mike21BW

Number:	Boundary condition:	Applied at:	Type of boundary condition:
[I]	$\nabla^2 \phi^S = \frac{\partial^2 \phi^S}{\partial x^2} + \frac{\partial^2 \phi^S}{\partial y^2} + \frac{\partial^2 \phi^S}{\partial z^2} = 0$	$\mathcal{D}$	Laplace or continuity condition
[II]	$\frac{\partial^2 \phi^S}{\partial t^2} + g \frac{\partial \phi^S}{\partial z} = 0$	$z = 0$	Linearized kinematic free surface condition
[III]	$\frac{\partial \phi^I}{\partial n} + \frac{\partial \phi^S}{\partial n} = 0$	$\mathcal{H}$	Neumann condition
[IV]	$\frac{\partial \phi^S}{\partial n} = 0$	$z = -h$ and W	Neumann condition
[V]	$\lim_{R \to \infty}(\phi^S) = 0$	$R \to \infty$	Dirichlet or radiation condition

Table A- 4: Boundary conditions incident/scattered wave problem

BC [I] follows from the assumption of incompressible and irrotational flow. BC [II] follows from the assumption that no water particles may leave the free surface. The normal velocity in the scattered wave is the opposite of the normal velocity in the incident wave (see BC [III]), such that the boundary condition $\vec{V} \cdot \vec{n} = 0$ at the hull of the ship is fulfilled. According to BC [IV] no fluid can cross the ship hull boundary by setting the velocity of the fluid equal to the velocity of the body boundary in the normal direction of the body surface. The radiation condition (BC [V]) ensures that the source radiate waves, instead of absorbing them and that the potential is outgoing at an infinitely large distance from the oscillating body.

The first order wave forces, due to both incident and scattered wave, follow from integration of the first order pressures over the mean submerged hull. The pressure p is obtained by applying the Bernoulli equation:

$$-\frac{p-p_0}{\rho} = gz + \frac{\partial \Phi}{\partial t} + \frac{1}{2}\nabla\Phi \cdot \nabla\Phi + \text{constant} \qquad \textit{Eq. A- 6}$$

In which:

gz	=	Hydrostatic pressure	[m^2/s^2]
$\frac{\partial \Phi}{\partial t}$	=	Linear component of dynamic pressure	[m^2/s^2]
$\frac{1}{2}\nabla\Phi \cdot \nabla\Phi$	=	Quadratic pressure related to the second order forces	[m^2/s^2]

The Froude-Krylov force can be calculated due to integration of pressures in the undisturbed incident wave and the diffraction force is found by integration of pressures in the scattered wave. The total first order wave force follows from summation of the Froude-Krylov force plus the diffraction force. Second order wave effects are included in the first order forces, since a nonlinear wave model is used to compute the incident wave field. Other second order contributions are however not taken into account. These remaining terms for the second order force and moment include the products of first order quantities, due to relative wave height (first term RHS Eq. A-11 and Eq. A-12), second order pressure (second term RHS Eq. A-11 and Eq. A-12), products of first order pressures and first order body motions (third term RHS Eq. A-11 and Eq. A-12) and the contribution of the product of first order rotations and first order inertia forces (fourth term RHS Eq. A-11 and Eq. A-12), see also Pinkster (1980).

The general formulas to calculate the wave forces or moments are given by:

$$\vec{F} = -\int\int_S p\vec{n}dS \qquad \textit{Eq. A- 7}$$

$$\vec{M} = -\int\int_S p(\vec{x} - \vec{x}_G)\cdot\vec{n}dS \qquad \textit{Eq. A- 8}$$

In which:

p	=	Fluid pressure	[kN/m^2]
$\vec{n}$	=	Outward pointing normal vector of surface element	[-]
dS	=	Surface element	[m^2]
S	=	Total wetted surface of the body	[m^2]
$\vec{x}$	=	Coordinate of surface element	[m]
$\vec{x}_G$	=	Coordinate of the centre of gravity	[m]
$\vec{F}$	=	Force	[kN]
$\vec{M}$	=	Moment	[kNm]

The first order wave forces and moments due to the incident and scattered wave are given by:

$$\vec{\mathrm{F}}(\mathrm{O}^1) = \int\int \left(p^I - \rho \frac{\partial \Phi^S}{\partial t} \right) \vec{n} dS \qquad \textit{Eq. A- 9}$$

$$\vec{\mathrm{M}}(\mathrm{O}^1) = \int\int \left(p^I - \rho \frac{\partial \Phi^S}{\partial t} \right) (\vec{x} - \vec{x}_G) \cdot \vec{n} dS \qquad \textit{Eq. A- 10}$$

And the second order wave forces and moments are given by:

$$\vec{\mathrm{F}}(\mathrm{O}^2) = \frac{1}{2} \rho g \int_\Gamma (\zeta - \alpha_3)^2 \vec{n} dl - \rho \int\int \left(\frac{1}{2} \nabla\Phi \cdot \nabla\Phi + \vec{\alpha}(O^1) \cdot \nabla \frac{\partial \Phi}{\partial t} \right) \vec{n} dS + \vec{\Omega}(O^1) \cdot \boldsymbol{M} \ddot{\vec{X}}(O^1) \qquad \textit{Eq. A- 11}$$

$$\vec{\mathrm{M}}(\mathrm{O}^2) = \frac{1}{2} \rho g \int_\Gamma (\zeta - \alpha_3)^2 (\vec{x} - \vec{x}_G) \cdot \vec{n} dl - \int\int \left(\frac{1}{2} \nabla\Phi \cdot \nabla\Phi + \vec{\alpha}(O^1) \cdot \nabla \frac{\partial \Phi}{\partial t} \right) (\vec{x} - \vec{x}_G) \cdot \vec{n} dS + \vec{\Omega}(O^1) \cdot \boldsymbol{M} \ddot{\vec{\Omega}}(O^1) \qquad \textit{Eq. A- 12}$$

In which:

$\vec{\alpha} = \vec{X} + \vec{\Omega}(\vec{x} - \vec{x}_G) \cdot \vec{n}$	=	Total displacement	[m]
α_3	=	Displacement in vertical direction	[m]
Ω	=	Rotational displacement	[rad]
dl	=	Line element of the waterline	[m]

Appendix B. Physical model results

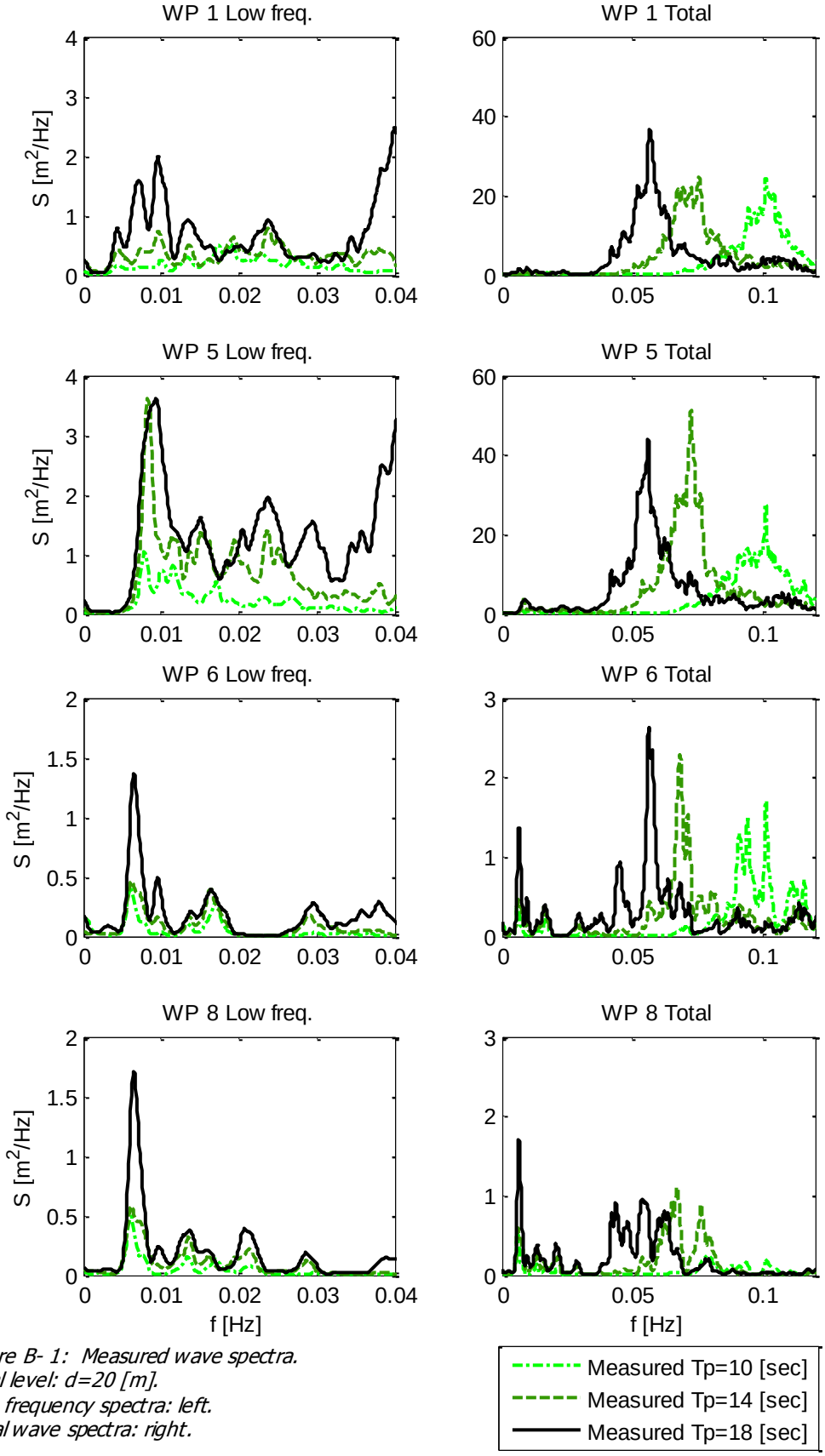

Figure B- 1: Measured wave spectra.
Tidal level: d=20 [m].
Low frequency spectra: left.
Total wave spectra: right.

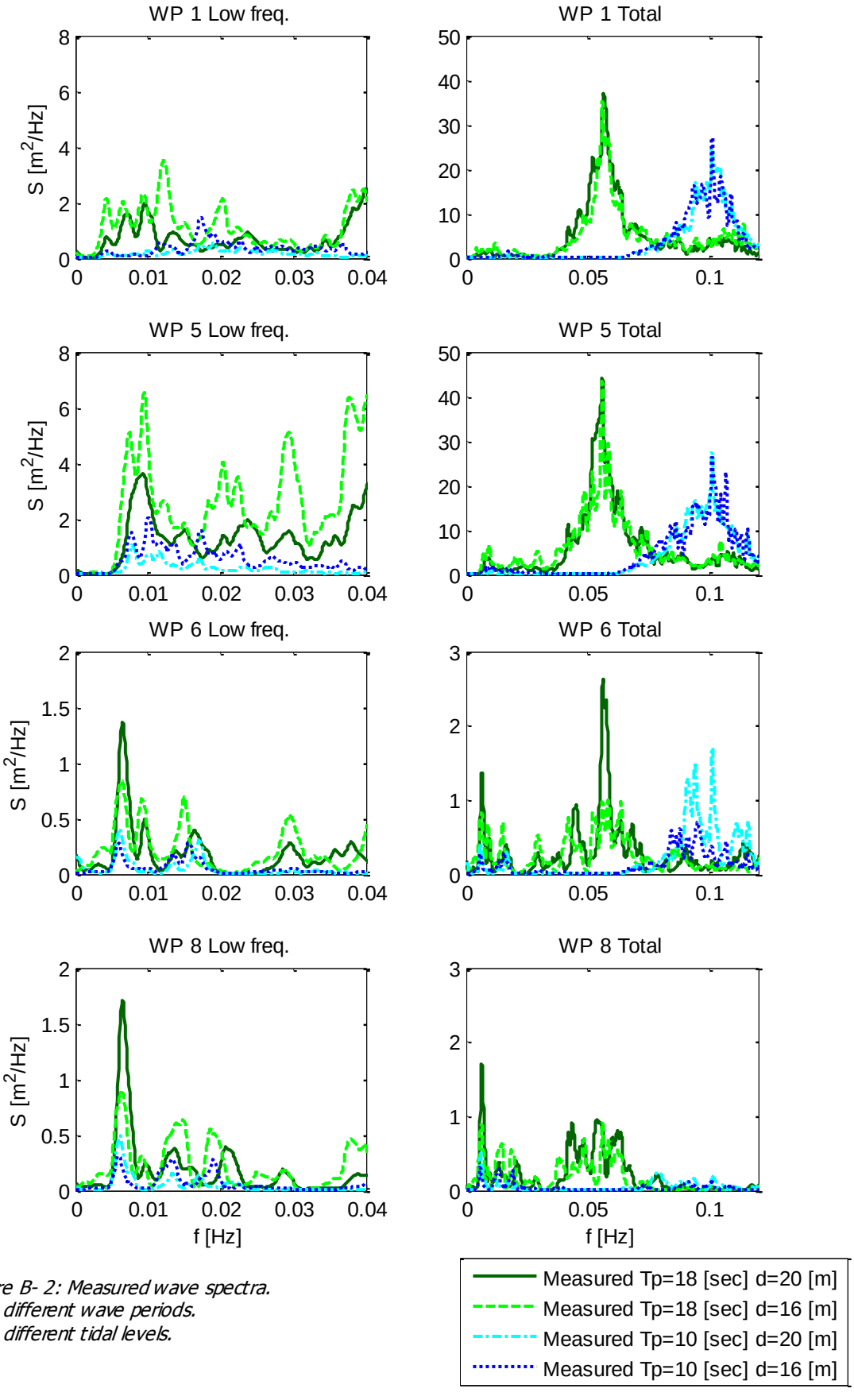

Figure B- 2: Measured wave spectra.
Two different wave periods.
Two different tidal levels.

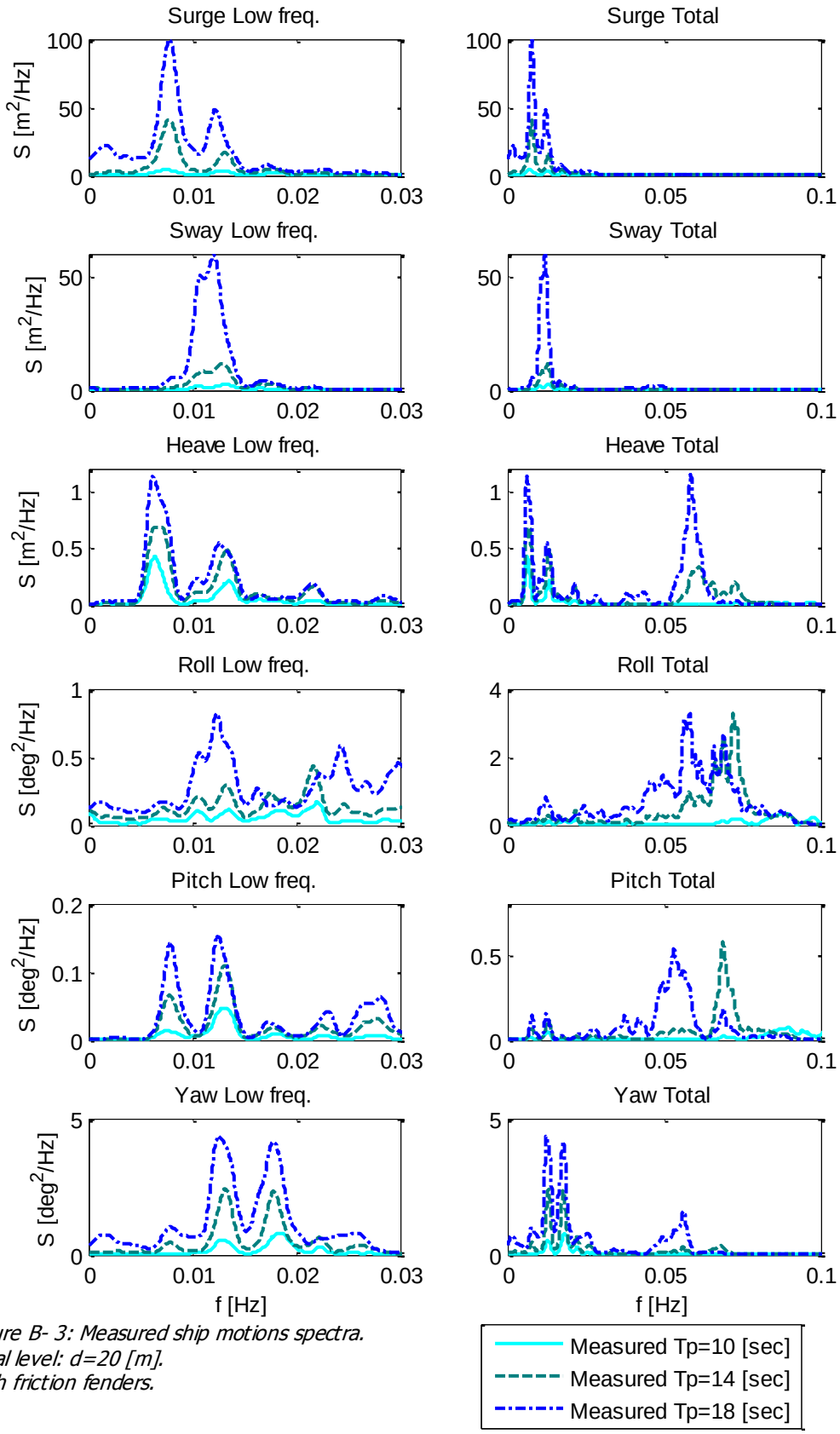

Figure B- 3: Measured ship motions spectra.
Tidal level: d=20 [m].
High friction fenders.

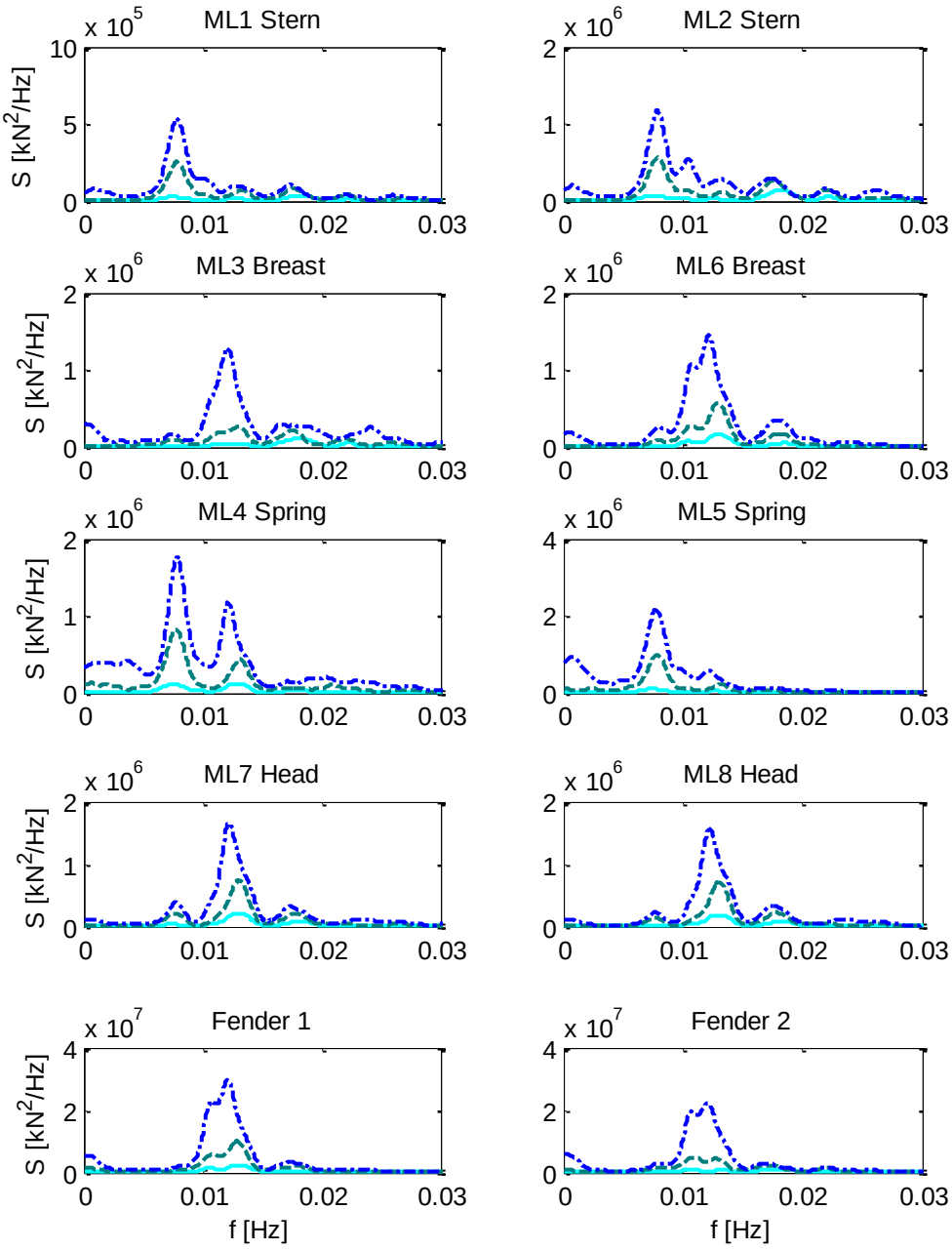

Figure B- 4: Measured spectra mooring lines.
Tidal level d=20 meter.
High friction fenders.

Appendix C. TRITON simulations

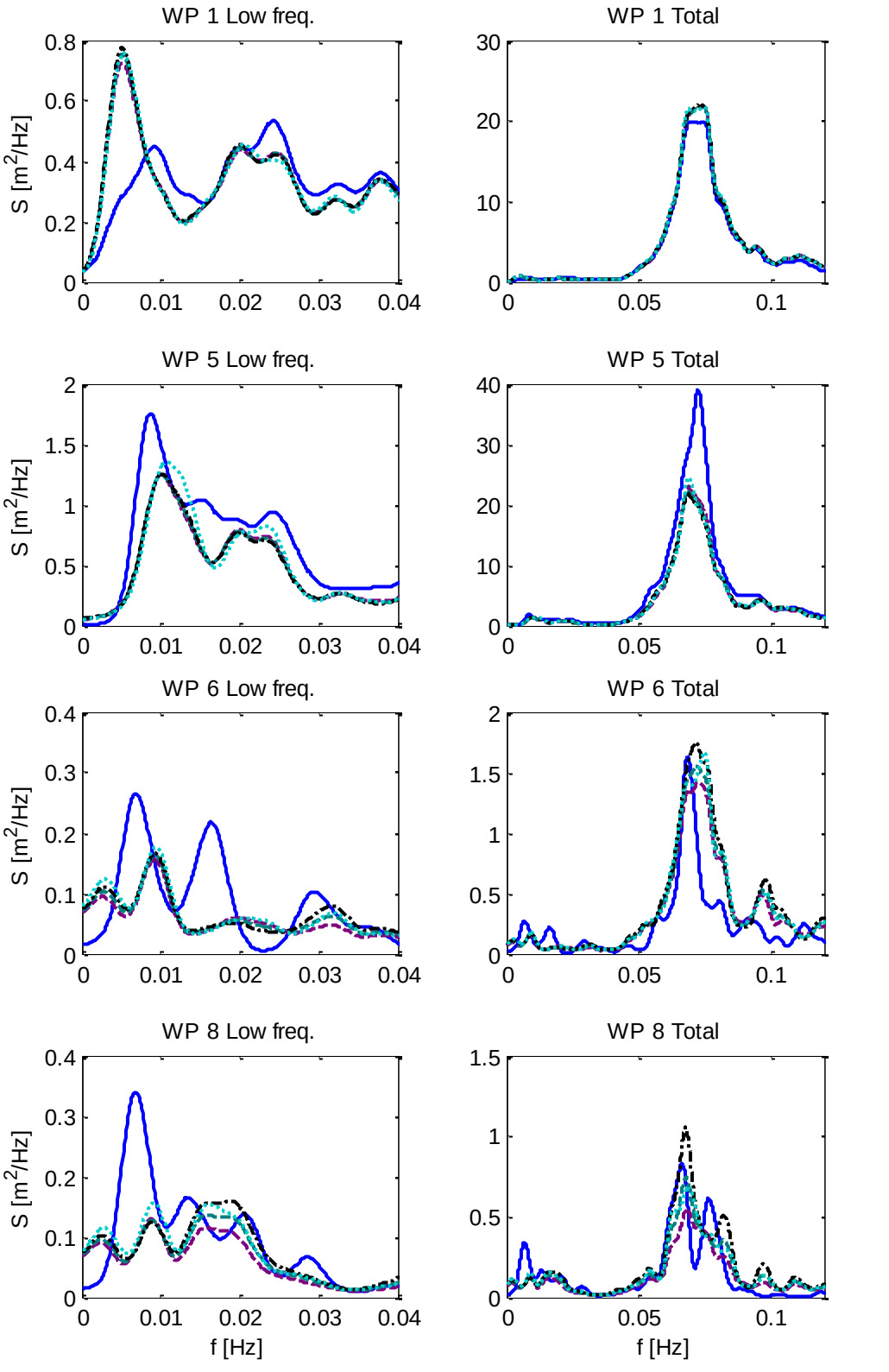

Figure C- 1: Results of run 01 to run 04. Sensitivity different reflection coefficients partial reflecting boundaries.

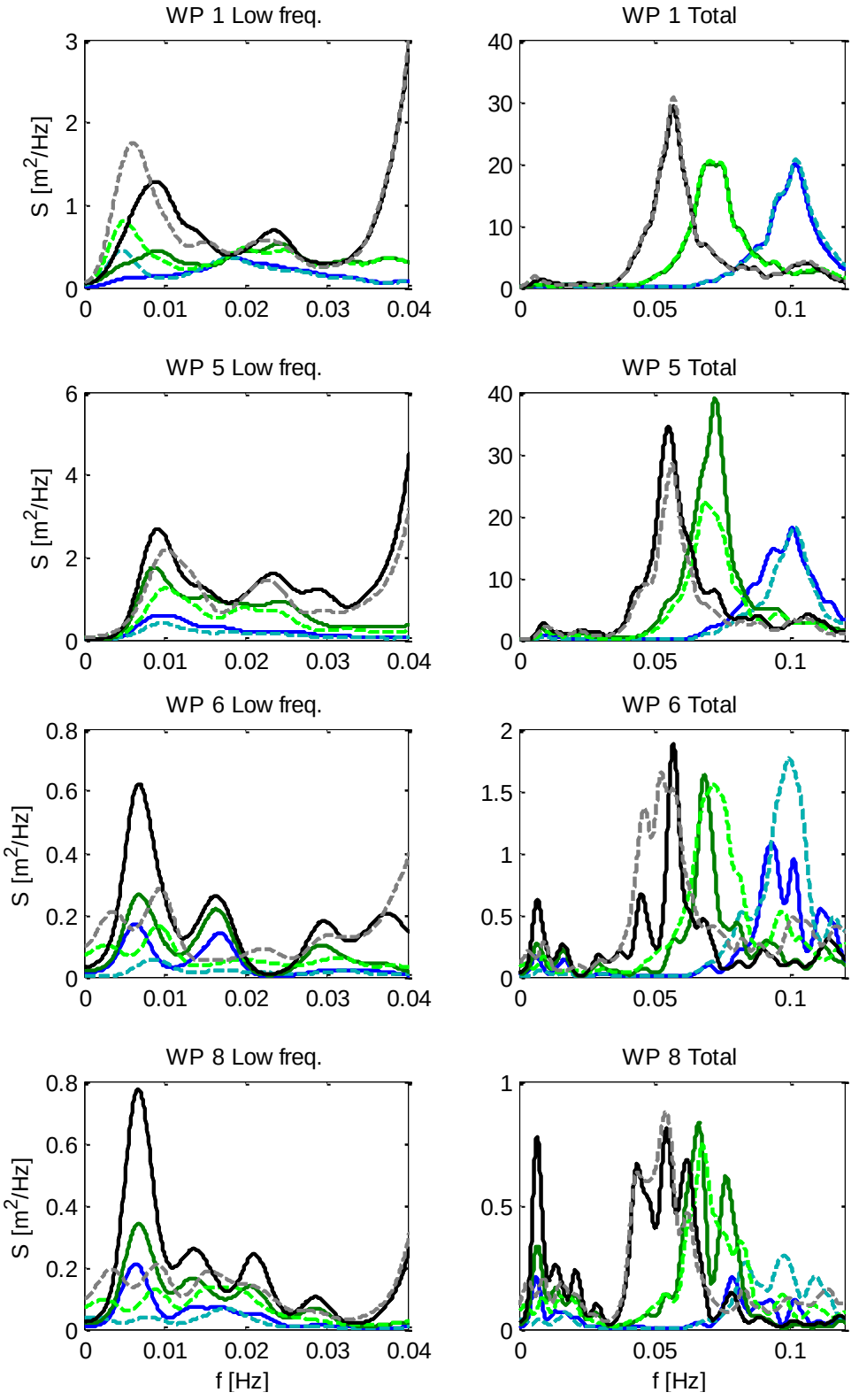

Figure C- 2: Results of run 05 and run 06. Verification partial reflecting boundaries for different wave periods.

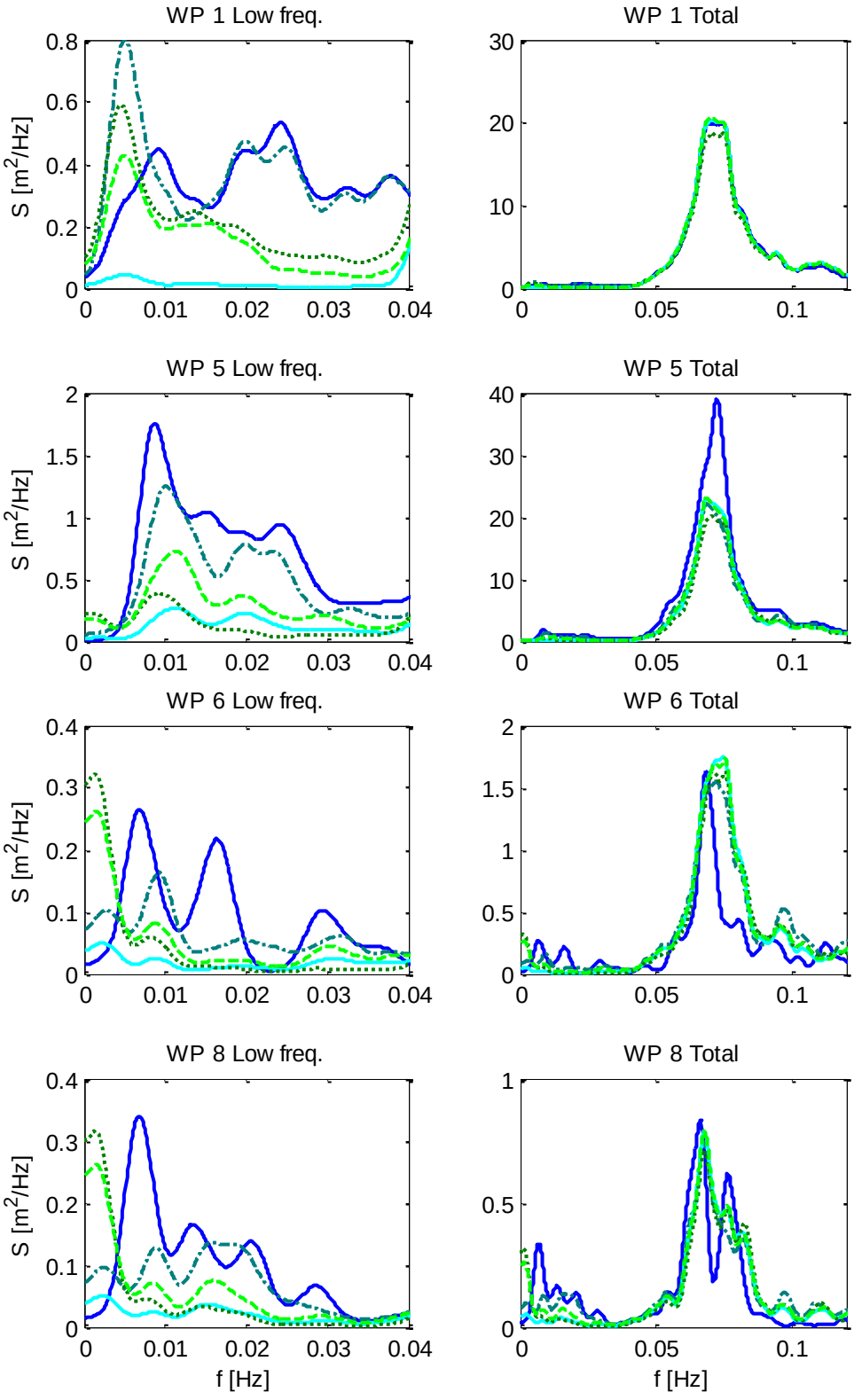

Figure C- 3: Results of run 07 to run 09. Sensitivity generated waves.

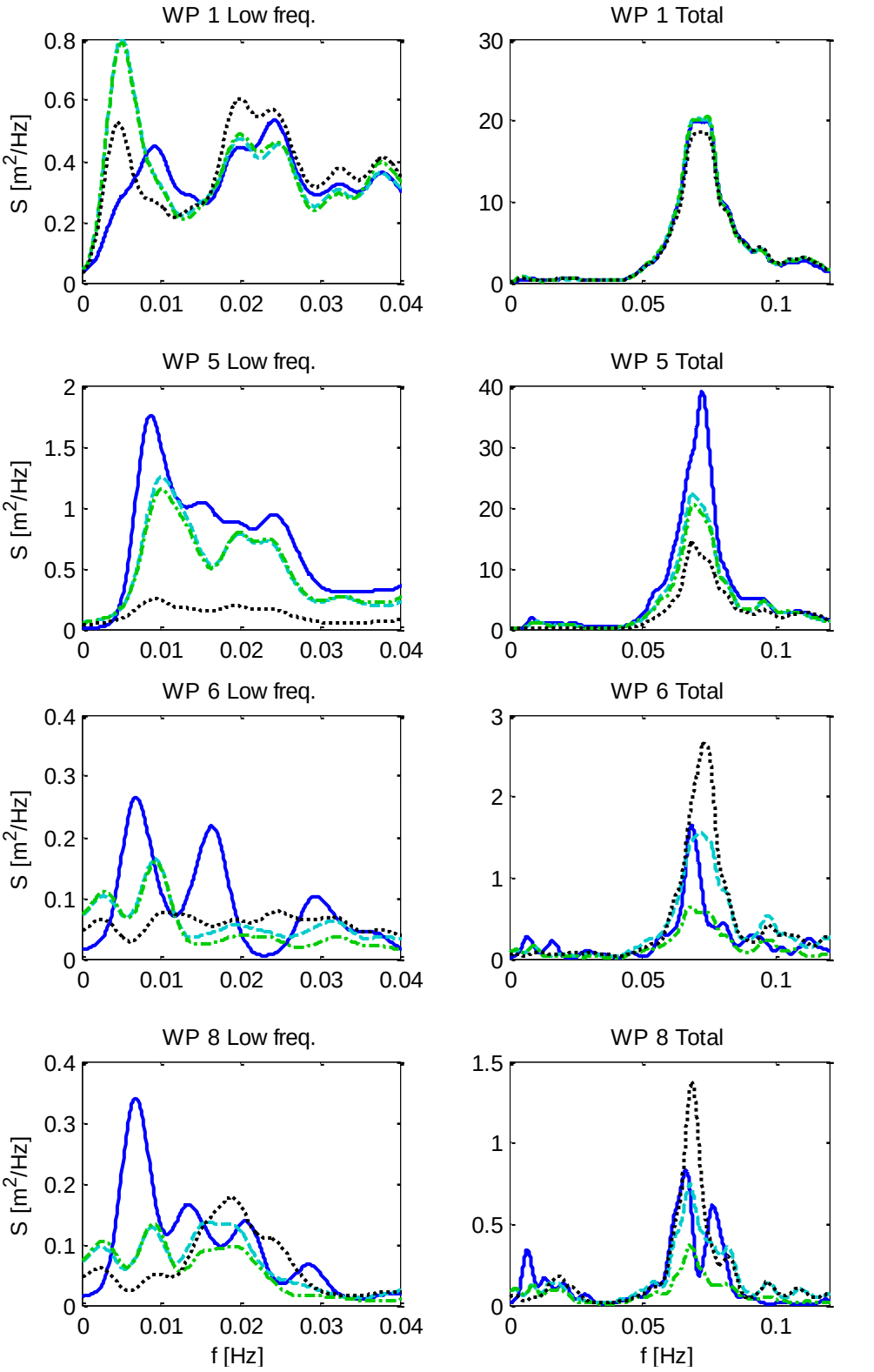

Figure C- 4: Results of run 10 and run11.
Additional simulations
Adaptation of breakwater head.
Partial reflecting side wall I.

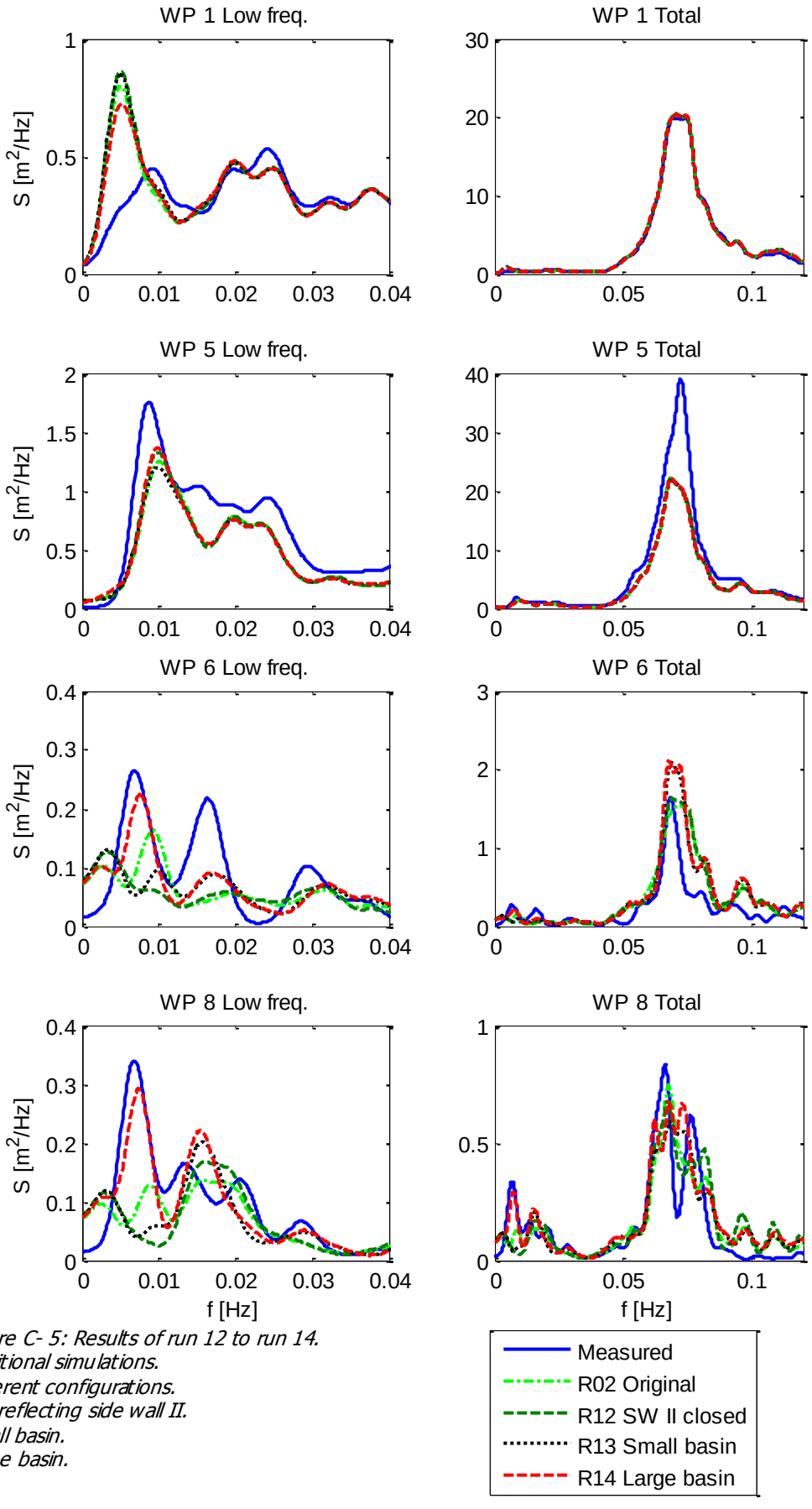

Figure C- 5: Results of run 12 to run 14.
Additional simulations.
Different configurations.
Full reflecting side wall II.
Small basin.
Large basin.

Appendix D. Modification of model set-up boundary conditions in Boussinesq-type wave model TRITON

Within TRITON a boundary condition procedure calculates the reflected wave, see section 4.2.2. From previous studies it is known that oblique model boundaries may cause numerical instabilities within TRITON. These instabilities are due to discretization of the dispersion boundary conditions along oblique model boundaries. The effect of an instable model boundary is illustrated in Figure D- 1: and Figure D- 2, in which the same time-serie was used under the same conditions except for the descritization of the partial reflecting boundary.

A numerical instability in the velocity field is noticed in case of oblique model boundaries, which grew in time. After longer period of simulation this instability dominates the total velocity field, see Figure D- 2. By avoiding oblique model boundaries, no numerical instabilities were noticed in the flow field. In case of a stable flow field, the applied model boundaries were defined parallel along grid lines, see Figure D- 3. In simulations with applied oblique model boundaries flow velocities above 3 [m/s] along the model boundaries in TRITON were calculated. These small instabilities finally formed a jet along the model boundaries effecting the total flow field (simulations not presented in this thesis). The occurrence of such a numerical instability along the model boundaries was already noticed in the case of an uniform bottom with low energetic waves (simulations not presented in this thesis).

If the flow velocities are calculated incorrect, but far outside the area of interest, the results from the Boussinesq-type wave model simulations can be used in further processing to calculate the wave forces on the ship. If incorrect described fluxes and/or velocities are located in the area of interest (the vicinity of the ship) this may lead to an incorrect description of the flow field around the ship and hence an incorrect description of the wave forces on the ship.

Due to an alternative model set-up of the model boundaries in TRITON no numerical instabilities in the flow field are observed. TRITON is robust enough to calculate the flow over a long period of simulation.

Conclusion

For the simulations carried out with TRITON during this study the following can be concluded:
Generated numerical instabilities along the model boundaries are responsible for the generation of eddies within the computational domain of TRITON. During longer period of simulation these eddies may increase in size as well as velocity magnitude. The existence of these very large eddies with large velocities amplitudes in the numerical model is physically not possible and is purely due to numerical instability along the model boundaries.

Numerical instabilities along model boundaries in TRITON can be avoided or minimized. Adaptations in the set-up of the model boundaries ensured that unwanted eddies were avoided during further performed simulations within TRITON.

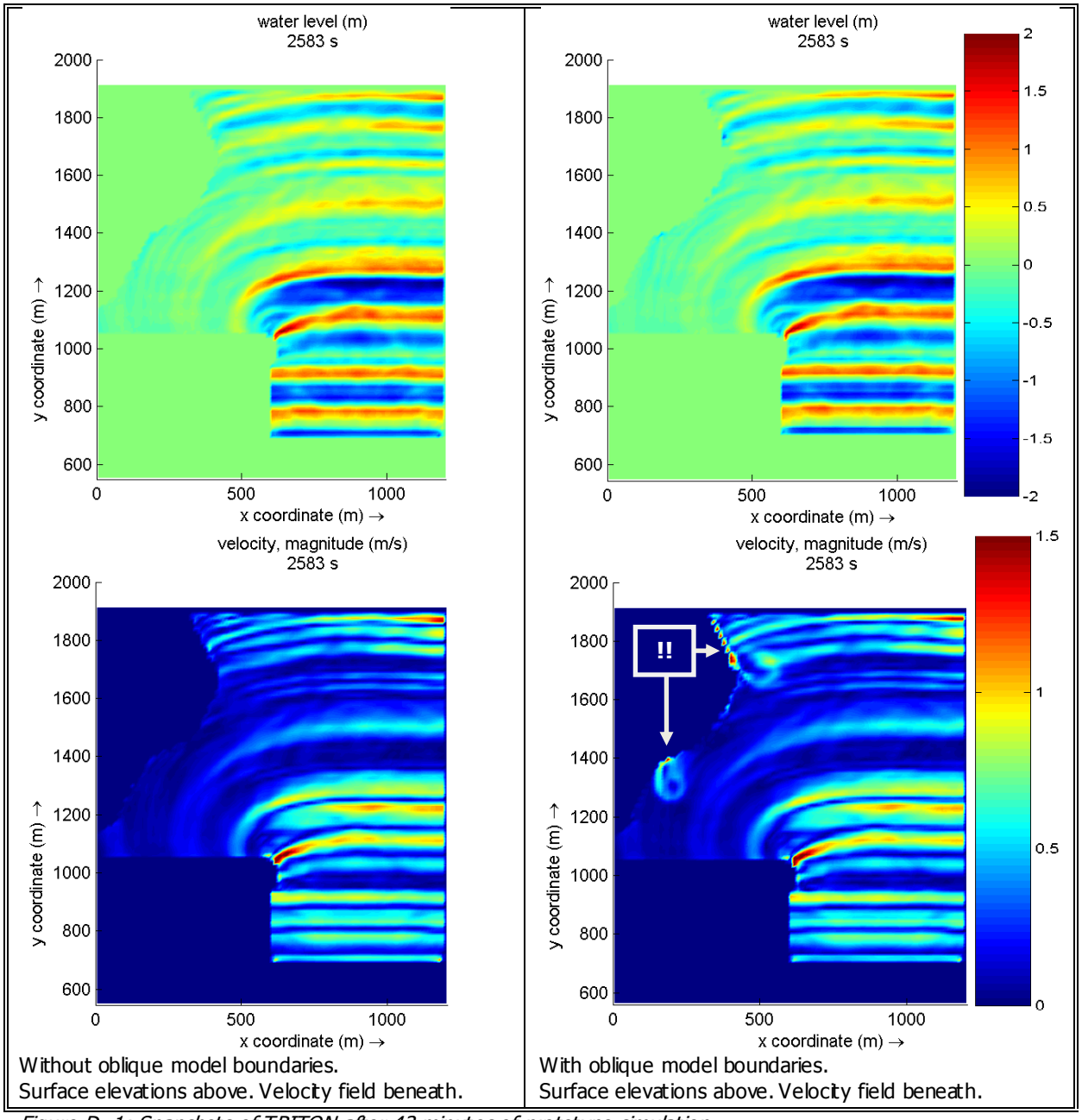

Figure D- 1: Snapshots of TRITON after 42 minutes of prototype simulation.

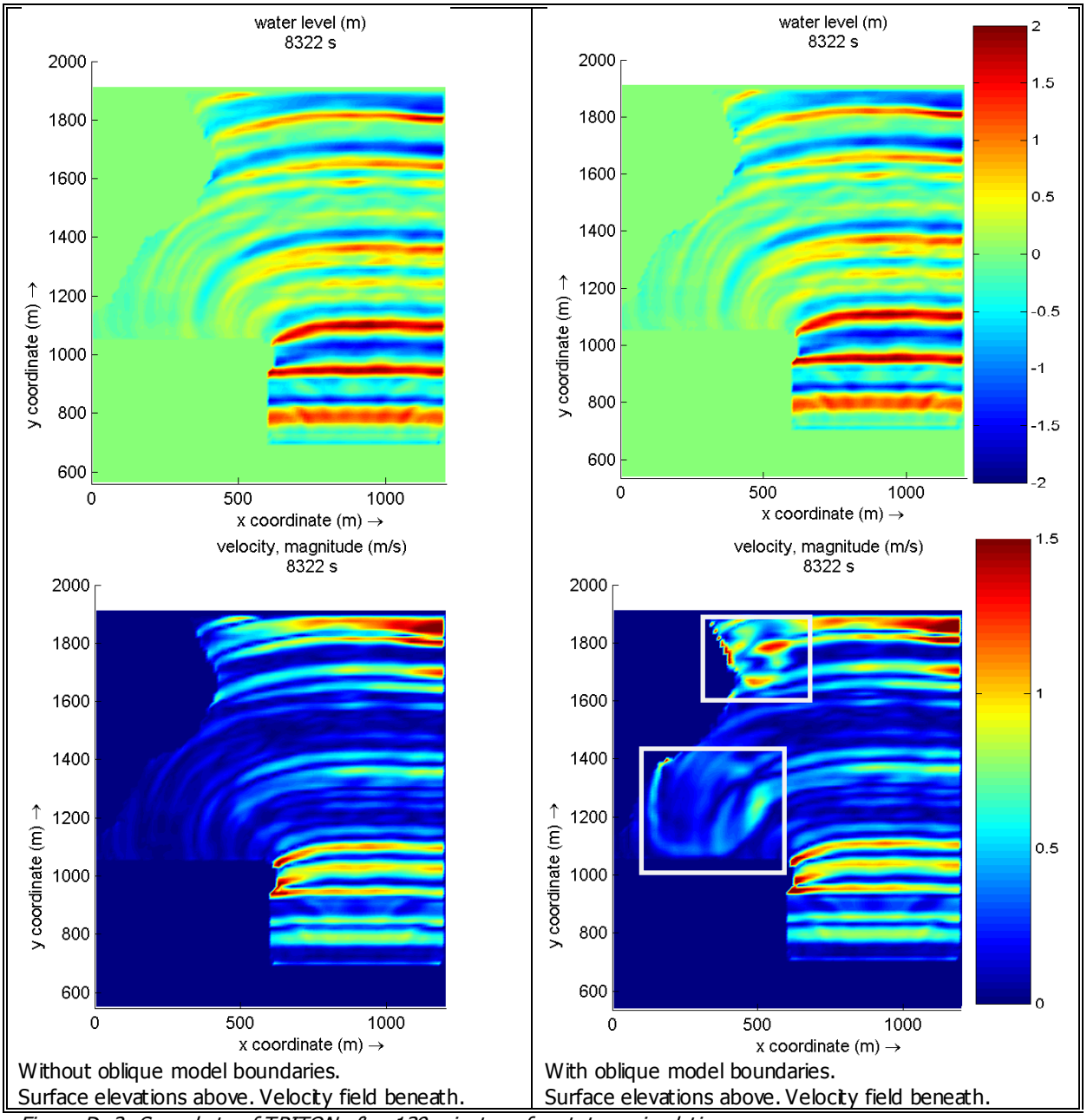

Without oblique model boundaries.
Surface elevations above. Velocity field beneath.

With oblique model boundaries.
Surface elevations above. Velocity field beneath.

Figure D- 2: Snapshots of TRITON after 139 minutes of prototype simulation.

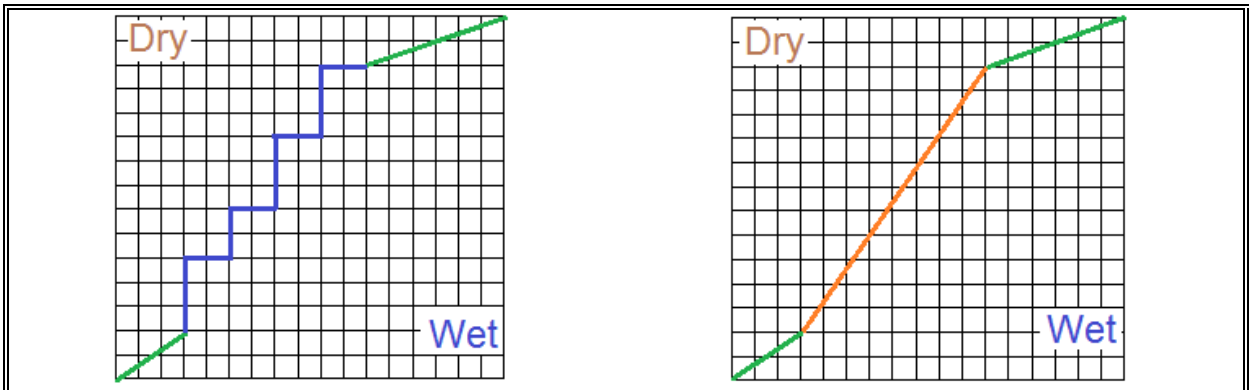

Use of stair case model boundaries (left) and oblique model boundaries (right) in computational domain TRITON.

Figure D- 3: Discretization of model boundaries in computational domain

Appendix E. Alternative resonance mechanism

The following comments were handed in by Dr. P. Rosa Santos from the Faculty of Engineering University of Porto. These comments should be taken into account during further research of wave modelling and/or moored ship response calculations.

Together with the transversal resonance mode mentioned in the dissertation, the following hypothesis should also be analysed: resonance of the mass of water limited by the north breakwater, the old north breakwater and the south breakwater. This mass of water may be considered as a triangular edge, with constant water depth (conditions in the physical model).

For d=20 m water depth and a height of the triangular edge of about 650 m, the following results may be obtained: a period of nearly 172s (0.0058Hz) for the first resonance mode considering some curvature at the triangle summit and a period of about 142s (0.0070Hz) if a perfect triangular edge is considered. As the triangular edge is reasonably wide it is expected that the associated response curve will be smooth, corresponding to a poorly selective situation. Nevertheless, pure reflective non-resonant situations caused by the corner between the two breakwaters may occur for a wider range of periods.

This mechanism may explain why energy measured in WP5 at frequencies about 0.006 Hz is not very high. Long waves reflected from the absorbing beach and "Prainha" (both are close to the left side wall of the wave basin) will be subjected to diffraction phenomena, either to Matosinhos Beach and the wave maker (see red lines in Figure E- 1).

In a previous study numerical simulations, for monochromatic long period waves, were carried out. Harbour geometry, bathymetry and surroundings were taken into account (i.e. simulation of real prototype conditions). For a period of 80 s (0.0125 Hz) and 100 s (0.01 Hz) a nodal line is located nearby the centre of Berth "A". So WP6 & WP8 do not measure correctly this standing wave. As the long wave period increases, the node line approaches the head of the north breakwater. For periods between 140 ~ 170s it should be placed nearly in the base of the triangle represented in Figure E- 1 and measured by WP6 and WP8.

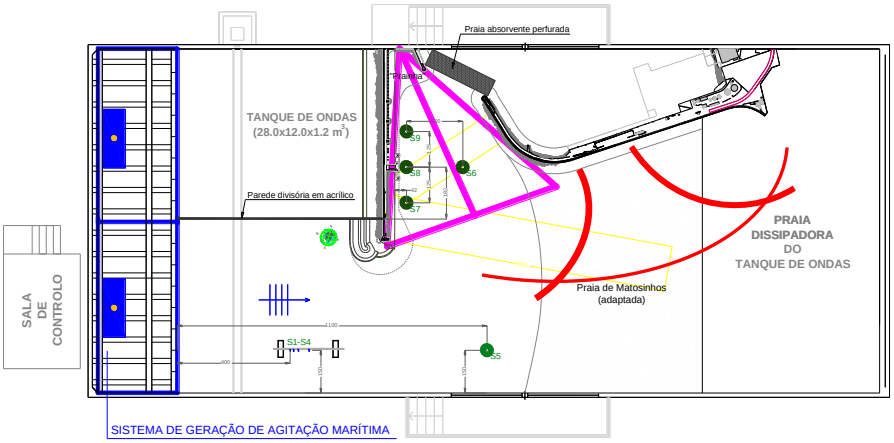

Figure E- 1: Resonant mechanism between North breakwater, old North breakwater and South breakwater.

Considering L= 350 ~ 500 m, d=20 m and the simplified expression for resonance of a closed basin, the periods obtained for the 1st mode of resonance are between 50s (0.020Hz) and 71s (0.014Hz).

It is difficult to be sure about the resonant mechanisms that occur (and are dominant) in the physical model. When planning the second phase of the study, this kind of issues was taken into account. It is remarkable to confirm that despite limitations and simplifications, resonant mechanisms identified in the model have correspondence with the prototype.

After diffraction, most of the wave´s energy will be directed to the south breakwater and then reflected to the Berth "A" location (see representation bellow). Then that energy will be re-directed to the south breakwater and Matosinhos beach (effects not too much different from what happens in the prototype).

Only a small amount of the incident (or generated) long wave energy will be directly directed to the left side of the wave tank. Part of this energy will be reflected in 'Prainha' (beach that exists in the prototype). The remaining energy will enter the inner harbour basin (very simplified due to space limitations), by the gap between the two breakwaters, but only after being partially dissipated in the perforated beach installed there.

> *Morais, C. C.; Abecasis, F., 1978. Storm surge effects at Leixões. Laboratório Nacional de Engenharia Civil, Memória Nº503, Lisboa* - this paper was presented at Fourteenth Coastal Engineering Conference, Copenhagen, 1974.

This reference reports an accident occurred at Berth "A" with a 137000 dwt oil tanker on the 21st and 22nd January 1974. Long period waves of 2 to 4 minutes with amplitudes of up to 50 cm, probably amplified, occurred. It was hypothesized that the situation was worse for periods near two minutes, because for the conditions existing at the time, the resonant period of the triangular edge mentioned before was of about 133 s. The oil tanker was unloading. In the worse situation the surge amplitude was of about 10 to 15 m and the sway amplitude of about 3 to 4 m from the berth. With tug assistance those peak-to-peak amplitudes reduced to 8 and 2 m, respectively.

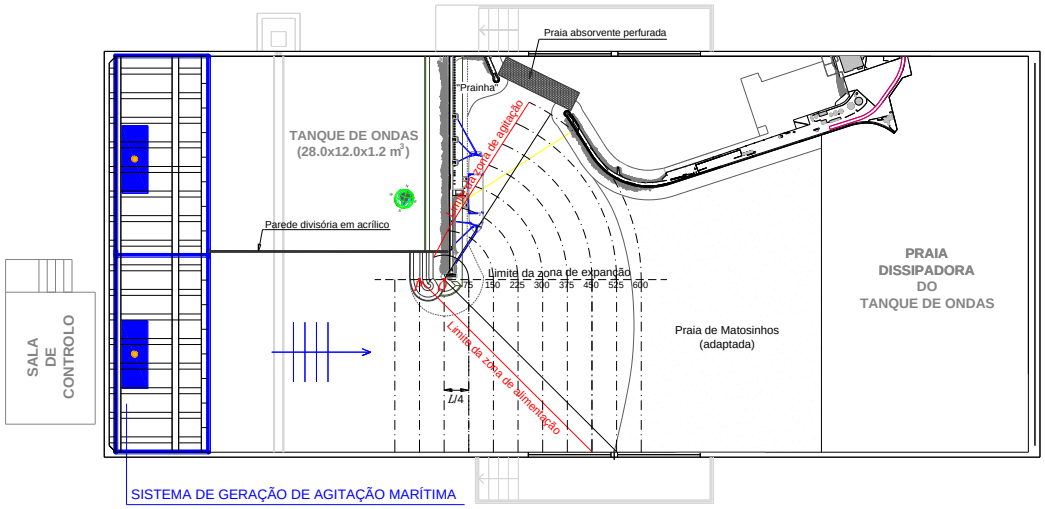

Figure E- 2: Diffraction in physical model.

Almost all the low frequency energy measured by WP1 to 4 is measured in WP5. WP5 is also close to a beach. In beaches, bound long waves are released and start to travel as free waves. Beaches may also generate low frequency energy by a so called "breakpoint forcing mechanism". According to the location of WP5, and taking into account the conditions of the previous figure, some reflections from the south breakwater may also be measured at the location of WP5. The low-frequency spectrums of WP5 show a high concentration of energy in the range between 0.007 to 0.01 Hz. The lengths associated with those frequencies are between 1000 m and 700 m (1st mode of oscillation). The wave tank is 12 m wide (1200 m in prototype dimensions). Considering the second mode of resonance, the possibility of WP 5 being close to an anti-node reduces considerably.

Most of the low frequency energy travels in the longitudinal direction. Low frequency energy may reach berth "A" area by diffraction or after reflection on the south breakwater or Matosinhos Beach. In the analysis presented in the dissertation it is considered that low frequency energy is trapped in the transversal direction. Low frequency energy travels, mainly, in the longitudinal direction. Diffraction will occur either in the propagation to the berth (right > left) or from the berth (left > right).

Considering only the 1st mode of resonance, length associated with those critical 'resonant' frequencies are between 1000 and 700 m, which are difficult to fit transversally in an alignment including the berth "A". In this case WP5 & WP8 are not in a node. In practice partial standing wave systems occur. Therefore, WP placed where the amplitude is minimal will record some energy.

For the triangular edge mentioned before and a d=20 m, the period of the first resonance mode was between 172 s (0.0058Hz) and 142 s (0.0070 Hz). As the triangular edge is reasonably wide, it is expected that the associated response curve will be smooth, corresponding to a poorly selective situation.

Analysis of Figure 3-6 > results of WP8. Three peaks can be seen between 0.005 Hz and 0.01 Hz in the wave spectra. Consider three partial standing wave systems associated with those three peaks. All may be explained as a result of the edge mechanism described before (0.0058 Hz and 0.0070 Hz) and therefore can have correspondence with reality. It is important to mention that the right side wall of the basin may also have some effect on that. below presents, as example, results of numerical simulations carried out for long period waves. In the example results are for T=120s.

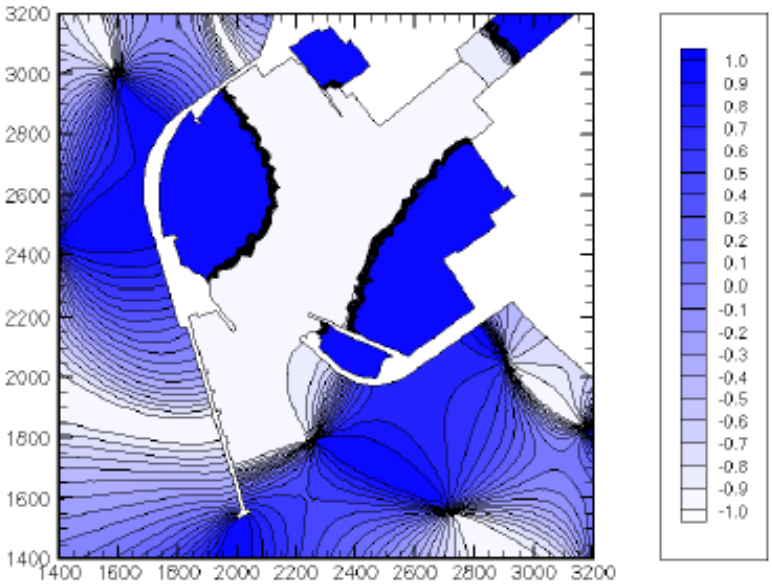

Figure E- 3: Monochromatic long wave computations for port of Leixões (T=120s).

Three 'resonant' situations could be associated with those three peaks. The first one, with a T~160 s (~0.0062 Hz), may correspond to a situation with a mode nearby the head of the breakwater. This standing wave is the more easily measured by WP8. The second one, with a T~143 s (0.007 Hz) and a node between the head of the north breakwater and the bow of the ship. A higher response is measured from the ship. Because the node is more close to WP8 this 'standing wave' is not so easily measured. The third one, with a T~125 s (0.008 Hz) and a nodal line in the space occupied by the ship's bow. This hypothetical 'standing wave' is therefore more difficult to measure but leads to the bigger response from the ship. The natural period of oscillation of the moored oil tanker in the surge direction is about 70 to 80 s (0.013 to 0.14 Hz), what may partially explain the second observed peak in the surge spectra.

Sway motion should mainly be associated with reflections from the south breakwater (or Matosinhos beach), but also the possible installation of partial standing wave systems between the two breakwaters. Smaller lengths lead to higher resonance frequencies. The sway natural period of oscillation is also in the range of 70 to 80 s (0.013 to 0.14 Hz). Differences of mooring system stiffness longitudinally and transversally are not very high. Some sway may also be due to coupling between surge and sway.

From Figure 3-6, it can be seen that the spectral energy density of surge decreases when approaching 0.01Hz (from the left), however it seems that the relative importance of sway is very high around 0.01 Hz. Sway would certainly be more easily excited if a transversal standing wave system were installed between the two breakwaters. Only simple reflections (i.e. without resonance) from the south breakwater may significantly contribute to the obtained results. Due to surge and sway coupling, large surge motions may also leads to significant sway motions.

Long waves could pass the perforated dissipation beach, but suffer energy dissipation when doing that. The rubble slopes installed inside that small basin (in all sides except in the right side wall of the wave basin) provided additional damping.